Abstract

In the first part, an attempt was conducted to clarify the effects of sediment extraction and dam construction on the change in the riverbed characteristics over yearly to decadal scales in the lower Tedori River, Japan. This goal was pursued by first comparatively analyzing the survey data on the bathymetry and human activities over a 58-year span. Empirical orthogonal function (EOF) analysis was then carried out to derive the principal variation trends in the dataset.

The results indicate that the riverbed degraded in excess of 0.5–3.5 m in the entire study area over the period 1950–1991. The riverbed sediment volume of the reach 0–16 km decreased by 12.7×10^6 m^3. The considerable reduction in sediment budget along the lower Tedori river was observed. The intensive sediment extraction was the dominant cause of degradation of the riverbed in this period. As another effect of sand and gravel mining, in the period of 1975 to 1990, the sediment mean diameter in the main course was smaller than that in the lateral lane. The temporal adjustment of the riverbed elevation at each cross section indicates that the riverbed experienced five phases of adjustment: I-A, I-B, I-C, II and III, four of which were well described by an empirical model.

In the period 1991–2007, the increase in the riverbed sediment volume of 0.6×10^6 m^3 resulted in accretion of the riverbed at an average depth of 0.04 m. Concurrently, sediment budget slightly recovered partially along the lower Tedori river. The riverbed variation in this period corresponds to the phase III of the adjustment. It is deemed that operation of the Tedorigawa Dam resulted in the deposition of sediment in the lower sub reaches.

An overall decrease in bankfull channel width of the lower Tedori river was observed through the period of 1950-2007. The variation in the channel width followed the variation in the riverbed elevation: namely, channel narrowing and the river bed degradation; channel widening and the river bed aggradation.

Over the period 1950–1979, the main trends of the change in the riverbed and its controlling factors were clearly captured by the first four modes of EOF analysis. That is, the first mode explained the mean profile of the riverbed and temporal variation in the riverbed sediment volume. The second to fourth spatial eigenfunctions reflected the spatial variation in the rate of vertical adjustment for the phases I-B, I-C and I-A, respectively. The corresponding temporal eigenfunctions explained the respective

effects of sand and gravel mining, of imbalance between sediment transport capacity and sediment supply, and of dredging activity on the riverbed. In addition, a collation of river and coastal EOF results indicate that the time lag of the onset of accelerated erosion in the Mikawa coast was several years when compared with that in the downstream river.

In the second part, in order to reproduce the bore propagation over a channel with complex topography, a numerical model is developed to solve the Nonlinear Shallow Water Equations on the basis of TVD-MacCormack scheme. The model incorporates the surface gradient method , a simple wetting and drying method and an improved surface gradient method. The applicability of the numerical model is tested through comparison with existing theoretical and experimental studies. The verification of the model against with analytical solution include tide wave over steps, preservation of still water surface, dam-break, run-up and back-wash on a sloping bathymetry. Excellent agreement between analytical and numerical results was achieved. Subsequently, the validation of the model with the experimental data consist of bore propagation over a triangular bottom sill, dam-break wave propagation over a complex topography, 3D schematic dam break. In general, numerical results agree well with the experimental ones. Finally, bore propagation and run up over a river bank was modeled.

Acknowledgments

Contents

List of Figures

List of Tables

Part I. Introduction

1.General background

River plays a crucially important role in human life. Most of us live near rivers and rely on them for water supply, food, power, transport, recreation, waste disposal, and as a source of raw materials (Bridge, 2003). In order to maximize economic and environmental values of rivers, it is required to sustain health of river in dynamic equilibrium state. Prior to anthropogenic intervention, river systems are usually in a quasi-steady state wherein erosion, transport, and deposition are adjusted to the prevailing conditions of climate and geology (T.Hack, 1960). In recent decades, human activities and extreme events have strongly affected morphological evolution of rivers. It is realized that disturbances induced by climate change may progress exceedingly slowly and be practically imperceptible by human standards (Simon, 1989). In contrast, human-induced disturbances often accelerate or alter natural processes and trends rapidly, resulting in a compressed time scale for river adjustments (Rinaldi and Simon, 1998). Lower rivers which is located downstream of the rivers and adjacent to coasts are prone to be influenced by both disturbances occurring in river basins and disasters originating from seas.

Morphological change in lower rivers due to human impacts generally occurs as a result of change in flow, sediment regime and/or boundary condition. Typically, natural transporting processes of flow and sediment from mountains to coasts are disrupted by anthropogenic impacts such as material extraction and dam constructions. Consequently, these interventions could adversely affect the morphology of the lower river such as: riverbed mobilization, scouring, erosion, and deposition, etc.

After the World War II, many countries in the world have experienced a rapidly economic growth period, which is accompanied with a high need for concrete aggregate and energy. Regarding the aggregate demand, sand and gravel has been prevailingly utilized because of its advantages: durable, well-sorted, rounded and cheap. In many areas, aggregate is derived primarily from alluvial deposits, notably from active river changes, their flood plains, and older terrace deposits (Sandecki, 1989). It is realized that sediment mining produces a large variety of physical, ecological, and environmental effects. In term of morphological effects, sediment mining could induce upstream incision, downstream incision, lateral channel instability, bed armouring, impacts on infrastructures and sediment deficit in coastal zone (Rinaldi et al., 2005). In addition, for various purposes, many dams have been con-

structed in many rivers. Most regions of the world experienced an extreme acceleration of dam-building activity from 1950 and the rate of dam building appears to have peaked in 1968 (Beaumont, 1978). In almost all cases, dams interrupt and modify the downstream flux of sediment through watersheds; they typically also affect the flow regime (Grant, 2012). It is known that flows and sediment are two key factors which decide river form. Thus, dam constructions have the potential to alter the entire hierarchy of channel variables (Schumm and Lichty, 1965). It is therefore especially important for rational river management to more insightfully understand how human activities such as sand and gravel mining and dam construction affect morphology of lower rivers.

Besides, lower rivers may be vulnerable to bore inundation which is originated from dam-break flow in the upstream area or from tsunami intrusion following great earthquakes. For example, the tsunami induced by the 2011 Tohoku earthquake in Japan hit Sendai Plain. Subsequently, the tsunami runs up a number of rivers and overflowed into surrounding areas. Many structures were severely damaged, and huge numbers of human lives were lost in the flood. In order to mitigate such disasters, it is vital to better understand hydrodynamic responses of a bore during propagating into the lower river as well as its adjacent area.

2.Needs for research

Among various human activities, dredging activity (DA) and sand and gravel mining (SGM) most notably reduce the amount of sand-and-gravel-sized sediment and consequently alter the river morphology (Collins and Dunne, 1989; Kondolf, 1994; Kondolf, 1997; Rinaldi and Simon, 1998). According to Simon (1989), the dredging and straightening of alluvial channels between 1959 and 1978 in West Tennessee in the United States degraded sites upstream of the area of maximum disturbance and lowered bed levels by as much as 6.1 m. The Gállego River in Spain was subjected to incision amounting to more than 5 m between the early 1970s and 2004, and the mining of gravel is the only plausible cause for this severe degradation (Martín-Vide et al., 2010). Along alluvial rivers of Tuscany, central Italy, there was significant acceleration of channel incision during the period 1945–1980, in concomitance with the maximum sediment mining activity at a regional scale (Rinaldi, 2003). Additionally, the river pattern evolved from being generally braided to a more singular thread

(Kondolf and Swanson, 1993; Martín-Vide et al., 2010; Rinaldi et al., 2005). These results were investigated over time spans of less than 40 years, and the possible indirect effects of sediment extraction on the river morphology are therefore not well understood. Hence, there is a need for more thorough research to examine the interaction of the disturbed rivers with sediment extraction.

Many rivers around the world have been affected by dam constructions superimposing or succeeding the process of intensive sediment extraction. Dam constructions affect the morphology of rivers below by reducing the flood peak and blocking the upstream bed load supply. Incision below dams is most pronounced along rivers with fine-grained bed materials (Alekseevskiy et al., 2008; Isik et al., 2008b). By contrast, along several gravel-bed rivers, there is riverbed aggradation because the reduced flood peak is insufficiently powerful to pick up and transport tributary-supplied sediment (Church, 1995; Topping et al., 2000). The effects of in-stream gravel extraction are often exacerbated downstream of reservoirs (Kondolf and Swanson, 1993). However, the long-term response of the riverbed to damming subsequent to mining remains unresolved.

In Japan, the morphology of the pristine river is characterized due to the combination of steep landforms and frequent storms, and its change is often accelerated by the effects of earthquakes and volcanic eruptions (Oguchi et al., 2001). Therefore, Japanese rivers differ from most continental rivers in the world because they are short (max. length: 367 km), steep (average slope: 0.44%), and exhibit very flashy flow regimes(Yoshimura et al., 2005). Since around 1960, when Japan entered a period of high economic growth, a substantial amount of sand and gravel has been extracted from rivers to be used as concrete aggregate. Additionally, many dams have been built to control floods, generate electricity, and secure water for various uses (Inoue, 2009). This has seriously affected the river morphology. Nevertheless, there has been little research on such problems owing to the inherent complexity of the problem and deficit data coverage, especially on decadal scales (Yuhi, 2008a). Sato et al. (2004) indicated the significant degradation of the longitudinal profile of the Samegawa River, Japan, in the region 1 km from the river mouth in 1977. This degradation was attributed to the dredging of a sand bar in the early 1970s although there is no official record of the amount of sand dredged. Through analysis of the sediment budget at the reach scale, Huang (2011) deduced that the riverbed sediment volume in the lower Tenryu River decreased as a result of sand and gravel extraction and dam construc-

tions, which were conducted intensively before 1968. A similar view for the Tedori River and neighboring coast was presented by Yuhi (2008a); (Yuhi et al., 2009). However, these investigations mainly considered the variation in the riverbed sediment volume rather than the morphologic features.

Recently, the Tedori River has been profoundly affected by continuous anthropogenic activities such as dredging activities, sand and gravel mining and multi-purpose constructions. These activities have disturbed the preceding equilibrium condition of the Tedori River. In particular, significant amount of sediment was moved out due to mining and trapped in the Tedorigawa Dam. This has induced intensive change in the riverbed elevation and the corresponding sediment storage volume from 1950 and 2007. Therefore, research on response of the lower Tedori river to sediment extraction and dam constructions using datasets spanning over 50 years is the utmost important to contribute to implement rational management of the Tedori river as well as other rivers in Japan.

Bore propagation in rivers and inlands is mathematically described by the shallow water equation. The most challenging feature of the shallow water wave equations is that they admit discontinuities as well as smooth solutions. Even the case in which the initial data is smooth can lead to discontinuous solutions in finite time. Although much effort has been made to analytically solve the shallow water equation, yet theoretical solutions are still very limited in several simplified cases, which are insufficient to capture complicated hydrodynamics of real flows. Therefore, together with the development of high-performance computers, numerical methods have become a productive tool to reproduce the various flow phenomenon which include discontinuities in the solution. Many researches on improving the accuracy of the numerical schemes for solving the hyperbolic equation system have been conducted. However, the treatment of source terms in that equation system and the modeling of the moving wet-dry interface at a shallow water wave front remain difficult (Liang et al., 2009; Wei et al., 2006). The problem becomes more difficult when simulating tsunami propagation over the complex topography in which artificial numerical wave is often created in free water surface. This imposes the need to further study the well-balanced numerical schemes which are more accurate and robust to model discontinuous free-surface shallow flows like tsunami propagation over the complex boundary. This work is considered as a preparation step to deal with the tsunami in the lower Tedori river as well as surrounding areas.

5

3. Objective and scope of study

The first main object of this study is to quantify the effect of sediment extraction and dam construction on riverbed characteristics over the period of 1950-2007 in the lower Tedori river, which is from the Tedori river mouth to 16km upstream from the river mouth. The specific objectives of the present investigation are (i) to analyze the variation in the riverbed of the lower Tedori River, focusing on establishing an empirical model of temporal variation in the riverbed elevation, (ii) to quantify the effect of sediment extraction and Tedorigawa dam construction on the riverbed, and (iii) to highlight the variation in the riverbed in relation to its controlling factors through empirical orthogonal function (EOF) analysis. These goals will be pursured by first comparatively analyzing the survey data on the bathymetry and human activities. EOF analysis is then employed to derive the main trends in the dataset.

The second object of this study is to develop a numerical model which is capable of solving the Nonlinear Shallow Water Equations based on the TVD-MacCormack scheme, which is 2nd order accurate in time and space. It aims to achieve well-balancing through modifying local bed elevation and using the surface gradient instead of the depth gradient for TVD corrections. The accuracy and robustness of the model will be tested against several analytical solutions and experimental data in order to confirm that the model is able to simulate the 1D, 2D discontinuous flow over the complex topography.

Part II. Long-term responses of the riverbed in the lower Tedori River, Japan to sediment extraction and dam construction

1.Introduction

In recent decades, morphological evolution of river have been strongly dominated by human activities through change in sediment transport and flow. Such activities often occur over a large temporal and spatial scale. Therefore, mechanisms of their effect on river channels are complicated to fully recognize. Existing knowledge on shedding light the problem has been obtained by a variety of researches (Rinaldi, 2003; Rovira et al., 2005; Yuhi, 2008b) in the last decade. Yet, in order to achieve better management in river systems, it is necessary to further investigate the variation in river channel in relation to anthropogenic activities in a long term at a large scale(Piégay and Hicks, 2005).

In rivers, morphologic characteristics and sediment transport have a mutual interaction. These features simultaneously respond to a deficit of bed sediment induced by human activities such as bed sediment extraction and dam constructions. A temporal and spatial trend of variation in the river bed level is closely related to the imposed disturbance in a river as well as in its basin (Isik et al., 2008a; Rinaldi and Simon, 1998; Simon, 1989).

Recently, the Tedori River has been profoundly affected by continuous anthropogenic activities such as dredging activities, sand and gravel mining and multi-purpose constructions. These activities have disturbed the preceding equilibrium condition of the Tedori River. In particular, significant amount of sediment was moved out due to mining and trapped in the Tedorigawa Dam. This has induced intensive change in the riverbed elevation as well as the corresponding riverbed sediment volume from 1950 to 2007*(Dang et al., 2012).*

In part I, we aim (a) to analyze the change in morphological characteristics of the lower Tedori river, (b) to analyze the temporal and spatial variation in sediment budget components and their mutual relation and (c) to use EOF analysis to capture the main variation trend in the lower Tedori river and its controlling factors.

2.Literature review

2.1.Effect of material extraction and dam constructions on river morphology

River morphology is naturally formed by alluvial processes such as erosion and deposition. Erosion and deposition are responses of the rivers to external impacts to maintain an approximate balance between available sediment and sediment transport capacity. Erosion occurs when the sediment transport capacity exceed the sediment supply. Conversely, deposition appears. Theoretically, morphological evolution of the rivers is considered on the basis of three simple principles regarding water flow – hydraulic selection, path of least resistance, and energy dissipation- and on a principle of finite relaxation times (Phillips, 2010).

Human activities exert the river morphology thereby via direct or/and indirect ways. The former often directly alter morphological characteristics of rivers such as riverbed elevation, width, slope, sinuosity and so on. Material mining and channelization are typical for such activity. The river morphology instantly responds to material extraction and channelization. The latter change the river morphology through adjustment of controlling factors, which leads to imbalance between sediment supply and sediment transport capacity, ultimately inducing degradation or aggradation in rivers. For example, dam construction is considered as one of the second activities. Besides, the direct impact could trigger the indirect one on change in river morphology.

Sand and gravel mining is an activity which uses heavy equipment to physically remove sand and gravel–sized material from riverbeds. Accordingly, pits is excavated in some places such as river channels, floodplains and terraces to extract sand and gravel (Fig. 2.1). Another way is bar skimming involving scraping off the top layer from a gravel bar without excavating below the summer water level (Kondolf, 1994). Through using these methods to extract sand and gravel, morphological characteristics of rivers are intensively altered. However, researches on the adverse effects of sediment mining on the riverine environment in general and on the river morphology in particular have remained limited, which leads to negative impacts of sediment extraction to be commonly neglected in the past (Rinaldi et al., 2005). Existing literatures have addressed morphological effect of sediment extraction as follows.

9

Sediment extraction from the riverbed exceeding the sediment supply firstly causes degradation of the riverbed. It was recognized that presence of a large pit in the riverbed creates discontinuities of sediment transport at both its upstream and downstream. Here, discontinuities of sediment transport means that the transport rate of bed-material load changes abruptly. The sediment transport discontinuity at the upstream limit of the excavated pit where there is a sudden increase in slope and consequently a rapid increase in sediment transport rate. This leads to exceeding transport capacity to sediment supply. This deficiency of sediment is compensated for by entrainment from the bed and the discontinuity usually moves upstream over time (Collins and Dunne, 1989; Erskine, 1990; Galay, 1983; Kondolf, 1994; Kondolf and Swanson, 1993; Lane, 1947; Surian and Rinaldi, 2003). The discontinuity occurs at the downstream limit of the pit where there is a deficiency of bed-material supply in relation to transport capacity, inducing the erosion of the bed below the pit and subsequently moving this erosion downstream over time (Galay, 1983; Rinaldi, 2003; Rinaldi and Simon, 1998).

Exceeding degradation of riverbed due to sand and gravel mining could trigger bank instability thereby down-cutting and toe removal, subsequently induce changes in channel width, channel migration in formerly stable reaches (Collins and Dunne, 1989; Rinaldi, 2003; Rinaldi et al., 2005; Surian and Rinaldi, 2003).

Direct extraction of gravel and sand from the riverbed, also can result in amouring, the development of a lag deposit of cobbles and boulders on the bed (Kondolf, 1994). Additionally, sediment deficit caused by in-stream mining leads to the selective erosion of finer grains from bed material and the development of bed amour (Rinaldi et al., 2005). As a result of bed degradation, bridges and channelization structures can be undermined, and pipelines or other structures buried under river beds can be exposed and damaged.

With the same mechanism of influence as that of pit excavation, gravel bar skimming also make the processes of sediment transport discontinuous and may induce downstream incision and lateral instability of the channel, even when the extraction rate are typically smaller than that by pit mining. Removal of the coarser surface layer of sediment due to skimming in natural rivers stimulates bed erosion and increases bed load transport (Kondolf, 1994; Rinaldi et al., 2005).

When pits are constructed near the river and separated only by a strip of land (typically along inactive channels), an avulsion or a more gradual channel migration

may cause the pits to be captured during floods. The former off-channel pit is then converted into an in-channel pit, and the effects typical of in-stream mining can be expected. Another important concern of floodplain mining is that wet pits typically intersect the water table, and therefore constitute a preferential path of ground-water contamination and pollution.(Rinaldi et al., 2005)

Another significant effect of sand and gravel mining on morphology is erosion of downstream coast. Because 95% of sediment discharge delivered to the downstream coast is from rivers (Syvitski et al., 2003), sand and gravel extraction in rivers cause deficit of coastal sediment (Huang, 2011; Yuhi, 2008b).

Dams significantly change flow regimes downstream and disrupt continuous processes of sediment transfer from headland to downstream areas. These alterations of the primary fluvial processes below dams lead to change in river morphology. In recent 6 decades, such alteration have been realized as a crucially important issue for river managers: aggradation and degradation having adverse effects upon flood capacity, channel migration, diversions and a range of river uses (Hathaway, 1948). Morphological processes in a reach below dams are qualitatively explained based on the general expression of Lane (1955), which indicates that fluvial systems adjust so as to maintain an approximate balance between available sediment and sediment transport. Namely, to transfer a given supply of water and sediment load, it requires rivers to change the size of width, depth and slope. According to Petts (1984), response of rivers below dams was categorized into different three types of adjustment: Passive response, where flows are reduced below the river's competence threshold and channel dimensions are reduced accordingly but without significant change in bed elevation; Degradation, where bed elevations and lateral deposits are scoured as the channel moves toward a new equilibrium with the reduced sediment supply; Aggradation, where reductions in discharges and competence due to dam operation are of sufficient magnitude to limit the channel's ability to entrain and transport sediment delivered by tributary or other inputs downstream of the dam, resulting in an increase in bed elevation. Prior to 1980, due to the paucity of data, researches on behaviors of rivers to dams upstream were mainly conducted in term of qualitative analysis. Accordingly, rate and extent of degradation was reported by Wolman (1967), Hathaway (1948), Lawson (1925); aggradation was addressed by Makkaveyev (1974), Malhotra (1951), Stanley (1951) and Arroyo (1925). After 1980, with application of new analysis technology such as airborne multispectral imagery, aerial

photography and GIS, coupled with the longer data sets produced advance in river morphology. Thanks to these improvements, narrowing was investigated in Peace River, Canada(Church, 1995) and Green River, USA (Lyons et al., 1992). More specifically, narrowing following aggradation or local degradation was observed in Mangrove Creek, Australia (Sherrard and Erskine, 1991), but widening accompanied with degradation appeared in Osage River, U.S.A (Germanovski and Ritter, 1988). Conversely, widening in accordance with aggradation was present in Fortun River, Norway (Fergus, 1997). Interestingly, slight change was witnessed in River North Tyne (Sear, 1995) and River Tay in U.K. (Gilvear and Winterbottom, 1992). Besides, change in river pattern was seen: from straight to more sinuous in Mangrove Creek, Australia (Sherrard and Erskine, 1991); from meandering to braided in Green River, U.S.A. (Lyons et al., 1992). Overall, morphological response of each river to dams upstream vary river by river and depends on its condition of climate, geology and topography. It, therefore, needed to conduct more case studies in order to extract an useful framework.
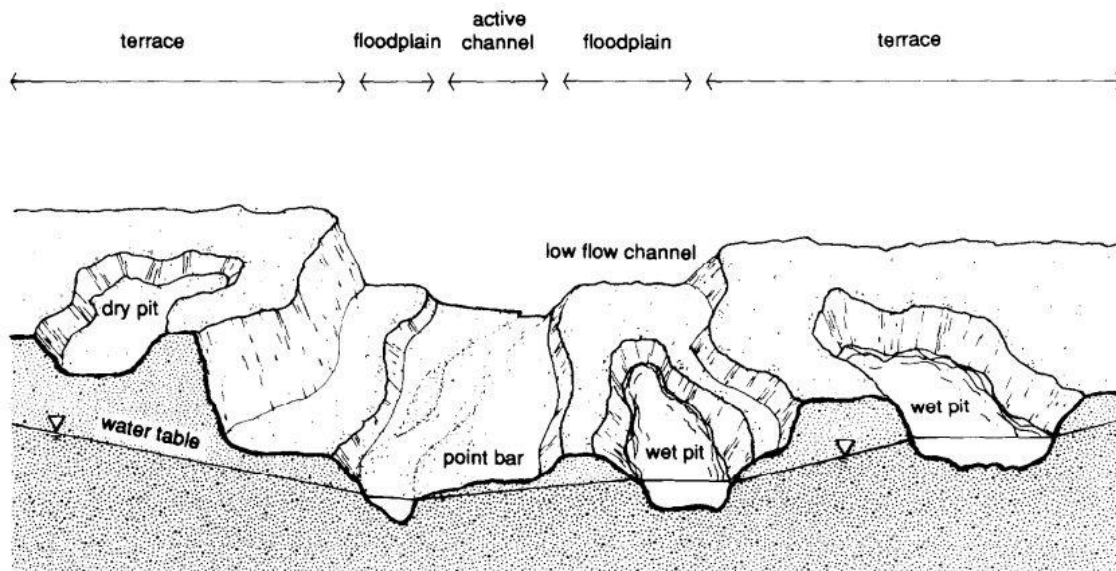
Figure 2.1. Alluvial deposits exploited for aggregate depicted in relation to river channel morphology and alluvial water table (Kondolf, 1994).

2.2. Rate of vertical adjustment in riverbed

Morphological responses of rivers to disturbances or climate-induced change decrease with time and subsequently asymptotically reach a condition of minimum variance. Such variation trend could be well described mathematically by nonlinear

functions. In the last century, nonlinear decay functions was used to properly address the evolution and alteration of the rivers (Bull, 1979; Graf, 1977; Hey, 1979; Rinaldi and Simon, 1998; Robbins and Simon, 1983; Schumm and Lichty, 1965; Simon, 1989).

Above literatures indicate that types of nonlinear decay function vary with different rivers. Graf (1977) used exponential functions to describe the 'relaxation time' necessary to achieve new equilibrium following a disturbance. Robbins and Simon (1983) used exponential decay regressions between water surface slope and time to describe quantitatively gradient adjustment along a particular reach experiencing channelization. A convenient way to interpret temporal and spatial trends of aggradation and degradation is to fit nonlinear functions to bed elevations measured through time, and to plot a measure of these functions versus the distance from the river mouth (Rinaldi and Simon, 1998). Accordingly, Williams and Wolman (1984) found that hyperbolic functions well describe degradation in rivers below dams. Simon (1989) use both exponential and power equations to fit to the observed data in West Tennessee. In this case, the power function is more appropriate to fit the empirical data than the exponential function. Therefore, it was chosen to describe temporal variation in bed levels at each cross-section. By using this way, parameters of the empirical model sufficiently captured the morphologic responses of West Tennessee, USA in time and space. With some improvements of Simon (1992), an exponential function that describes the dimensionless change in bed elevations is used to simplify comparisons between the two fluvial systems: the Toutle and Obion-Forked Deer River systems. Based on a pair of parameters extracted from the empirical models, temporal and spatial variations in morphological processes of the Toutle and Obion-Forked Deer River Systems was addressed clearly. Similarly, the improved exponential function regression analysis was also applied to the Arno River, Italy. The results indicate that the magnitude and rate of the vertical adjustment of the Armo River experienced several phases corresponding to the impact of human activities on the river basin. However, it also reveals that in some cases, the parameter of the empirical model did not accurately reflect morphologic behaviors of the Armo River. It, therefore, needs to continuously advance the empirical model for applying to other rivers in the world.

2.3. EOF analysis

Empirical orthogonal function analysis was used to identify dominant patterns of variability within a data set. Eigenfunction approach considers the explanation of observed data by a set of shape functions (the EOFs) that is extracted from the data itself (Jackson, 1991; Preisendorfer, 1988). EOF separates the temporal and spatial dependence of the data, considering data as a linear combination of products of corresponding functions of time and space (Dai et al., 2013). The EOFs correspond to a statistically optimal description of the data with respect to how the variance is concentrated in the modes, where the variance explained decreases with the mode number (Larson et al., 1999). Therefore, since the explained variance typically decreases with the increasing mode number, most of the variance in the data is explained by only several modes. Thanks to this property, EOFs have been as a data reduction technique or a method to distinguish which is signal or noise. Statistically, it is known that the EOFs are optimal, yet no a priori reason is ensured for the eigen-functions to carry a physical meaning. Frequently, however, corroborating evidence can be used to provide a physical interpretation of the results (Miller and Dean, 2007).

Recently, EOFs have been widely used for describing morphological processes of coastal evolution. Firstly, this method has been most prevailingly applied to investi-gate change in characteristics of transversal profile (Aubrey, 1978; Dick and R.A.Dalrymple, 1984; Pruszak, 1993; Winant et al., 1975; Yuhi et al., 2007; Zarillo and J.T.Liu, 1988). Secondly, it can also be found in application to other types of problems: Losada et al. (1991), Larson et al. (1999) and Liang and J.Seymour (1991) applied this technique to analyse the alongshore variation of specific level contour lines; Medina et al. (1991) used the EOF method to study transversal transport of sediment; cross-shore distribution of sediment has also been studied by Larson et al. (1999), R.Medina et al. (1994) and R.Medina et al. (1992); both cross-shore and alongshore interactions have been analyzed by means of three modes EOF method (R.Medina et al., 1992). Larson et al. (1999) considered short and long term responses of beach fill. It is realized that EOFs has captured very well the morphological change in the coast. Besides, there have been a few researches on using EOFs to describe the morphological behaviors of rivers. Most typically, Hsu et al. (2006) proposed a two-dimensional empirical eigenfunction model to analyze and predict the variations of riverbed profile. Such a model is then applied to analyze the riverbed variations of the

downstream of Chou-Shui River in Taiwan. The results show that the proposed method can reasonably analyze and predict the riverbed variations. This initial work of Hsu et al. (2006) opened a potential application of EOF to morphological analysis of rivers at larger scale in time and space.

3.Regional setting and datasets

3.1.Characteristics of the Tedori River Basin
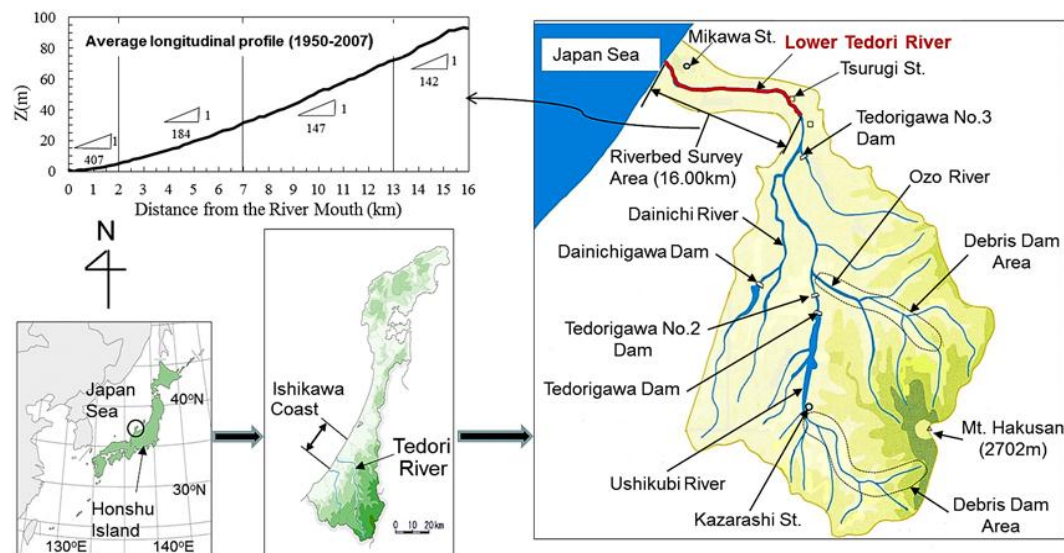
Figure 3.1. Tedori River Basin

The Tedori River, which originates at Mt. Hakusan, has catchment area of 809 km2 and channel length of 72 km (Fig. 3.1). The main tributary of the Tedori River is the Ushikubi River, with other tributaries being the Ozo River, the Danichi River and other small rivers. The Tedori River flows through the Tsurugi gauging station, on its westward journey through the Kaga Plain to the Japan Sea. The lower Tedori River referred to in the remainder of this paper (the reach downstream of the Tedorigawa Dam) is the portion of the river between the river mouth and 16 km upstream. The Tedori River is one of the steepest rivers in Japan, with average slopes of 1/27 and 1/145 for the entire river and the lower Tedori River, respectively. Based on homogeneity related to slope, width, and mean diameter of bed material, the lower Tedori River can be divided into four reaches located 0–2 km, 2–7 km, 7–13 km, and 13–16 km upstream of the river mouth (Teramoto et al, 2003) (Table 3.1).

The drainage area is underlain by various lithologies, including ancient Hida metamorphic rocks and volcanic rocks from eruptions of Mt. Hakusan. Nobi rhyolites (pyroclastic rock) from the Mesozoic to the Cenozoic era are distributed around the Mt. Hakusan area while Tedori Layers are present in the area east of the Tedorigawa Dam the and Ozo River. Both the Tedori Layers and Nobi rhyolites are prone to massive collapse. Therefore, a large amount of gravel and sand sized sediment has been flowing into the Tedori River.

Table 3.1.Characteristics of the four distinct reaches in the lower Tedori River (Teramoto et al, 2003)

Characteristics	Reach 1	Reach 2	Reach 3	Reach 4
Distance upstream of river mouth (km)	0.0–2.0	2.0–7.0	7.0–13.0	13.0–16.0
Channel width (m)	350	358	289	146
Channel slope	1/365	1/190	1/140	1/130
Mean diameter of bed material (mm)	67	77	166	187
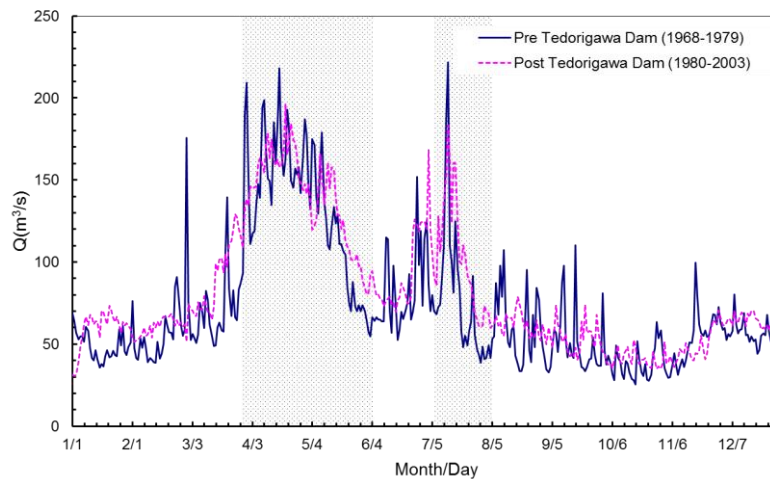
Figure 3.2. Temporal variation in daily averaged discharge in the lower Tedori River

The climate of the catchment area is dominated by the monsoon winds blowing in from the Japan Sea. The mean annual rainfall in the Tedori River catchment is about 2,600 mm/yr on the plains, and 3,300–3,600 mm/yr in the mountain ranges. In 1980, the Tedorigawa Dam (Fig. 3.1) was constructed, resulting in changes in the flow regime of the lower Tedori River. The highest average daily discharges in the lower Tedori River typically occur from mid-March to late May (due to snow melt) and

from mid-June to mid-July (owing to seasonal rainfall) both before and after the Tedorigawa Dam construction (Fig. 3.2).

3.2. Datasets

The present study focused on variations over the lower Tedori River during 1950–2007. The 58-year span of the data surveyed with high resolution provided good data coverage in time and space to capture the main trends of long-term variation in the river morphology and its controlling factors. The following datasets were used in this study, that were provided by the Hokuriku Regional Development Bureau of the Ministry of Land, Infrastructure, and Transport of Japan (hereafter referred to as HRDB).

- Sand and gravel volumes mined from the river channel from 1951 to 1991 based on annual permissions by local government
- Annual volume of dredged material in maintenance activities from 1949 to 1963
- Annual sediment deposition in sabo dams from 1936 to 1983 with some missing years
- Annually maximum river discharge (Q_{max}) from 1928 to 2006 measured at the Tsurugi station, located 14 km from the river mouth (Fig. 3.1)
- Thirty-six annual surveys of the riverbed topography (1950–1979, 1991, 1997, 1998, 2002, 2003 and 2007) consisting of 81 river cross-sections at intervals of 200 m along the 0–16-km reach
- Sequential aerial photographs at scales of 1:15,000 for the years 1947, 1955, 1968, 1984, 1995, and 2000

4.Methods of analysis

4.1.Mean bed level at cross-sections

The mean riverbed level of each cross-section was averaged over the cross-sectional extent located below high water level (HWL). Here, HWL in river channel was computed by using a hydraulic model (RIC-Nays) developed by the International River Interface Cooperative (iRIC)(Jang and Shimizu, 2005). The model was calibrated against the Manning roughness coefficient using the high-water marks measured for the flood of the Tedori River at 1441 m^3/s on July 13, 2002. The model validation was carried out for another large flood at 2852 m^3/s on September 22, 1998 by using the calibrated coefficients. The results show that the calculated and observed water surfaces were qualitatively in good agreement.

Subsequently, an annual longitudinal profile was established from the mean riverbed levels. Note that the bed elevation was described herein relative to the Tokyo Peil (T.P.) datum, which is the standard ground elevation in Japan based on the mean sea level of Tokyo Bay.

4.2.Vertical adjustment

Initially, a comparative analysis of existing surveyed data was conducted to quantify the dominant variation trends in time and space. On the basis of the presence or absence of different human activities, the entire period was divided into three sub periods: (I) 1950–1979, (II) 1980–1990, and (III) 1991–2007.

To quantify the yearly variation in riverbed, the rate of vertical adjustment (K, m/yr; $K > 0$ for deposition, $K < 0$ for erosion) at each cross-section of the lower Tedori River was computed. Over all cross-sections of the Tedori River, nonlinearly temporal variation in the riverbed elevation at each cross-section has undergone five different phases (Fig. 4.1). The sub period of 1950-1979 (I) includes first three phases I-A, I-B and I-C. Given the paucity of data, the sub period of 1980–1991(II), corresponding to phase II, was not considered. The remaining sub period of 1991-2007(III) corresponded to the phase III. Note that the transitional years between two successive phases were addressed based on the criteria that high goodness of a fitting function with the riverbed was simultaneously attained in both phases. Accordingly, the transitional years between phase I-A and I-B varied from 1958 to 1962 and between

phase I-B and I-C from 1968 to 1973. Both exponential and power functions were tested to fit the riverbed of the various phases. The exponential function was chosen to describe the temporal trend of the riverbed of the lower Tedori River because it yielded the better fit than the power function. Subsequently, *K* was calculated for each phase at each cross–section, as follows.
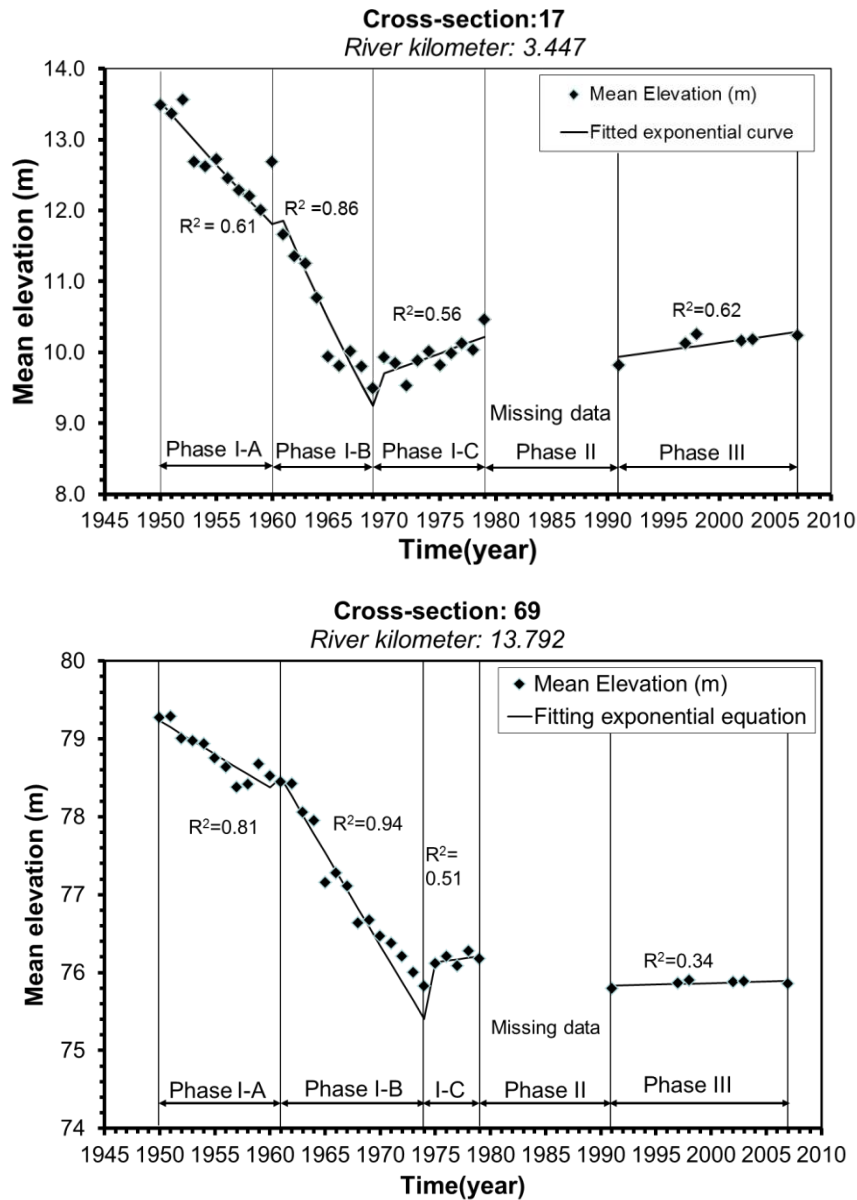
Figure 4.1. Fitting exponential equations to temporal vertical adjustment at the 17 th and 69 th cross –section

The temporal adjustment of the river bed at a cross- section was described well by the exponential functions:

$$Z(t)-(Z_{min}-c)=ae^{bt} \tag{4-1}$$

19

where $Z(t)$= elevation of the riverbed; a= coefficient determined by regression analysis, representing the riverbed elevation at the initial year to=0; Z_{min} is the lowest riverbed elevation during a given period for each cross-section, in meter above sea level; b= coefficient determined by regression analysis, expressing the rate of nonlinear change in the riverbed per year: $b>0$ for degradation, $b<0$ for aggradation; c is coefficient ensuring that the left hand side in Eq (5.1) is always positive, $c=1$m was used for this study; t= the time since the year the onset of adjustment process.

To eliminate effect of the cross section position on coefficient b, the riverbed elevation was extracted by $(Z_{min}-c)$ before being fitted by the exponential function. Rate of vertical adjustment ($k(t)$) at the t-th year was defined as follow:

$$k(t) = \frac{dZ}{dt} = -abe^{bt}$$

The average rate of vertical adjustment (K) over the period t_o-t was calculated as follow:

$$K = \frac{1}{(t-t_0)}\int_{t_0}^{t} k(t)dt = \frac{1}{(t-t_0)}\int_{t_0}^{t}\frac{dZ}{dt}dt = \frac{1}{(t-t_0)}Z\Big|_{t_0}^{t} = \frac{a(e^{bt}-e^{bt_0})}{t-t_0}$$

4.3. Horizontal variation

To investigate the temporal change of the riverbed along the cross-sectional direction, we compared the cross-sections surveyed in 1950, 1979, and 2007. The comparison was carried out for 16 cross-sections at intervals of 1 km.

To evaluate the effect of sediment extraction on the sediment grain size of the Tedori River, the sediment mean diameter (d_m) of the in-river sediment from 1963 to 1993 was investigated on the basis of an unpublished internal report of HRDB.

To investigate the variation trends in vegetation cover in the lower Tedori River, the aerial photographs were digitally scanned at resolution of 600 dpi. The area of vegetation cover was then measured for each aerial photograph using CAD software.

To investigate the relation between horizontal and vertical adjustment of the river channel, the temporal change in channel width was examined. Channel width at each cross-section was defined based on the width of the water surface, which was calculated by using the RIC-Nay model for channel-forming discharge of 1775 m^3/s.

4.4. Sediment volume of river bed

At each cross section, the sediment volume of the riverbed was calculated for the cross-sectional extent between two benchmarks located immovably on the left and right riverbanks (hereafter mentioned as *L*). In the original survey, the number and location of the survey points varied yearly; we thus divided *L* of each cross-section into 51 fixed points that were spaced uniformly. The riverbed elevations at these fixed points were calculated through linear interpolation. Finally, the sediment volume of the riverbed was calculated on the basis of the riverbed level at fixed locations.

4.5. Sediment budget

Analysis of the variation in the sediment budget of a river reach is an effective way to quantify the contribution of natural and human-induced effects to changes in the riverbed (Kondolf, 1994; Martín-Vide et al., 2010; Rovira et al., 2005). It is therefore essential to establish an equation for the bed sediment balance of the lower Tedori River (0–16 km) to clarify how different components have affected the riverbed sediment volume. This equation indicates that difference between incoming and outgoing sand and gravel equals the variation in the riverbed sediment volume within the study reach.

$$\underbrace{(V_{RSV}^{n} - V_{RSV}^{1950})}_{1} = -\underbrace{\sum_{i=1950}^{n} V_{DA}^{i}}_{2} - \underbrace{\sum_{i=1950}^{n} V_{SGM}^{i}}_{3} + \underbrace{(\sum_{i=1950}^{n} V_{in}^{i} - \sum_{i=1950}^{n} V_{out}^{i})}_{4} , \qquad \text{(4-2)}$$

where *i* is the index of the year; V_{in}^{i} and V_{out}^{i} are bed material transport rate over the *i*-th year, calculated at the cross-sections located at the upstream and downstream ends of the study area; V_{DA}^{i} is the volume of sediment extracted from the river by DA in the *i*-th year; V_{SGM}^{i} is the SGM volume mined from the river in the i-th year; V_{RSV}^{n} is the sediment volume of the river bed in the *n*-th year; V_{RSV}^{1950} is the sediment volume of the river bed at 1950.

4.6. Sand and gravel transport rate

To calculate the sand and gravel transport rate along a segment, an equation of material balance was established, as follows.

21

$$Q_{out}^i = Q_{in}^i - (1-\rho)(\Delta V_{RSV}^i + V_{DA}^i) - \beta V_{SGM}^i$$

<div align="right">(4-3)</div>

where i is the index of the segment; Q_{in}^i and Q_{out}^i bed material transport rate over the i-th segment, calculated at the cross-sections located at the upstream and downstream ends of the segment; V_{DA}^i is volume of sediment extracted from the river by DA in the ith segment; V_{SGM}^i is official SGM volume mined from the river in the i th segment; ΔV_{RSV}^i is volume variation of the river bed sediment in the ith segment; ρ is the porosity of the bed, $\rho = 0.25$; β is a coefficient accounting for various factors such as the porosity of the bed and the ratio of real to official SGM.

4.7. EOF analysis

Furthermore Empirical Orthogonal Function (EOF) analysis (Hsu et al., 2006; Winant et al., 1975) was conducted in order to highlight the long-term characteristics of channel variation and the effect of anthropogenic activities over the periods 1950–1979 and 1991-2007. In this study, the non-demeaned riverbed level Z_{ki} (averaged over each cross-section) was explained by the summation of eigenmodes:

$$Z_{ki} = \sum_{n=1}^{N} C_{nk} e_{ni}$$

for the i-th profile position and k-th survey,

The deviation of the riverbed level between k-th and q-th surveys for the i-th profile position is explained by the summation of eigenmodes as below.

$$\Delta Z_{kq} = \underbrace{(C_{1k} - C_{1q})e_{1i}}_{first\,mode\,component} + \underbrace{(C_{2k} - C_{2q})e_{2i}}_{second\,mode\,component} + \underbrace{(C_{3k} - C_{3q})e_{3i}}_{third\,mode\,component} + \underbrace{(C_{4k} - C_{4q})e_{4i}}_{fourth\,mode\,component} + ...$$

<div align="right">, (4-4)</div>

where e_{ni} are the normalized spatial functions, C_{nk} are the temporal functions. The subscript n indicates the variation mode. The subscript i changes from 1 to I, the total number of points along the longitudinal profile of the riverbed. The subscript k changes from 1 to K (K = 30, 17 for the period 1950-1979 and 1991-2007, respectively), the total number of times that profiles were recorded. The spatial functions that best fit the data in the least-squares sense were derived from the following equation:

$$Ae_n = \lambda_n e_n,$$

where A is a symmetric correlation matrix and λ_n is a corresponding eigenvalue of the matrix A. Using orthogonality, we have

$$C_{mk} = \sum_{i=1}^{I} Z_{ik} e_{mi}.$$

The first eigenfunction with the largest eigenvalue explains most of the riverbed variation. The variance explained decreases with the mode number, and each successively higher eigenfunction explains the variation unexplained by the preceding eigenfunctions (Wijnberg and Wolf, 1994).

5.Results and Discussion

5.1.Anthropogenic activities in the Tedori River Basin

During the 20th century, the channel features were strongly affected by a variety of anthropogenic activities (Fig. 5.1).

5.1.1. Sand and Gravel Mining

In the post-World War II period, sand and gravel were mined in the area from the river mouth to 15 km upstream. During the mid-1960s, SGM was conducted at its highest rate (Fig. 5.2), causing substantial degradation of the riverbed. To deal with this problem, a law was passed to prevent the overmining of sand and gravel in the mid-1970s. The mining was then completely prohibited in 1991. The total amount of sand and gravel extracted was 7.6×10^6 m^3 computed on the basis of licenses issued by local authorities over the period 1962–1991. Additionally, maintenance dredging of the river channel was conducted from 1949 to 1963 in the area from the river mouth to 15 km upstream, mainly to 4.9 km upstream. The total volume of dredged sediment was 2.1×10^6 m^3.
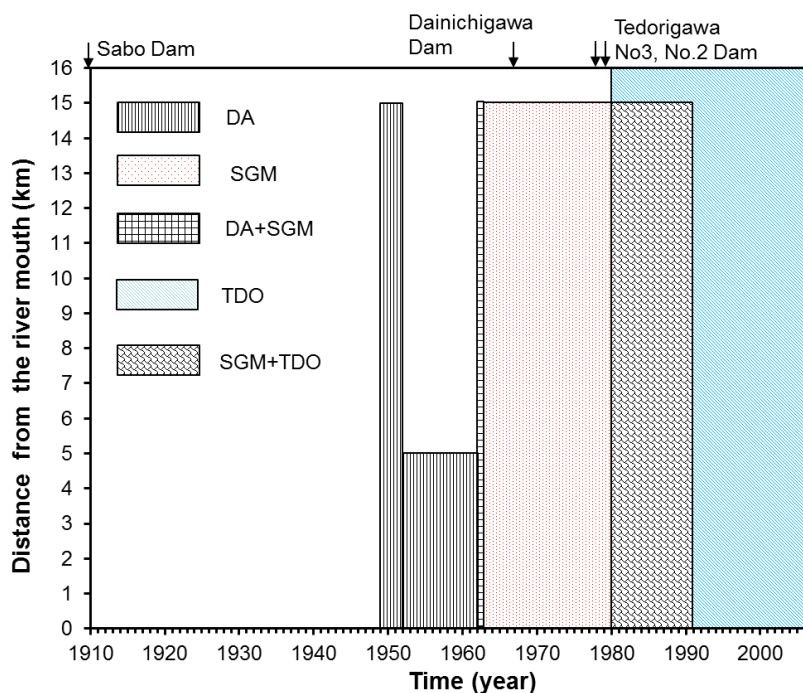
Figure 5.1. Temporal and spatial ranges of anthropogenic effects on the Tedori River (DA: Dredging activities; SGM: Sand and gravel mining; TDO: Tedorigawa Dam operation).
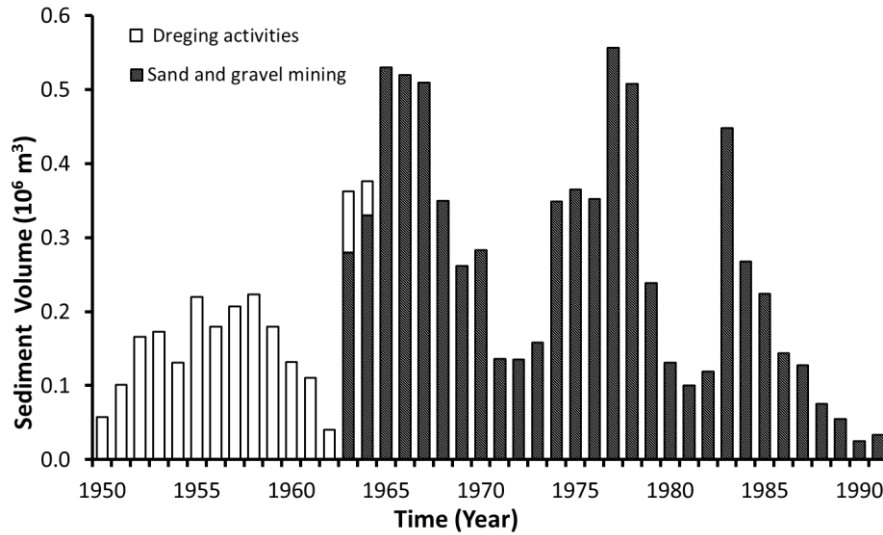
Figure 5.2. Volume of sand and gravel mining extracted from the Tedori River according to the license issued by the local government. It is considered that the values shown in this figure could significantly underestimate the real volumes.

5.1.2. Dam construction

A number of dams with different purposes have been constructed within the river basin (Fig. 3.1). Notably, Tedorigawa Dam operation (TDO) from 1980 has played a most important role in altering the flow regime and sediment transporting capacity. TDO has reduced the magnitude and frequency of large floods (Table 5.1). The flood discharge with a return period of 5 years in the post-dam period (1799 m^3/s) was 24% less than that in the pre-dam period (2357 m^3/s). The coefficient of the river regime, defined as the ratio of the annual maximum discharge to the annual minimum discharge, was 2279 and 190 for the pre-dam and post-dam period, respectively. The annual flow volumes for the pre- and post- dam periods were 2305.9 $\times$ 10^6 m^3 and 2547.4 $\times$ 10^6 m^3, respectively. These imply that TDO regulated the flow in the short term (i.e., flood events) rather than the middle-term (i.e., monthly or annual flows).

25

Table **5.1.** Flow characteristics of the Tedori River before and after Tedorigawa Dam construction (*RI is recurrence interval*)

Flow characteristics	Unit	PreDam (1968-1979)	PostDam (1980-2003)
Annual flow volume	$10^6 m^3$	2306	2547
Coefficient of the river regime		2279	190
Q(RI=5)	m3/s	2357	1799
$Q_{average}$	m3/s	1737.0	1159.0
Ω	kN/s	83.0	62.0
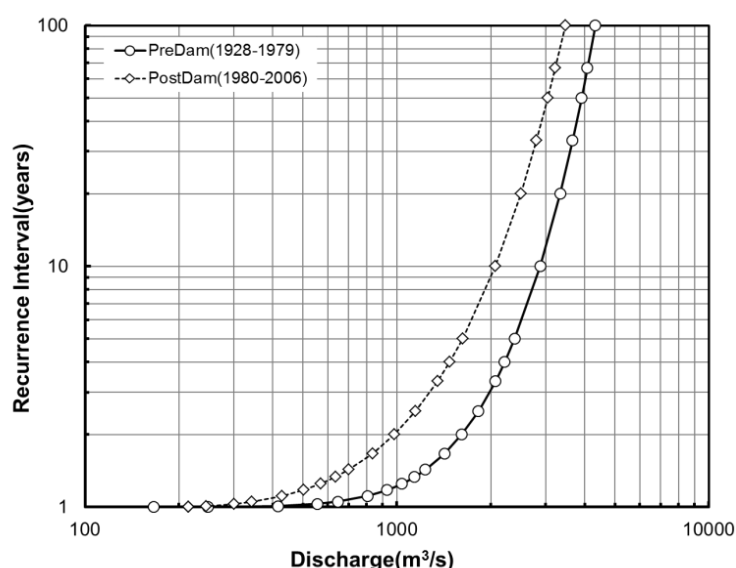
Figure 5.3. Flood-frequency curves derived from annual maximum flows at Tsurugi station for pre-and post-1980 periods.

In addition, the Tedorigawa Dam has trapped all the bed load and some of the suspended sediment originating from one of the main tributaries (the Ushikubi River). The accumulative sediment retained by the Tedorigawa Dam amounted to 8.2×10^6 m^3 by 2005.

Owing to flood control operations, the magnitude and frequency of flooding were less in the post-dam period than in the pre-dam period; the average flood peaks for the pre-dam and post dam periods were 1737 and 1159 m^3/s, respectively. In addition, expected probable flood discharges were calculated using annual maximum discharges observed at the Tsurugi station. Probable flood discharges were computed employing the Gumbel method. The results indicate that the 5-, 10-, and 100-year

26

probable floods were forecast to decrease by 24%, 19% and 12%, respectively (Fig. 5.3). Furthermore, the total stream power per unit channel length $\gamma.Q.s$ (Simon and Rinaldi, 2006) (where γ is the specific weight of water (N/m^3), Q is the flood discharge (m^3/s), and s is the energy slope (m/m), which may be approximated by the slope of the channel bed) was investigated for both pre- and post-Tedorigawa dam periods. The results show that the mean total stream power per unit channel length for the pre-dam period was 83.0 kN/s. This magnitude reduced by 25% to 62.2 kN/s for the post-dam period.

5.1.3. Representative floods

Naturally, morphological processes of rivers mainly occur in flood events. Channel-formed discharges have an average return interval in excess of 1.5 to 2 years, approximately corresponding to mean discharges. Figure 5.4 indicates that during 1950s there were two flood events exceeding the change-formed discharges of 1737 m^3/s. The same number of effective floods were also observed in 1960s. In the 1970s, channel-formed floods were more frequently present with 6 ones. After Tedorigawa dam constructions, a decreased number of effective discharges were witnessed: one in the period of 1980-1991 and three in the period of 1991-2007.
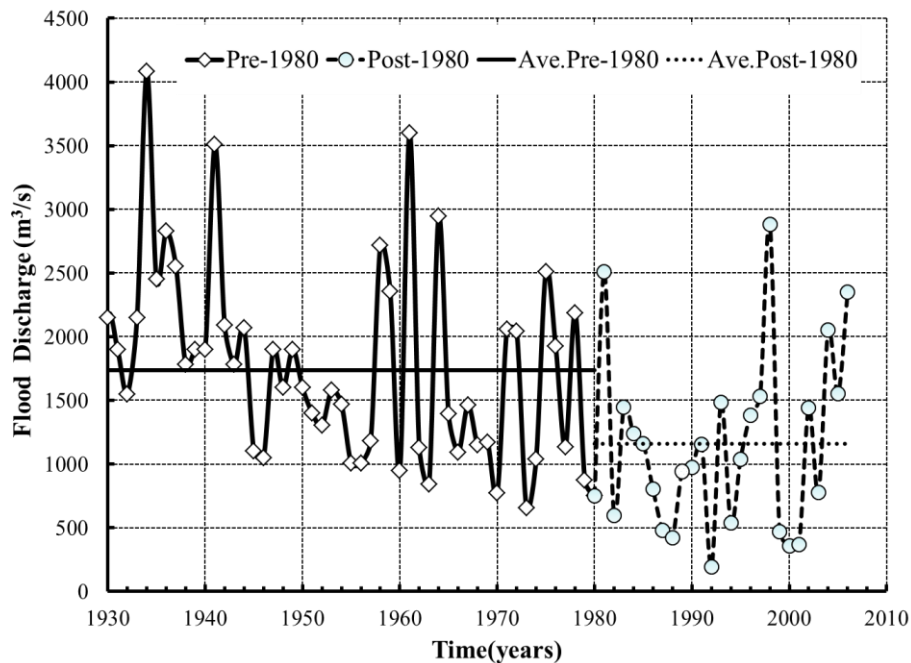
Figure 5.4. Temporal variation in flood discharge at the Tsurugi gauging station before and after Tedorigawa dam construction.

5.2. General features of riverbed response

5.2.1. Riverbed response dominated by natural factors before 1950

Depending on the type and rate of natural or anthropogenic effects on the Tedori River system, the lower Tedori River has experienced different types of changes in riverbed features in time and space. Nunomoto et al. (1980) estimated that the riverbed sediment volume decreased approximately 2.5×10^6 m^3 during 1934–1943. In contrast, from 1943 to 1950, the riverbed experienced deposition, especially near the river mouth (Table 5.2); as shown in Fig. 5.5a, the bathymetric contour lines shifted downstream. It is considered that in the former period, riverbed sediment was transported to the neighboring coast owing to a series of flood events exceeding 2500 m^3/s (occurring in 1934–1937 and 1941–1942). This reduced the riverbed sediment volume. During the later period, there was no such large flood event except for the flood event of 2040 m^3/s in 1944, which decreased the sediment transporting capacity of the flow and consequently resulted in the deposition of bed-material sediment delivered from upstream areas. Although many sabo dams have been built since 1910, the variation in the riverbed has still been closely related to the occurrence of flood events. It can thus be considered that natural factors (represented by large flood events) dominated the variation in the riverbed prior to 1950.

28
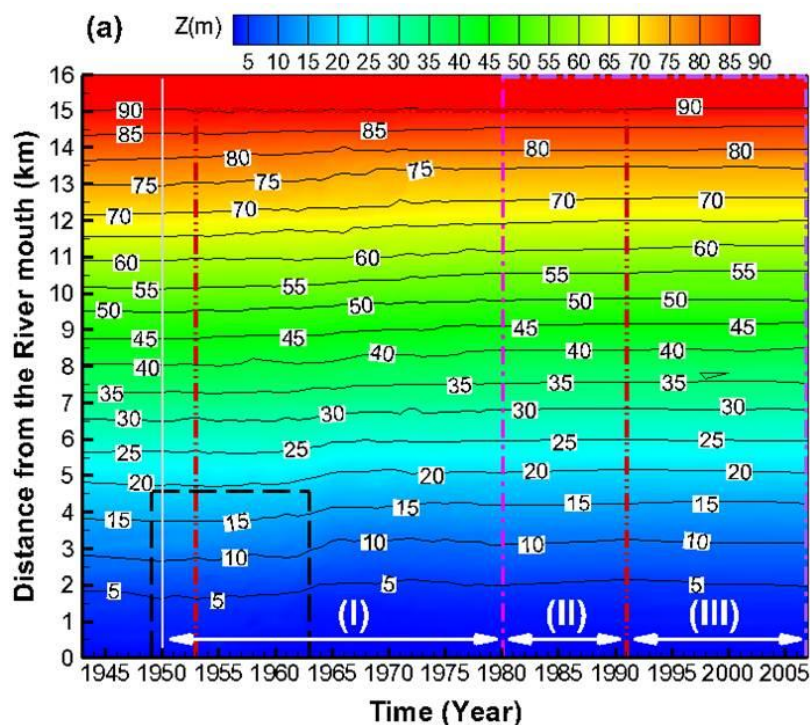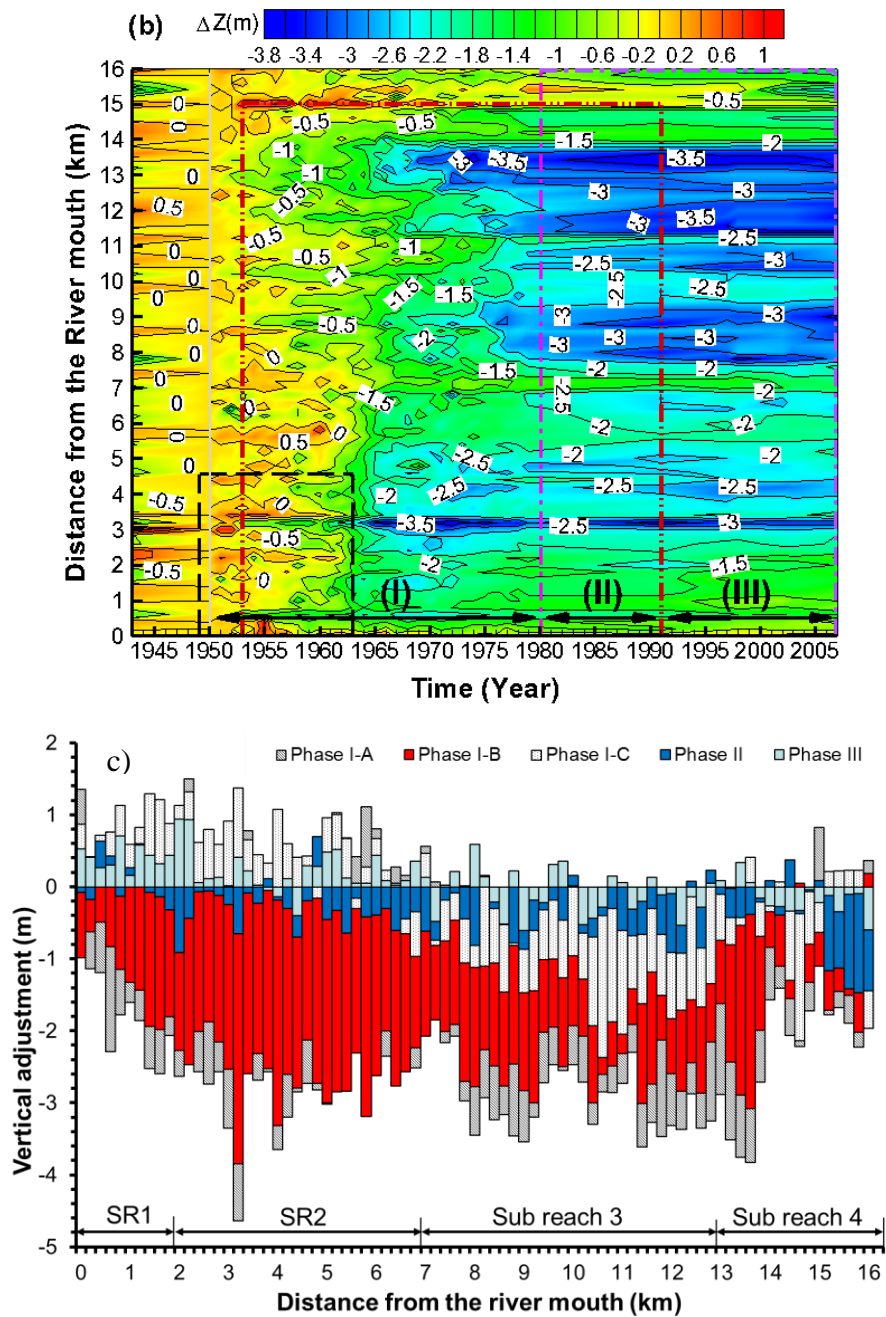
Figure 5.5. Temporal and spatial variations of the riverbed elevation of the Tedori River

(a) Mean riverbed elevation: The long-dash line shows the temporal and spatial ranges of DA; the dash–dot–dot line shows the temporal and spatial ranges of SGM; the dash–dot line shows the temporal and spatial ranges of the TDO effect. b) Vertical adjustment of the riverbed elevation from the river bed elevation in 1950. c) Vertical adjustment of the riverbed elevation in different phases.

5.2.2. Riverbed response dominated by human interventions after 1950

Since 1950, human interventions have become the dominant controlling variables of riverbed alteration. Originating from DA in the downstream area, erosion tended to

29

migrate upstream along the reach of 0–15 km from 1963 to 1979 (Fig. 5.5a). To analyze the variation in the riverbed elevation, the yearly deviation of longitudinal profiles with respect to the longitudinal profile of 1950 was examined (Fig. 5.5b). The change in the riverbed elevation of the different phases was also addressed in Fig. 5.5c. The result indicates that the eroding depth was in excess of 0.30–3.50 m over the period 1950–2007.

(I) Sub period I: 1950-1979

Owing to the combined effects of DA and intensive SGM, the erosion in the sub period I was highest with an average eroding depth of 1.98 m (Table 5.2). The spatial variation in the eroding depth from 1950 to 1979 indicates that the eroding depth of the reach of 2–13 km was significantly higher than that of the remaining areas. Temporal and spatial distributions of K are shown in Fig. 5.6a. Considering the phase I-A, high degradation with two highest peaks of 0.17 m/yr was observed from 0 to 5.4 km, where DA and possibly SGM were carried out, and almost all of the 6.6–14.5 km sub reach, where SGM was conducted. Minor deposition was observed at 5.4–6.6 km and 15 km upstream from the river mouth.

In phase I-B, the riverbed experienced considerable degradation as an instant and direct result of the most intensive SGM. The average eroding rates of sub reach 2 was 0.22 m/yr which is double as much as the K value in other sub reaches (Table 5.3). Additionally, the magnitude of K gradually increased to its highest value of 0.33 m/yr at 3.2 km, after which it decreased steadily until the upstream end of sub reach 2. The variation trend of K fluctuated in sub reach 3, attaining the second highest magnitude before diminishing considerably until the upstream end of sub reach 4.

In the phase I-C, the aggradation was evident in the sub reach 0–4.5 km upstream from the river mouth, with an aggradational rate of 0.05 m/yr. This can be attributed to natural recovery of the sediment transported from the upstream as a result of the restriction of SGM in the mid-1970s. That morphologic behavior of the Tedori River is similar to that of the Brenta River in Italy (Surian et al., 2007) and that of the Obion River in USA (Simon et al., 1989). However, there was a difference in the sediment source inducing the deposition in the downstream area: owing to the work in early era, no bank failure observed in the Tedori River. The sediment source in the Tedori River originated from the upstream riverbed and possibly tributaries while in the other

rivers the sediment came from the bank failure/channel-widening. In phase I-C, strong erosion was also observed in other areas, with a mean magnitude of 0.07 m/yr.

The temporal and spatial variation in the rate of the nonlinear vertical adjustment (b) was shown in Fig 5.6b. Although the magnitude of b is different from that of K, yet there is similarity in variation trend between b and K. Although b carries a mathematic meaning, K is more representative for description of a physical process.

(II) Sub period II: 1979-1991

SGM coupled with TDO caused the riverbed degradation in almost all of the study area. The riverbed slightly degraded with 0.03 m in the sub reach 1 while the eroding depths of the remaining sub reaches varied from 0.25 m to 0.30 m (Table 5.2). Even the sub-reach of 0-4.5 km where the aggradation was observed in the phase I-C also turned into degradation in this sub-period. However, compared with the previous sub period, there was a decrease in the rate of the degradation. The eroding rate was in excess of 0.02-0.03 m/yr.

(III) Sub period III: 1991-2007

In the last sub period, the riverbed was erosional in upstream sub reaches 3 and 4 and became depositional in downstream sub reaches 1 and 2. In this period, TDO trapped all the upstream bed material from the Ushikubi River transported to the lower Tedori River. This induced selected erosion of the fine-sized bed material (Dietrich et al., 1989) in sub reaches 3 and 4. Subsequently, sediment-starved flow, which was released from Tedorigawa Dam, carried that amount of erosion-induced sediment downstream (Kondolf, 1997) and deposited it in sub reaches 1 and 2. This effect of TDO could also have occurred at the same rate in the previous period, yet it was difficult to separate the effect from the impact of SGM.

In contrast to the variation trend of K in the first three phases, that for the phase III-D was minor. That is, a slight accretion trend was observed in the first two sub-reaches with rates of 0.03 and 0.01 m/yr, respectively (Table 5.3) while sub reach 4 underwent slight erosion at 0.01 m/yr. Simultaneously, local erosion and deposition was clearly documented in the sub reach 3. This could be due to the presence of vegetation in the riverbed which was considered as an indirect effect of Tedorigawa Dam operation. Accordingly, the deposition occurred at upstream of the vegetated area and the erosion at downstream (Tsujimoto, 1999).

In conclusion, the SGM most significantly affected the change in the riverbed during the entire study period. Accordingly, the adjustments of the riverbed simultaneously occurred along the lower Tedori River as a result of direct and/or indirect impact of mining. Depending on the magnitude and extent of SGM, the riverbed degraded moderately in phase I-A and rapidly in phase I-B; in phase I-C, the aggradation was observed in the downstream area while the riverbed remained degraded in the upstream area. Light variation in the riverbed in phase III indicates that the Tedori River was gradually re-gaining its equilibrium condition after the cease of SGM in 1991.

Table 5.2. Temporal variation in reach-averaged vertical adjustment

Distance[1] (km)	Bed level change (m)				
	1943-1950	1950-1979	1980-1990	1991-2007	1950-2007
0-2 (sub reach 1)	0.21	-1.27	-0.03	0.42	-0.87
2-7 (sub reach 2)	0.18	-2.01	-0.30	0.21	-2.10
7-13 (sub reach 3)	0.05	-2.46	-0.29	-0.09	-2.84
13-16 (sub reach 4)	0.08	-1.45	-0.25	-0.14	-2.04
0-16 (entire reach)	0.12	-1.98	-0.25	0.06	-2.21

[1]*Distances are measured from the river mouth*

Table 5.3. Mean value of the rate of vertical adjustment in different phases

Distance[1] (km)	K(m/year)			
	Phase I-A	Phase I-B	Phase I-C	Phase III
0-2 (sub reach 1)	-0.06	-0.11	0.05	0.03
2-7 (sub reach 2)	-0.03	-0.22	0.02	0.01
7-13 (sub reach 3)	-0.06	-0.14	-0.10	0.00
13-16 (sub reach 4)	-0.05	-0.09	-0.02	-0.01

[1]*Distances are measured from the river mouth*
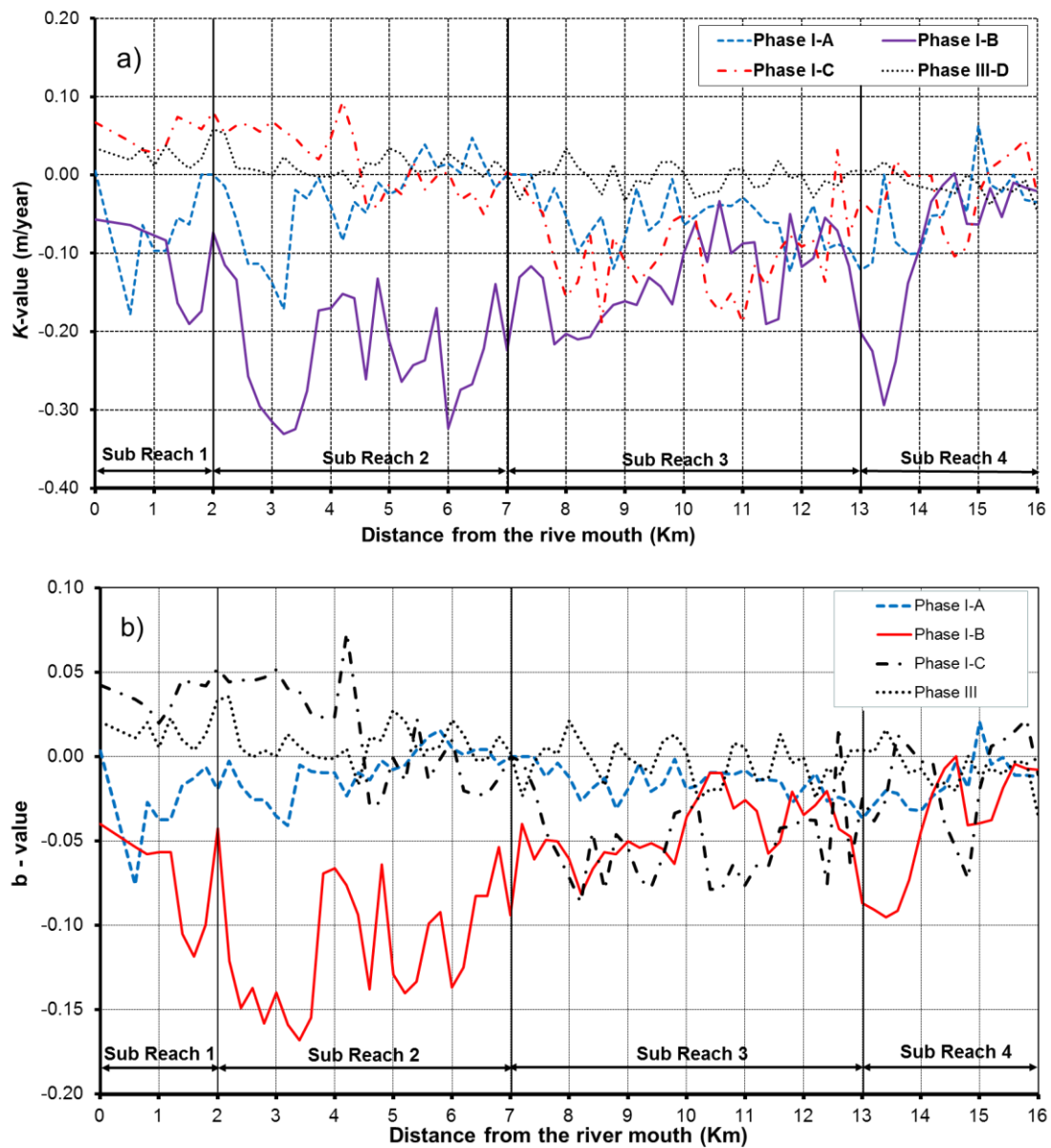
Figure 5.6. Temporal and spatial variations in the rate of vertical adjustment.

As a consequence of the direct effects of human activities or of change in other controlling factors, the slope of Tedori River (*S*) varied temporally and spatially at different rates during the period 1950–2007 (Fig. 5.7). It was found that variation in channel slope in sub reaches 1 and 4 was more significant than that in the other sub reaches. Simultaneously, the slope of the four sub reaches considerably varied from 1950 to 1991, and subsequently remained stable until 2007. Over the period 1950–1970, *S* for sub reach 1 decreased by 30% while there was a slight variation in *S* in sub reaches 2 and 3. Possibly, SGM lowered the riverbed at the upstream and downstream ends of sub reach 3 by the same magnitude and consequently *S* remained at a nearly constant level. In contrast, in sub reach 1, SGM lowered the upstream end

33

more than the downstream end. Additionally, SGM in the upstream sub reaches decreased the sediment load supplied to sub reach 1. These actions decreased S in sub reach 1 to establish the new equilibrium condition. This behavior of the riverbed is similar to the finding of Lane (1955). From 1950 to 1972, *S* of sub reach 4 increased by 15% because there was SGM downstream but not upstream. Subsequently, the opposite trend was observed in sub reach 4 as a result of legal enforcement preventing the over-mining of sand and gravel in the mid-1970s. A change in *S*, therefore, could be considered as a response of the Tedori River to anthropogenic activities, especially SGM.
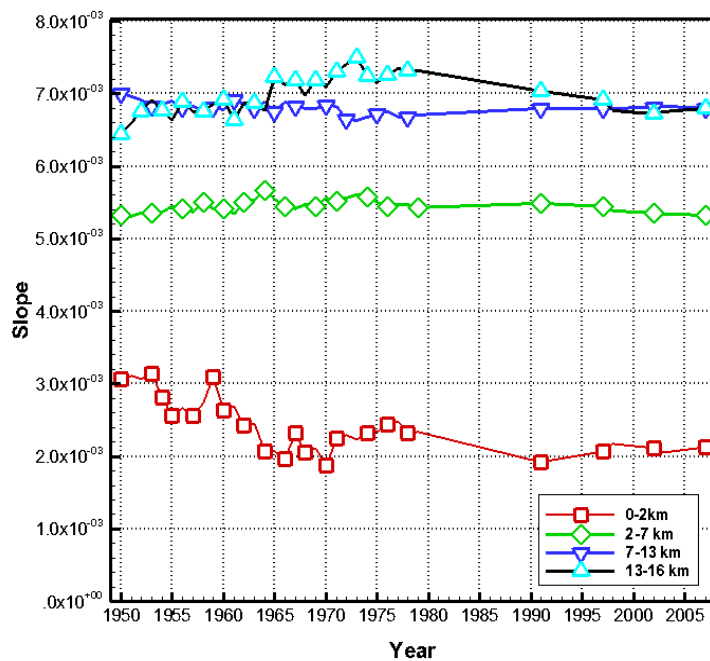
Figure 5.7. Spatial and temporal variations in slope

5.2.3. Horizontal variation

Here, four representative cross-sections located at the middle of each sub reach are shown (Fig. 5.8). The first notable point is that there was only degradation throughout the entire extent of a cross-section in the period 1950–1979 (Fig. 5.8, Fig. 5.9) while both degradation and aggradation simultaneously took place in different parts of a given cross-section over the period 1979-1991. The synchronous degradation in the former period could be due to SGM which was conducted in the whole extent. A reason for the latter period is that the total absence of SGM from 1991 together with the irregularity of the flow velocity field which could induce the transversal nonuni-

34

formity of erosion and deposition, meaning that either scouring or settling of sediment particles prevails in different parts of a given cross-section of a river channel (Alekseevskiy et al., 2008). In reality, a change in structure of the flow velocity field along cross-sectional direction is attributed to several factors such as seasonal variation in flow discharge and sediment supply, the presence and destruction of turbulent eddy currents. This process led to developing bars and islands in the river channel.

We can realize that the artificial dykes have disrupted the connection between the river channel and its floodplain and no bank failure was observed from 1950 to 2007. In this case, the bank of the dykes played a role as the protection of the river channel. The bank protection of the dykes implemented earlier was considered to be effective as a countermeasure to the instability of riverbank due to erosion in river channel. The early presence of the dykes with embankment disrupting the connection between the river channel and its floodplain makes the adjustment of the lower Tedori River different from that of other disturbed rivers in USA and Europe. The embankment has confined the river channel, resulting in no widening due to bank failure in the lower Tedori River during the period 1950-2007. Early presence of bank protection along the lower Tedori River may trigger the erosion in the riverbed. Overall, not significantly horizontal but vertical adjustment in cross-sections of the lower Tedori River was observed from 1950 to 2007.

The river configuration changed from braided in 1955 into transitional patterns in 1968 (Fig. 5.10). More specifically, aerial photograph of the study area in 1968 (not present here) indicates that the river pattern turned into single thread in the significantly erosional areas of 3-4 km and 11-14 km while it remained braided in the other erosional areas. Subsequently, the river pattern became braided in 2000 (e.g. as seen in aerial photograph in the year of 2000 (Fig. 5.10). The temporal variation in the river configuration reveals that the braided pattern could co-exist with the degradation of the riverbed.
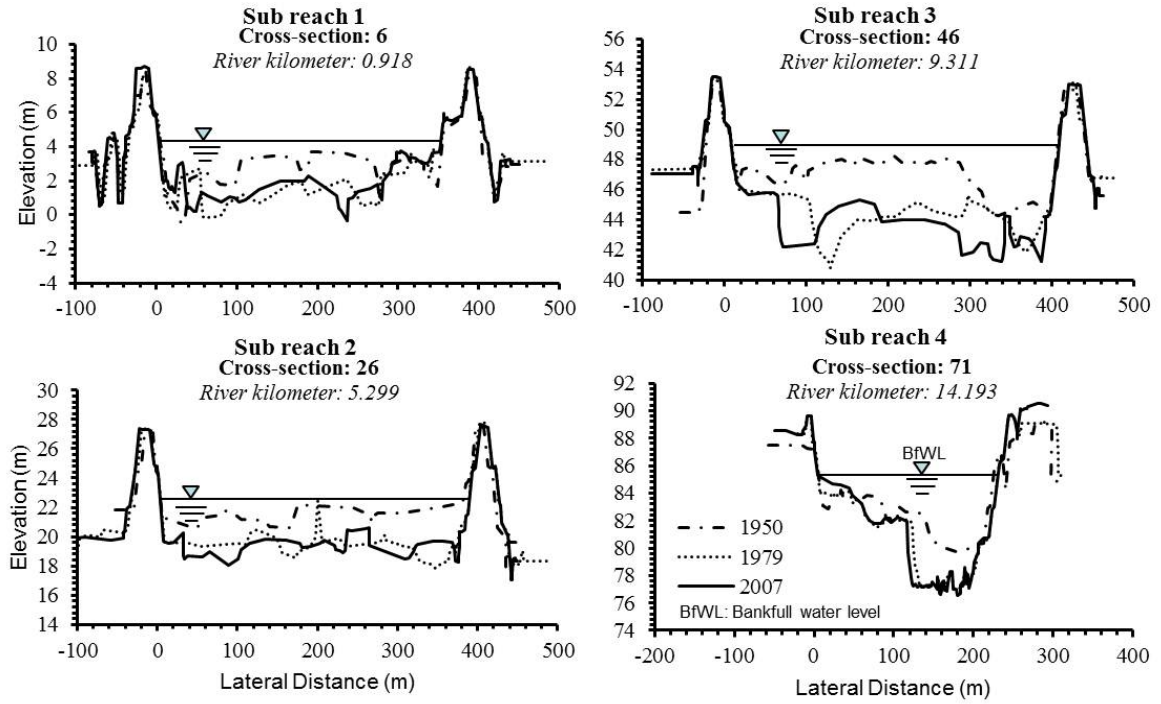
Figure 5.8. Superimposed cross-sectional profiles of the Tedori River at four sites for the years 1950, 1979, and 2007.
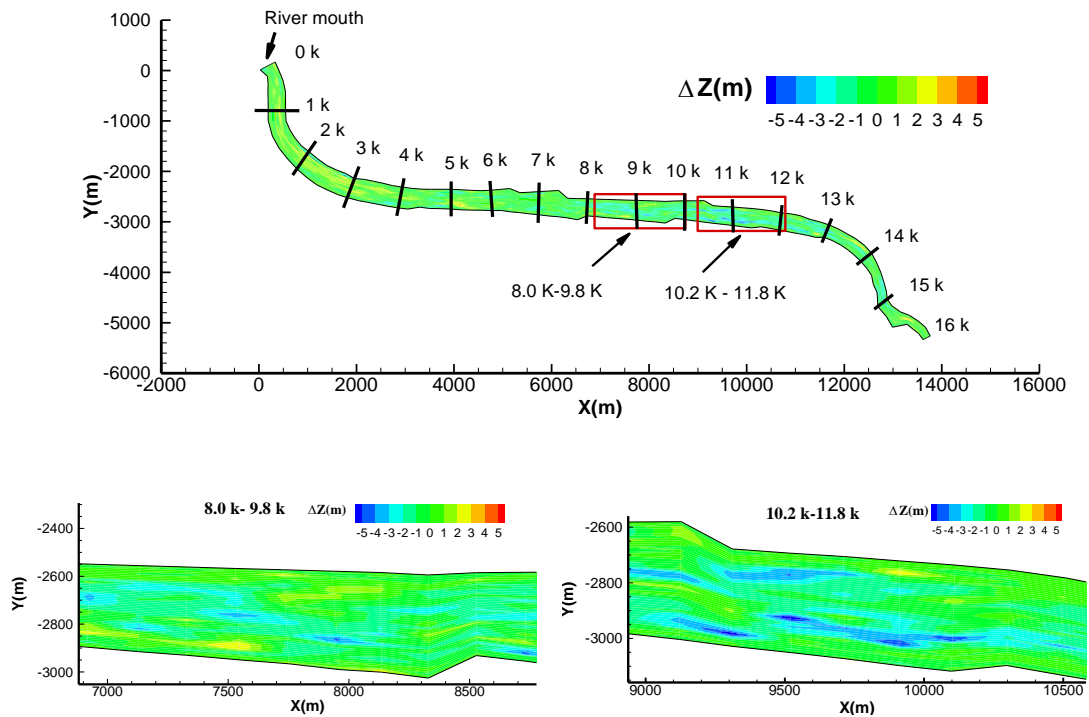
Figure 5.9. Variation in riverbed level (1950–1979)
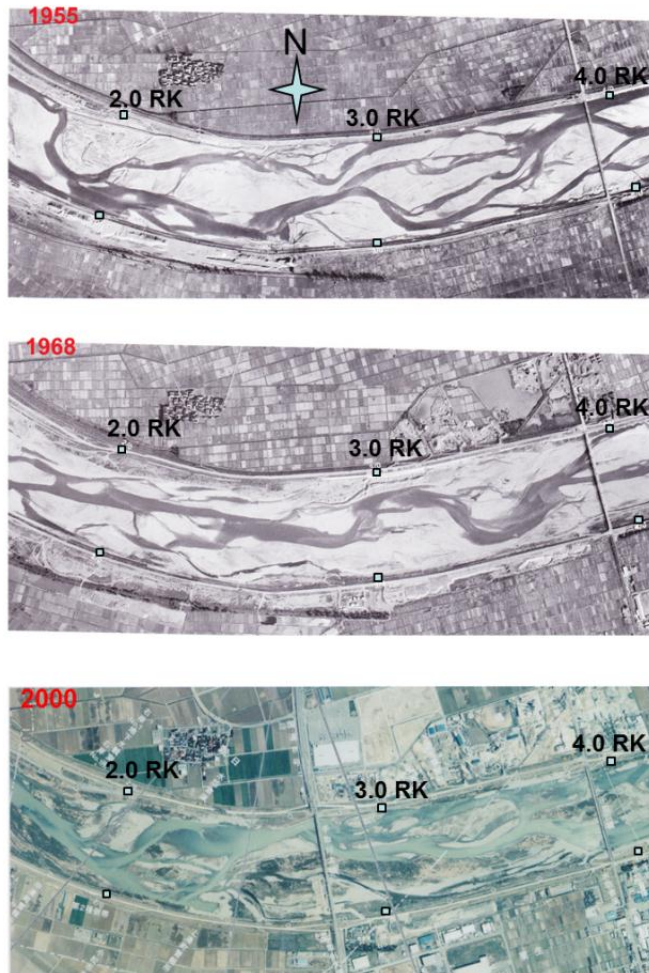
Figure 5.10. Comparison of aerial photographs of the 2-4 km sub reach over three different dates (RK, river kilometer, represents the distance from the Tedori river mouth).
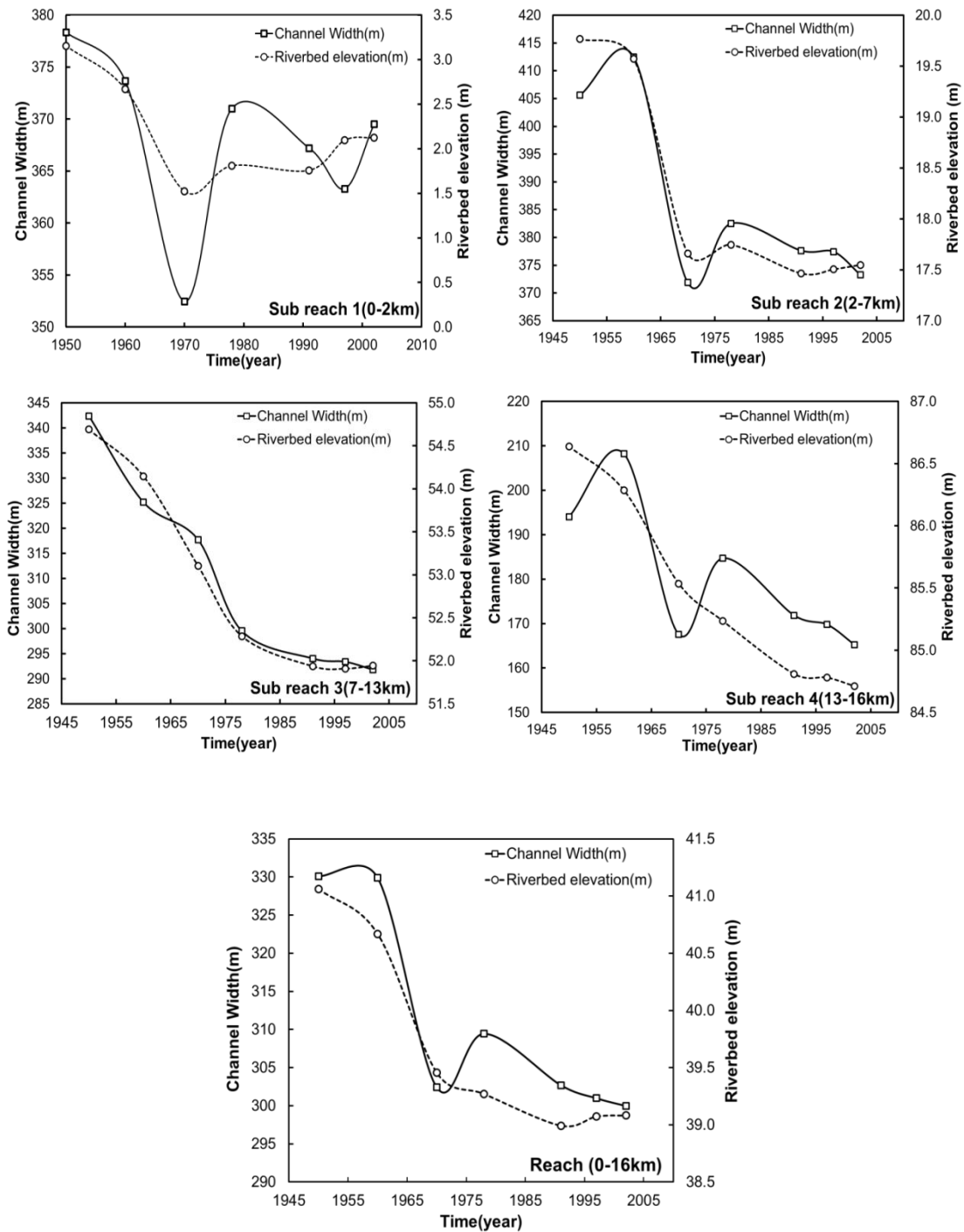
Figure 5.11. Temporal trends of average channel width and riverbed elevation in four sub reaches and entire reach.

The sub reach-averaged channel width and mean riverbed elevation for each sub reach and entire reach are then computed for years 1950, 1960, 1970, 1978, 1991, 1997 and 2002 as shown in Fig. 5.11. The average channel width of the entire study reach has decreased from 330 m in 1950 to 300 m in 2002. The temporal variation in the channel width indicates that a significant decrease in the channel width simultane-

ously took place in the four sub reaches from 1950 to 1970, coinciding with the trend of the considerable erosion occurred in this period along the lower Tedori River. This relation could be explained by the characteristics that when the riverbed was lowered, the flow concentrated in a narrower cross-section (Rinaldi, 2003). Similarly, the rapid decrease in the channel width was still observed in the sub reach 3 during the period of 1970-1978. On the contrary to such phenomenon, the channel width in the sub reaches 1 and 2 increased by the average magnitude of 15 m as a direct consequence of the aggradation trend occurred from 1970 to 1978. The channel width in the entire reach slightly decreased in the period of 1978-1991 and subsequently remained stable during the last period of 1991-2002. In conclusion, the variation in the channel width is accompanied with the variation in the riverbed elevation: namely, decreased bankfull width and the river bed degradation; increased bankfull width and the river bed aggradation.

5.2.4. Variation in sediment characteristics

A general reduction in grain size in the downstream area accompanying the general decrease in bed slope was observed (Fig 5.12). The decline in grain size also reflects the attrition of gravel in transit along the rivers (Collins and Dunne, 1989). During 1965–1975, d_m increased in the area of 4.5–14 km, ranging from 150 to 400 mm in the main course and from 100 to 200 mm on the near-riverbank area. From 1980 to 1993, d_m for the river channel decreased to 50–100 mm, while on the lateral area, d_m coarsened in a range from 200 to 400 mm in the reach of 3–14 km. Similar to the previous studies on SGM effects (Kondolf, 1994; Rinaldi et al., 2005), it was considered that SGM was responsible for the coarser d_m value in the riverbed for two reasons. The first is that an amount of sand and gravel-sized grain was moved out of the river, leaving the bed sediment layer with larger grains. Second, SGM triggered erosion in the upstream and downstream of the excavation pit, and finer sediment was thus transported to the downstream area.
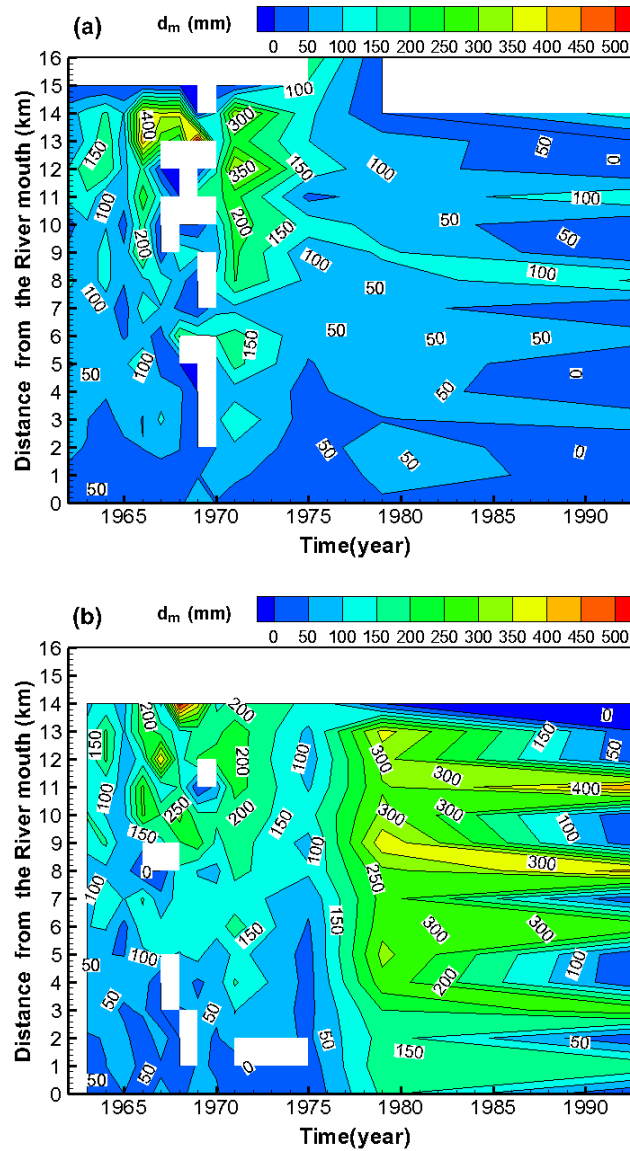
Figure 5.12. Temporal and spatial variations in the sediment mean diameter in the main course (a) and on the lateral area (b) (zero values or blank areas indicate missing data).

Another investigation of the variation in median sediment diameter (d_m) in both the main course and lateral area in relation with SGM was conducted by annual surveys of sediment samples from 1963 to 1971. Figure 5.13 shows the temporal variation in d_m in relation to the temporal variations in the slope and flood discharge product ($Q.S$). The $Q.S$ is representative of stream power per unit channel length (Bridge, 2003) and, consequently, can an important factor that influences the variation in d_m. In sub-reaches 1, 2 and 3, the temporal variation in both d_{mc} (median sediment diameter in the river channel) and d_{mp} (median sediment diameter on the lateral area) is closely related to the temporal variation in $Q.S$ during 1963–1971. In sub reach 4, although a close relationship was also observed between d_{mc} and $Q.S$ from 1963 to

40

1971, the variation in d_{mp} is opposite to the $Q.S$ from 1966 to 1969. In particular, in 1966 and 1968, when the minimum values of $Q.S$ were measured, maximum values of d_{mp} were recorded (Fig. 5.13d). This unusual relationship could be related to the effect of intensive sand mining that occurred in the lateral area of sub reach 4, as gravel and sand extraction could have made the bed surface more armored.
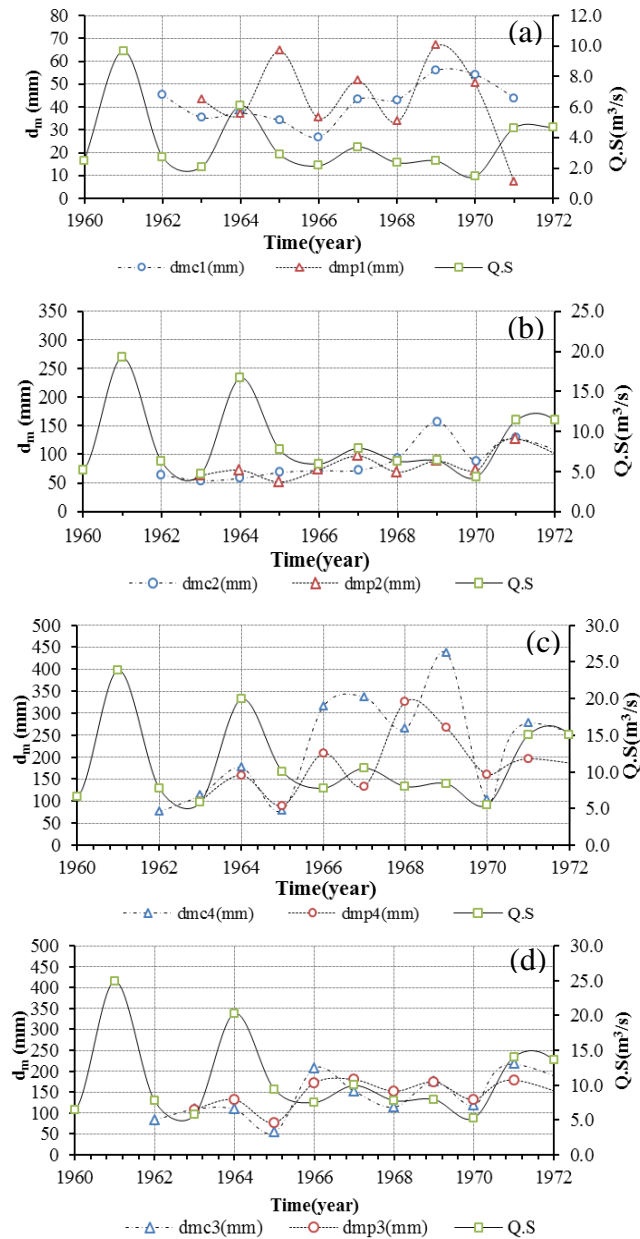
Figure 5.13. Temporal variation in the slope and flood discharge product ($Q.S$) and d_m of the lower Tedori River.

(a) Reach 1 (0–2 km); (b) Reach 2 (2–7 km); (c) Reach 3 (7–13 km); and (d) Reach 4 (13–16 km upstream of river mouth).

41

5.3. Effects of human activities on sediment budget

5.3.1. Estimation of sand and gravel supply rate

To calculate the sand and gravel budget along the lower Tedori river, it is nessesary to know gravel and sand transport at a cross-section. As a boundary condition, it is necessary to evaluate the sand and gravel transport at the upstream end of the study reach. For this purpose, we estimated the sediment budget of the Ushikubi River and Ozo River (Fig. 5.14). Firstly, the sediment budget of the Ushikubi River was defined based on the sediment deposition coupled with the removed sediment volume from the Tedorigawa Dam during the period of 1979 to 2006. We assume that the sediment yield of the Ozo River catchments is similar to that of the Ushikubi River. Accordingly, the sediment budget of the Ozo River was computed by multiplying the sediment yield of the Ushikubi River by 0.75 (the area fraction between Ozo and Ushikubi Rivers). The river sediment budget of the upstream Tedori river was then a summation of those of the Ushikubi and Ozo Rivers (Fig. 5.14). The percentage of sand and gravel of the sediment deposition in the Tedorigawa Dam was 54% (referred to several sediment samples in Tedorigawa Dam surveyed by HRDB). This value was also adopted for the percentage of sand and gravel in the sediment of the upstream Tedori River. Therefore, the sand and gravel transport at the upstream end of the study reach prior to and after Tedorigawa Dam operation were estimated to be $0.28 \times 10^6 m^3$ and $0.11 \times 10^6 m^3$, respectively.
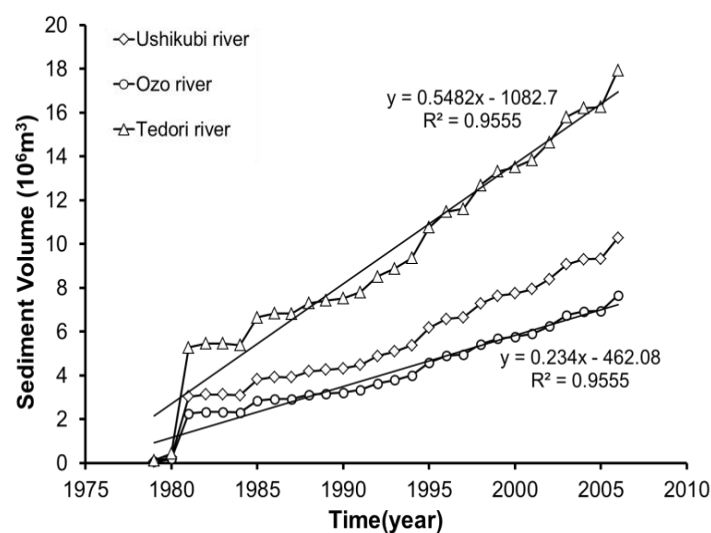
Figure 5.14. Estimation of the sediment yields in the Ushikubi river, Ozo river and upstream Tedori River.

5.3.2. Variation in riverbed sediment volume

The temporal variation in the in-river sediment volume (RSV; term 1 in Eq. (5.2)) was first examined on various spatial scales, including the entire reach and the four sub reaches (Fig. 5.15a). The cumulative variation in RSV was computed with respect to the riverbed elevation in 1950. It should be noted that the overall variation trend for all the spatial scales was a significant decrease from 1950 to 1979, and there was subsequently a slight decrease until 1991. From 1991 to 2007, an increasing trend was observed at all spatial scales, except for a decrease of 2.5×10^5 m^3 in sub reach 3. The remaining erosion in sub reach 3 can be partially attributed to the secondary effect of intensive SGM that was conducted in the previous period. The reduction in RSV in the whole area peaked in the 1960s, when there was a reduction of approximately 7.88×10^6 m^3 in RSV, at 0.72×10^6 m^3/yr (Fig. 5.16). A similar trend was also observed in sub reach 3 in the 1960s. This is considered to be due to the intensive SGM during the 1960s. According to the HRDB, SGM in the 1970s was mainly carried out in the reach of 7.4–15 km. As a result, the RSV in sub reaches 3 and 4 decreased by 1.5×10^6 and 1.3×10^5 m^3 respectively in the 1970s, while there was an increase in RSV in the remaining sub reaches. Therefore, the features of change in RSV along the entire study reach were closely related to those of the 7–13 km reach. For the entire reach of 0–16 km, Figure 5.16 indicates that RSV decreased at 0.38×10^6 m^3/yr during the first 30 years, then declined gradually at 0.09×10^6 m^3/yr from 1979 to 1991, and finally increased at 0.04×10^6 m^3/yr until 2007.
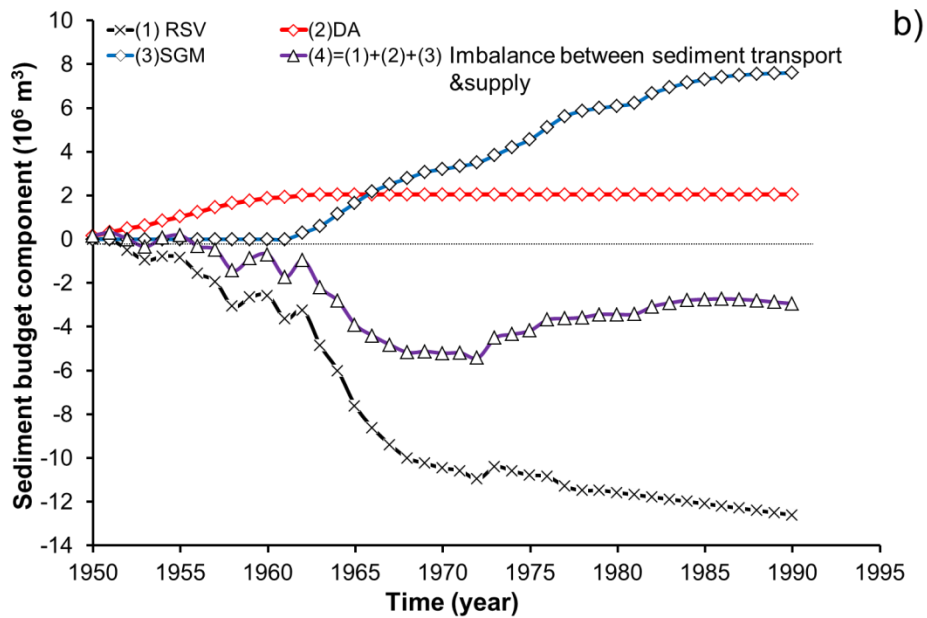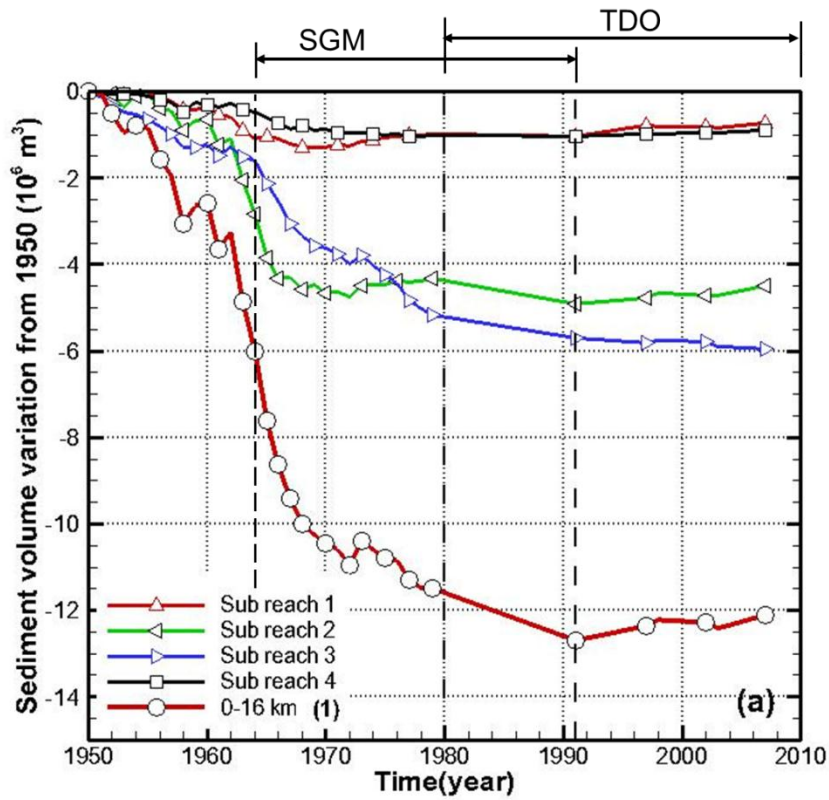
Figure 5.15. Temporal variations in cumulative sediment volume in the Tedori River Basin.

 (a) temporal and spatial variations in the riverbed sediment volume; (b) temporal variation in the sediment volume induced by human activities

Period (year)	1950-1960	1960-1970	1970-1979	1979-1991	1991-2007
■Vin	0.28	0.28	0.28	0.11	0.11
▨Vout	-0.35	-0.64	-0.09	-0.07	-0.07
▥SGM	0.00	-0.29	-0.29	-0.13	0.00
▢DA	-0.17	-0.07	0.00	0.00	0.00
-○- ΔV	-0.23	-0.72	-0.10	-0.09	0.04
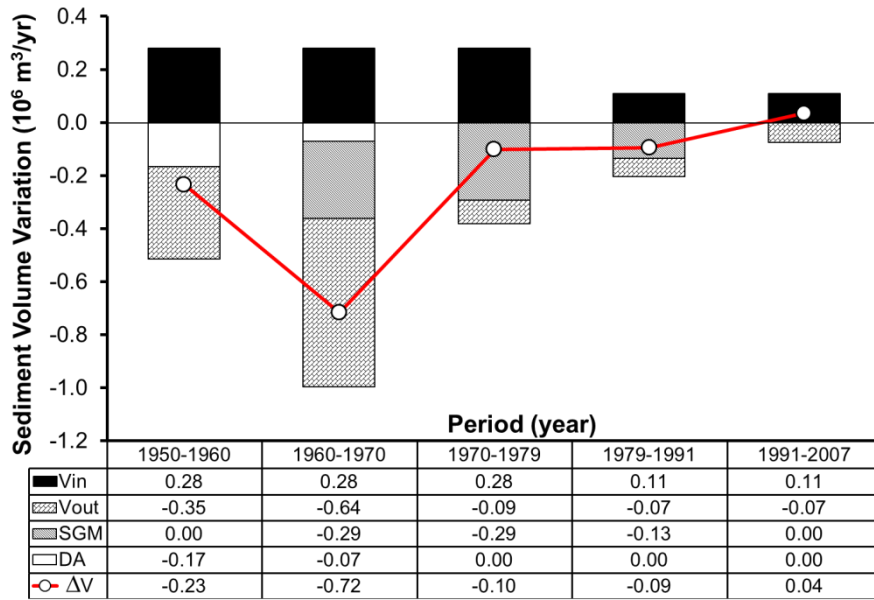
Figure 5.16. Decadal variations in components of sediment budget.

In this figure, for an easier descriptive purpose, sign of sediment budget components moving out of the river is minus. Sign of quantities entering the river is plus.

5.3.3. Direct effects of SGM until 1979

The decrease in RSV as shown above was primarily a consequence of the extraction rate being higher than the replenishment rate of upstream bed sediment. The amount of SGM (term (3) in Eq. (5.2)) was determined from the licenses issued by local authorities from 1950 to 1991 and the cumulative volume of SGM is plotted as curve (3) in Fig. 5.15b. This value is considered to be the minimum amount of SGM. According to Yamamoto et al. (2008a), it is projected that the SGM amount could be twice the amount permitted by local authorities (curve (3') in Fig. 5.15b). The amount of SGM based on Yamamoto's estimation is given in parentheses hereafter. From 1949 to 1963, DA resulted in the removal of $2.1 \times 10^6 \, \text{m}^3$ of sediment (curve (2) in Fig. 5.15b). The minimum amount of sediment extracted by SGM and DA from 1949 to 1979 was $8.1 \times 10^6 \, \text{m}^3$. The rate of extraction (including SGM and DA) was $0.17 \times 10^6 \, \text{m}^3/\text{yr}$ in the 1950s (Fig. 5.16), and it subsequently increased substantially to 0.36 $(0.65) \times 10^6 \, \text{m}^3/\text{yr}$ in the 1960s (Fig. 5.16). Owing to the legal restriction of SGM starting in the mid-1970s, the rate of SGM in the 1970s of 0.29 $(0.59) \times 10^6 \, \text{m}^3/\text{yr}$ (Fig. 5.16) was lower than that in the 1960s. It is notable that in the 1960s and 1970s, rates of extraction were greater than those of upstream bed sediment replenishment. For the mid and late 1950s, the official data in Fig. 5.16 indicates that there were DA

in the 0–4.9 km sub-reach, while in the early 1950s, the amount of DA in sub-reaches 3 and 4 was comparable to that in sub-reach 1. In addition, SGM activities during the 1950s, for which no official record of amount is available, might have some influence. Overall, material extraction removed the majority of gravel and sand from the riverbed, directly reducing the riverbed level where extraction was conducted.

5.3.4. Indirect effects of SGM and influence of natural factors until 1979

By removing sediment from the channel, SGM disrupts the preexisting balance between the sediment supply and transporting capacity, typically inducing degradatiom upstream and downstream of the extraction site (Erskine, 1990; Kondolf, 1997). The material extraction in rivers leaves various pits in the bed profile. These pits trap the bedload supplied from upstream during subsequent high flows, inducing a bed material deficit of downstream reaches and potentially inducing degradation downstream of the mining site. In addition, the upstream end of the pit is a knickpoint in which the slope changes abruptly, and this knickpoint typically migrates upstream, inducing degradation upstream of the mining site (Erskine, 1990; Huang, 2011; Kondolf and Swanson, 1993; Rinaldi et al., 2005). This degradation, in turn, induces higher average shear stresses on the bed under the same flows and therefore may aggravate the process of degradation (Martín-Vide et al., 2010). These could partially contribute to the decrease in RSV in the lower Tedori River from 1950 to 1991 (Fig. 5.15a).

On the other hand, although the rate of extraction in the 1950s was equal to or even less than that in the 1970s, yet the corresponding decrease in RSV in the 1950s was over twice as large as that in the 1970s; 0.23×10^6 and 0.10×10^6 m^3/yr, respectively. This can be explained by the fact that there were only two flood events exceeding 2000 m^3/s in the 1950s whereas there were four in the 1970s. These six flood events transported significant amount of bed material from upstream area to the lower Tedori River, but they may not be sufficiently large to be able to entrain and carry that entire sediment to the neighboring coast. Consequently, the deviation between V_{in} and V_{out} (term 4 in Eq.(5.2)) in the 1950s was lower than that in the 1970s: 0.04×10^6 m^3/yr and 0.19×10^6 m^3/yr , respectively. In conclusion, it can be considered that SGM indirectly contributed to term 4 in Eq. (5.2) and curve (4) in Fig.

5.15b; the remaining contribution is attributed to the imbalance in the sediment supply and sediment transporting capacity in flood seasons, which is a natural factor.

5.3.5. Combined effects of SGM and TDO during 1980-1991

For the period of 1980-1991 when the lower Tedori River was influenced by both SGM and TDO, the river experienced gradual decrease in RSV. Due to TDO, the replenishment rate decreased to 0.11×10^6 m^3/yr while the rate of extraction still stood at 0.13 (0.26) $\times 10^6$ m^3/yr. A collation of roles of SGM in the period of 1950-1979 (addressed above) and of TDO in the period of 1991-2007(as mentioned bellow) could indicate that SGM played a more important role than TDO in causing degradation in the lower Tedori River in the period of 1979-1991.

5.3.6. Direct and indirect effects of TDO after 1991

Immediately after 1991 when SGM was completely prohibited, there was slight accretion in the study area until 2007 (Fig. 5.15a). In this period, the RSV increased by 0.6×10^6 m^3 at 0.04×10^6 m^3/yr (Fig. 5.16). Such a trend was attributed to the sediment supplied from the Ozo River in flood seasons at the estimated rate of 0.11×10^6 m^3/yr and a substantial reduction in the sediment-carrying capacity of the lower river because of construction of the Tedorigawa Dam. In this case, reduction in the bed material transport capacity is greater than that in supply of bed load, thus transforming a naturally net degradational system into a system in which bed load may accumulate over time (Topping et al., 2000).

The vegetation cover changes with the varying magnitude of flood events. Through analysis of the aerial photographs for the years 1995 and 2000, the temporal variation in vegetation cover of the 0–2, 4–6-km, 9–11-km, and 14–16-km sub reaches was estimated. From 1991 to 1995, there was no large flood exceeding the channel-formed discharge of 1737 m^3/s; therefore, the vegetation cover along all sub reaches increased to its highest values; especially 44% in the sub reach of 14–16 km. Due to the flood in 1998 (2883 m^3/s), the vegetation cover considerably decreased to 18% on average in 2000. This variation trend in vegetation cover is similar to the those at 5 km, 8km and 10 km, which was addressed by Tsujimoto and Teramoto (2004). At the channel-formed discharge, the mean water depth of a cross-section varied in excess of 0.9-3.5m along the study area. By field and aerial photograph survey, it was realized that plants contributing to the vegetation cover in the lower

Tedori River were mainly willow and reed and almost all of which were submerged under condition of bankfull flow. Normally, submerged vegetation may induce more significant reduction in bottom shear stress than emergent one. Therefore, vegetation cover in the lower Tedori River could partially contribute to slight aggradation from 1991 to 2007. This is also is indicated by a significant correlation (Spearman R=-0.83, p<0.1) between increase in vegetation cover and reduction in the cumulative variation of the riverbed sediment volume.

5.3.7. Variation in sediment budget along the lower Tedori River

The variation in the riverbed sediment along the lower Tedori river in 5 different periods are shown in Fig. 5.17. The results indicate that a considerable reduction in the riverbed sediment volume was observed over the period of 1950-2007 in most of the study area, except for the segment of 15-16 km. In the three periods of 1950-1960, 1960-1970 and 1979 -1991, erosion occurred in nearly all of the segments. Notably, the rate of the erosion in the period of 1960-1970 was significantly higher than that in the other periods. Following the process of intensive erosion, a natural sediment recovery was realized in the periods of 1970-1979 and 1991-2007 in some areas. For example, the segment of 1-4 km in which the most serious erosion took place in the three former periods gained the highest rate of sediment deposition in the two later periods.
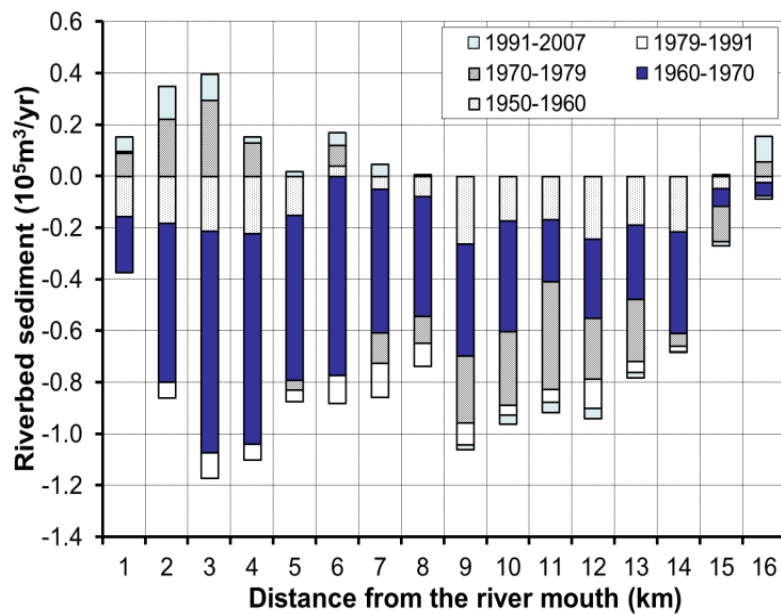
Figure 5.17. Temporal and spatial variation in the riverbed sediment volume.

Similar to other rivers, the real volume of the SGM in the lower Tedori river is considered to be higher than the official amount of 7.8×10^6 m^3 which was permitted by the authority. According to Yuhi (2008b), when such official value was taken into account a collation between the total response volume in the integrated watershed, consisting of the Tedori river and the neighboring coast, and removed amount, a deficit of 4.4×10^6 m^3 appeared. Several reasons were responsible for this imbalance, yet the underestimated amount of sand and gravel was considered as a main factor. Therefore, in this study we estimated that the real amount of sand and gravel extracted from the lower Tedori river in the period of 1950-1991 could be twice as large as the official amount (Yamamoto et al., 2008b) and the corresponding values of β are set as 1.1-1.95. We assume that SGM conducted at each segment is directly proportional to the riverbed sediment variation of such segment. Accordingly, SGM at each 1-km-segment was defined for four different periods as shown in Fig. 5.18. Moreover, the total volume of DA was 2.1×10^6 m^3. Similar to the way of distributing SGM, DA was also allocated along the segment of 0-4.8 km over the period of 1950-1963 (Fig. 5.18).
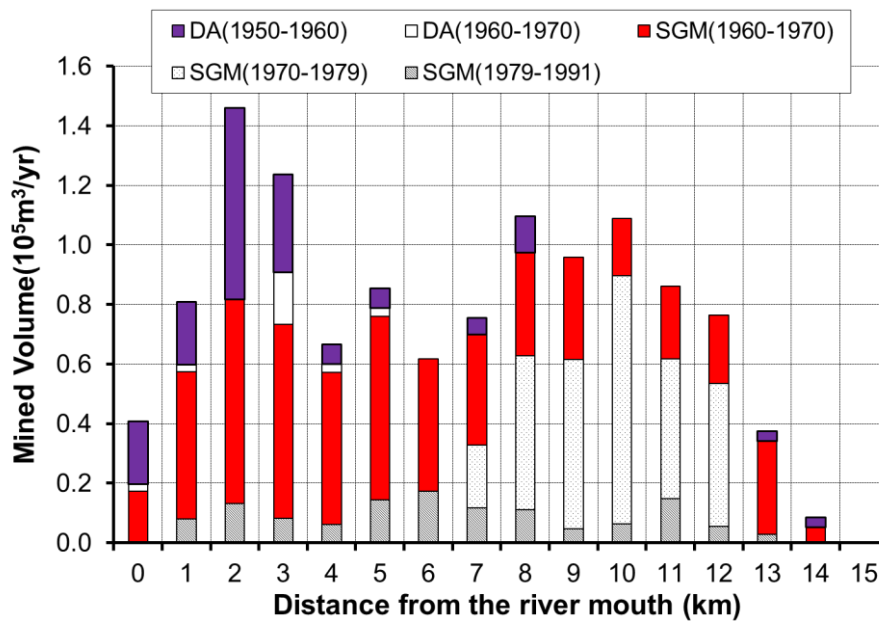
Figure 5.18. Temporal and spatial variations in the sediment volume mined from the downstream Tedori River.

49
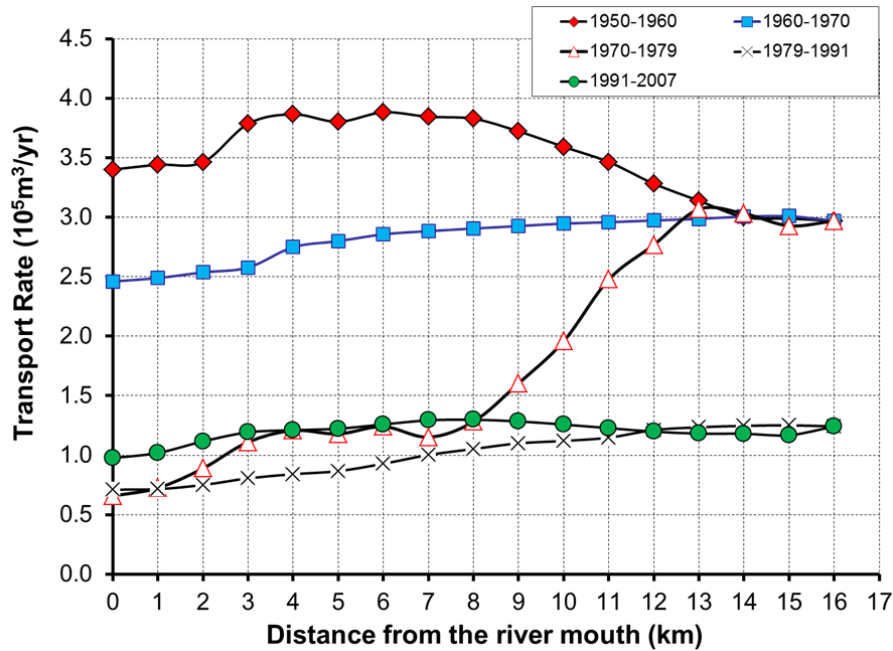
Figure 5.19. Temporal and spatial variation in bed material transport rate in the downstream Tedori River.

By using Eq (5.3), the sand and gravel transport through 16 cross-sections at interval of 1 km were conducted for 5 different periods as shown in Fig. 5.19. It was recognized that with SGM, the sand and gravel transport at all cross-sections generally decreased along the lower Tedori river. In the period of 1960-1970, SGM was most intensively conducted in the segment of 0-15km, making the sediment budget gradually decreased to $2.4\times10^5 m^3$/yr when reaching the down coast. A similar effect of SGM on the sediment budget was also observed in the period of 1970-1979 when SGM was mainly conducted in the area of 7-13 km. In particular, in such area there was a dramatic reduction by 1.8×10^5 m^3/yr in the sediment budget. Subsequently, the sand and gravel transported to the river mouth reached $0.6\times10^5 m^3$/yr, which was the lowest amount in comparison with other corresponding values for remaining periods. In the first period of 1950-1960, the sand and gravel budget gradually increased in flow direction in the segment of 6-16km, subsequently rapidly reduced to $3.4\times10^5 m^3$/yr at the river mouth. This rapid decrease could be explained as a combined influence of the DA conducted in the segment of 0-5 km. In the period of 1991-2007, the sand and gravel transport was dominated by TDO. In this period, only the Ozo river supplied the limited bed sediment to the lower Tedori river. Due to such sediment deficit, flow entrained fine sediment in the segment of 6-16 km and subsequently transported them to the segment of 0-6 km. As a result of this, the sediment

50

transport increased to the highest value of 1.3×10^5 m^3/yr at 7 km and subsequently decreased due to deposition occurred in the downstream areas. In conclusion, SGM induced a considerable deficit in sediment budget along the lower Tedori River; without SGM, sediment budget slightly recovered partially along the lower Tedori River.

Tedori River is main sediment source of the Ishikawa coast. It is realized that computed sediment transport at the Tedori River mouth in the whole period agrees very well with the long shore variation of coast in Mikawa district addressed by Yuhi (2008b).

5.3.8. Discussion on limitation of present analysis

Along the upstream segment of the river in the Hakusan Mountains, where the Tedori system comprises of two major tributaries (the Ushikubi River and Ozo River), a number of debris (sabo) dams have been built to monitor and control debris production and sediment runoff. Since the 1910s, approximately 150 sabo dams have been erected. Sabo dams have trapped sediment behind them (Fig. 5.15b). The sediment trapped by the sabo dams increased significantly and the deposits behind the sabo dams amounted to 8.2×10^6 m^3 by 1983. Although the majority of these deposits are much larger than the constituents of the downstream river, the deposits could be considered to partly reduce the upstream sediment supply to the lower Tedori River. However, it is difficult to quantify the effect of the debris dam on the lower Tedori River in this study.

Besides, the remaining uncertainty of this investigation may come from the survey datasets. Firstly, the volume of SGM may significantly underestimate the real volume. The cumulative error in the estimated volume of sand and gravel mining could be of $O(10^6)$ m^3. Secondly, the error arose from the estimation of sand and gravel replenishment rate (V_{in}) from the upstream area. In this study, V_{in} was derived based on the deposition of sediment in Tedorigawa Dam from 1980 to 2005. Difference between V_{in} used for this analysis and other V_{in} estimated by various methods is the order magnitude of $O(10^5)$ m^3 to $O(10^4)$ m^3.

5.4. EOF analysis

5.4.1. EOF analysis of riverbed elevation changes

EOF analysis was applied to highlight the decadal variation in the riverbed level and its controlling factors. On the basis of the availability of the data, EOF analysis was conducted for the periods 1950–1979. The variance associated with the first eigenfunction was 99.9854% of total variability of the data. The second, third and fourth modes account for 0.0119%, 0.0008% and 0.0003% of the variations, respectively. The spatial function of the first mode $e_1(x)$ (Fig. 5.21a1) represents the longitudinal profile of the mean riverbed over the period 1950–1979. Its associated first temporal function $C_1(t)$ (Fig. 5.21b1) gradually decreases in the 1950s, subsequently decreases rapidly in the next two decades. From these characteristics, $C_1(t)$ is considered to strongly correlate (with correlation coefficient $R^2=0.97$) to the reduction in the riverbed sediment volume of the reach of 0–16 km from 1950 to 1979, which was shown by curve (1) in Fig. 5.15a.

The spatial function of the second mode $e_2(x)$ (Fig. 5.21a2) is found to reflect the variations in the rate of the vertical adjustment of the riverbed for phase I-B ($R^2=0.48$). For example, at 3.2 km from the river mouth, $e_2(x)$ reached the minimum negative value with the absolute magnitude of 0.24. This value, multiplied by the positive value of the temporal function of the second mode during the period 1964-1970, likely indicates that the most severe erosion occurred at 3.2 km from 1964 to 1970. The corresponding temporal function $C_2(t)$ (Fig. 5.21b2) gradually increases in the 1950s, after which it sharply increases in the 1960s and reaches its highest value in 1972. It then slightly decreases before remaining at a stable value during the late 1970s. These trends show that $C_2(t)$ most likely corresponds ($R^2=0.97$) to the trend of the variation in SGM (curve (3) in Fig. 5.15b) in the period of 1950-1973 and weakly associates with it from 1974 to 1979. Such relation between the two curves indicates that the riverbed almost instantly responded to the most intensive SGM conducted in the 1960s and the reduction in SGM due to legal restrictions in the mid-1970s.

For the third mode, the spatial function $e_3(x)$ (Fig. 5.21a3) is observed to be almost positive in the sub reach of 0–4.5km, while it is negative in sub reach 3(7–13km). This curve is considered to correlate ($R^2=0.58$) to the variation in the rate of the vertical adjustment of the riverbed in the phase I-C. $C_3(t)$ (Fig. 5.21b3) fluctuates with small amplitudes in the 1950s, after which it decreases considerably in the early

1960s, and then increases until 1979. Notably, $C_3(t)$ turns into positive in the 1974-1979 period during which SGM was intensively conducted in the sub reach 3. At the same time, a similar trend is also observed at the curve (4) in Fig. 5.15b, which describes the imbalance between sediment transport capacity and sediment supply, suggesting that this mode could be attributed to both. Therefore, the third mode clearly describes degradation in the sub reach 3 and aggradation in the area 0-4.5km from 1974 to 1979. The degradation was induced due to both SGM and amount of bed material transported downward.

Regarding the fourth mode, the spatial function of the fourth mode $e_4(x)$ (Fig. 5.21a3) could be interpreted (R^2=0.56) as the variation in the rate of the vertical adjustment over the phase I-A. The corresponding temporal function $C_4(t)$ (Fig. 5.21b3) rapidly increases from 1950 to 1963, and then decreases suddenly to a stable level. This trend may be interpreted as the effect of DA in the sub reach of 0–4.8 km (Fig. 5.15b). Linear regression analysis shows that a high correlation (R^2=0.89) exists between $C_4(t)$ and the curve (2) in Fig. 5.15b describing the cumulative volume of DA from 1949 to 1963. The fourth mode indicates the most serious erosion occurring around 0.6 km and 3.2 km from 1958 to 1963. At the same time, it also addresses the local deposition in the area of 5.5-6.5 km.

In conclusion, through the correspondence between the first four eigenfunctions and their associated physical meanings, we find that the first four modes of EOF analysis almost fully capture the response of the riverbed and its controlling factors over the period 1950–1979. Namely, EOF analysis indicates the temporal variation in the magnitude and rate of the change in the river bed in terms of both elevation and sediment volume. Additionally, contribution of each controlling factor to such change was also realized with descending importance as follows: SGM, flood, and DA.
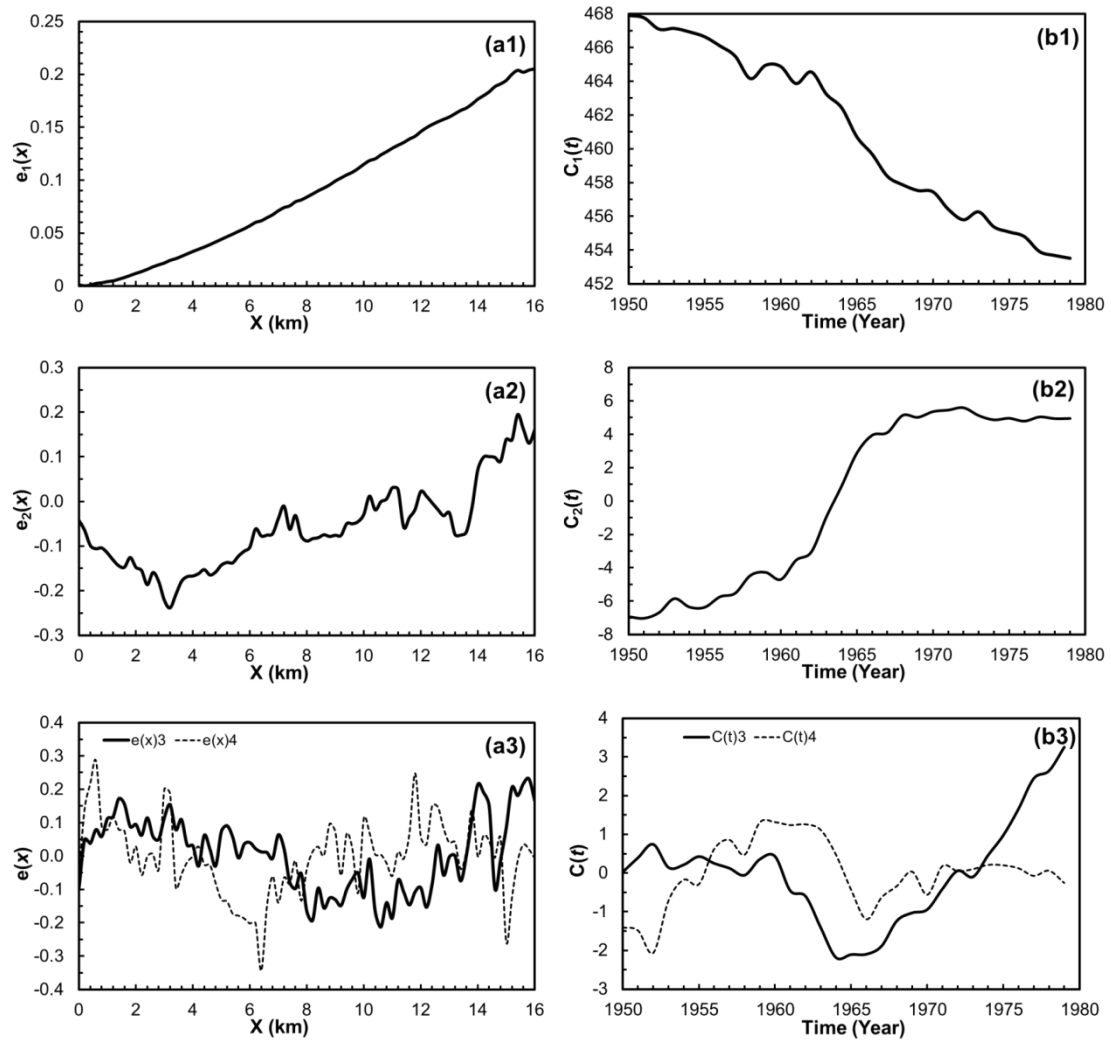
Figure 5.20. Temporal and spatial eigenfunctions for the first four modes

(a1) the first spatial eigenfunction; (b1) the first temporal eigenfunction; (a2) the second spatial eigenfunctions;(b2) the second temporal eigenfunctions; (a3) the third and fourth spatial eigenfunction;(b3) the third and fourth temporal eigenfunction

Figure 5.21 illustrates to what degree the four modes in Eq. (5.4) approximate the observed vertical adjustment of the riverbed over the different subperiods (1950–1959, 1960–1969, and 1970–1979). Four reproduced profiles of the vertical adjustment of the riverbed are defined by the superposition of the first mode, first two modes, first three modes, and first four modes, respectively. The degree of approximation is evaluated by the root-mean-square of the deviation between the reproduced and observed profiles (Table 5.4). The result indicates that the first mode primarily explains the overall vertical adjustment of the riverbed for the entire period. We now examine the role of the three remaining higher modes to highlight the dominant effect on the vertical adjustment of the riverbed in different periods. For the period 1950–1959, the contributions of the fourth and second modes are equivalent and much higher than that of the third mode. This implies that DA and SGM dominate the variation in the riverbed in this period. The highest contribution of the second mode is clearly observed in the 1960s. This provides evidence that SGM overshadows other impacts. In the last decade, the third mode becomes the most important because of the imbalance of sediment transport induced by frequent flooding. It is therefore reaffirmed that EOF analysis totally describes the temporal variation in the contribution of the human or natural influence on the decadal change in the lower Tedori River during 1950–1979.
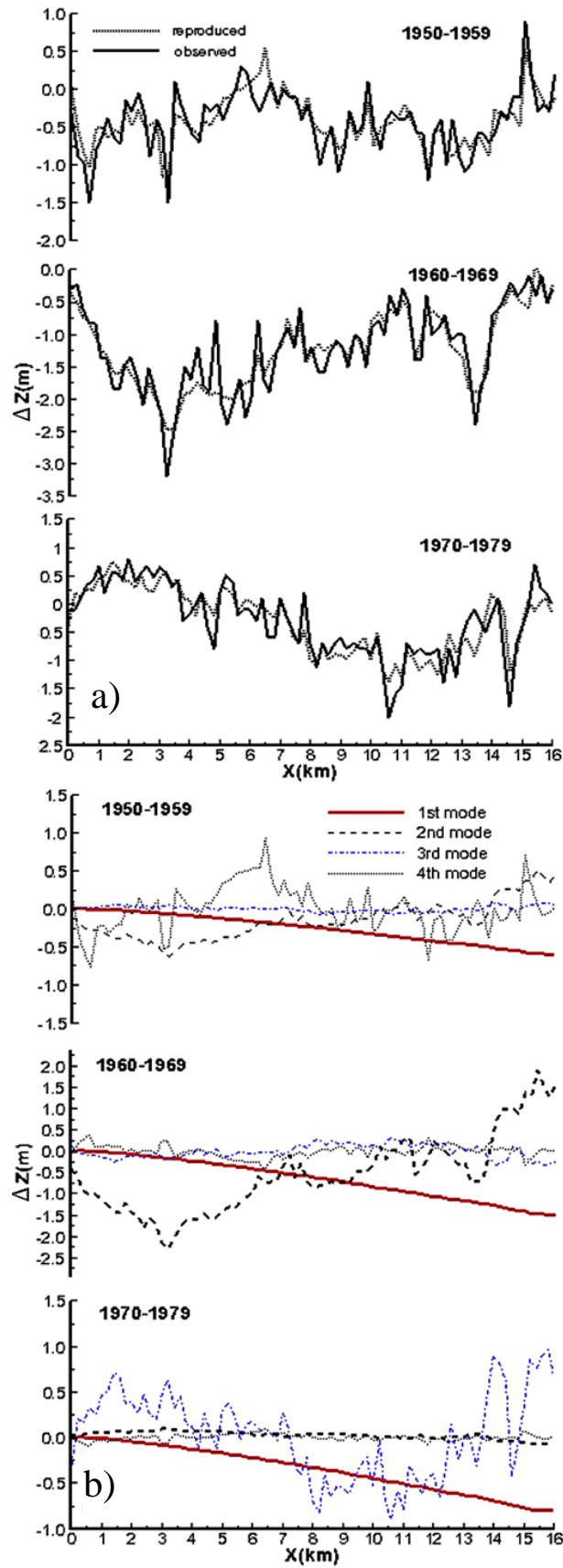
Figure 5.21. The observed and reproduced vertical adjustments over different periods

Table 5.4. Root-mean-square of the difference between the observed and reproduced vertical adjustments of the river bed

No.	Periods	Root mean squares (RMS)			
		1st mode	1st + 2nd mode	1st + 2nd +3rd mode	1st + 2nd+3rd+4th mode
1	1950-1959	0.49	0.38	0.38	0.24
2	1960-1969	1.13	0.35	0.31	0.27
3	1970-1979	0.55	0.55	0.30	0.30

EOF analysis was then employed to describe the variation in the riverbed and thus determine the main temporal and spatial patterns in the data from 1991 to 2007. During this period, the data for the riverbed were available only for 6 years; thus, the data for the remaining years were reproduced by linear interpolation. The temporal and spatial functions for the first and second modes are shown in Figs. 5.22 and 5.23, respectively. The first and second functions respectively explain 99.999% and 0.0004% of the variation in the data. The first spatial function $e_1(x)$ exhibits the longitudinal profile of the river bed averaged over the period 1991–2007. Figure 14b shows that the variation in the corresponding temporal function $C_1(t)$ is minor compared with that for the 1950–1979 period (Fig. 5.20b). This means that there was only a slight variation in the longitudinal profile of the riverbed over the period 1991–2007. The spatial function for the second mode $e_2(x)$ (Fig. 5.21a) reflects the rate of the vertical adjustment from 1991 to 2007 (Fig. 5.23a). The increasing trend of the temporal function for the second mode $C_2(t)$ corresponds to the increase in the riverbed sediment volume. The higher EOF modes could not provide clear physical meaning.
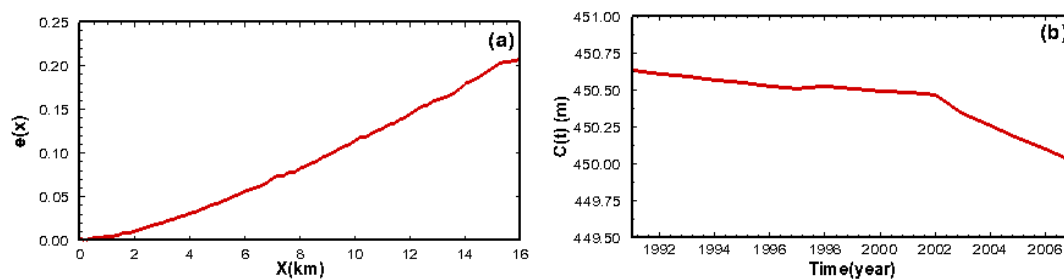
Figure 5.22. Temporal and spatial eigenfunctions for the first mode (1991–2007)

(a) spatial eigenfunction; (b) temporal eigenfunction
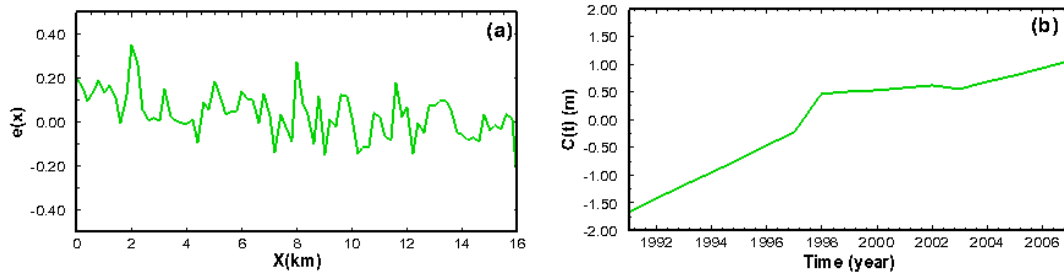
Figure 5.23. Temporal and spatial eigenfunctions for the second mode (1991–2007)

(a) spatial eigenfunctions; (b) temporal eigenfunctions.

5.4.2. Comparison of accelerated erosion in riverbed and downstream coast by EOF
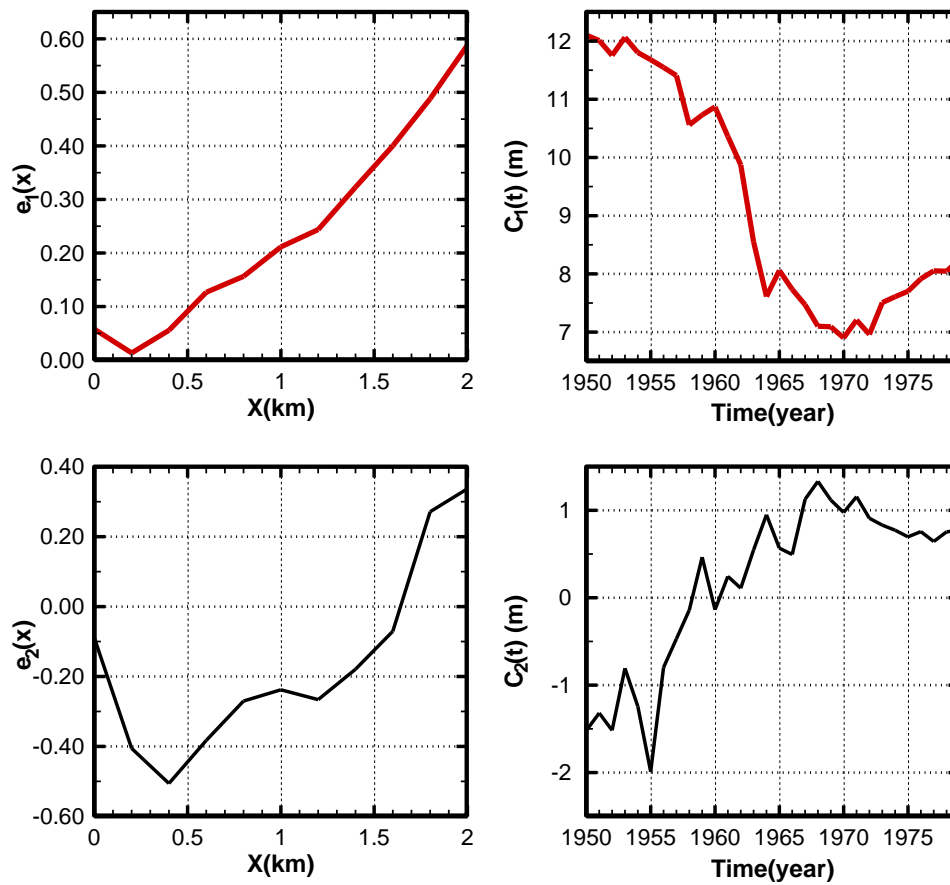
Figure 5.24. The temporal and spatial eigenfunctions for the 1st and 2nd modes of the river bed variation in sub reach 1 (0-2km)
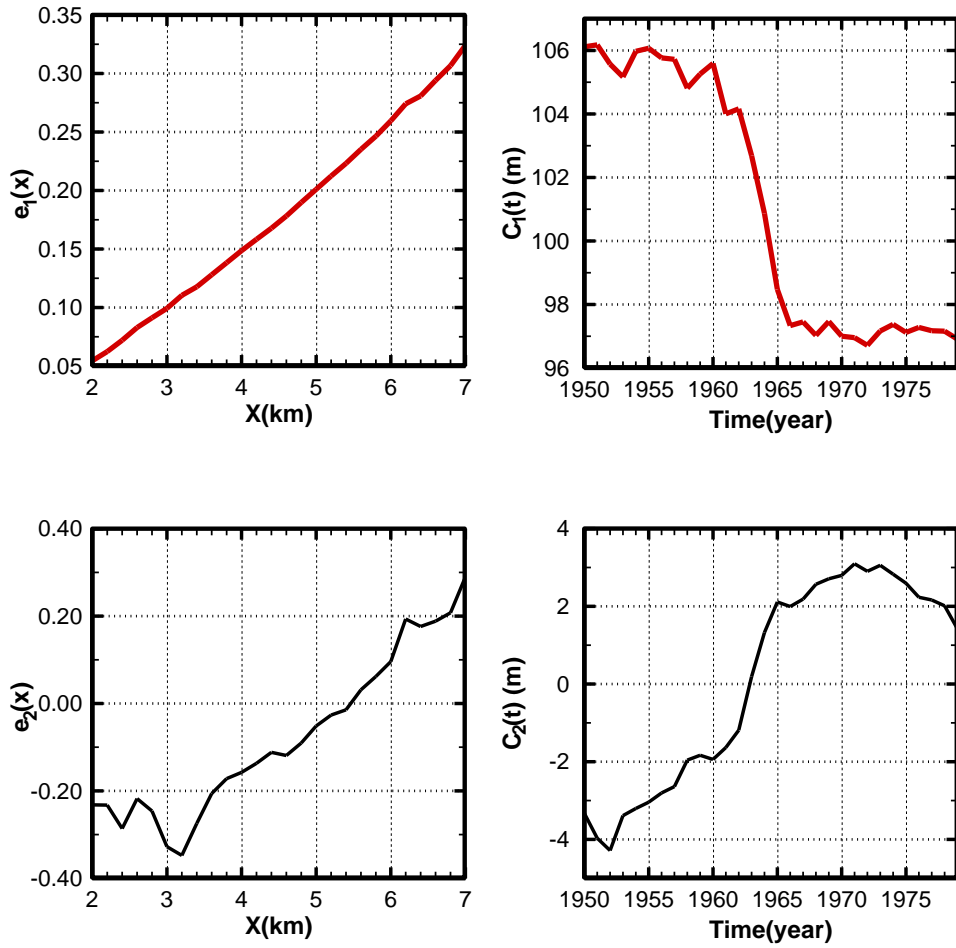
Figure 5.25. The temporal and spatial eigenfunctions for the 1st and 2nd modes of the river bed variation in sub reach 2 (2-7km)
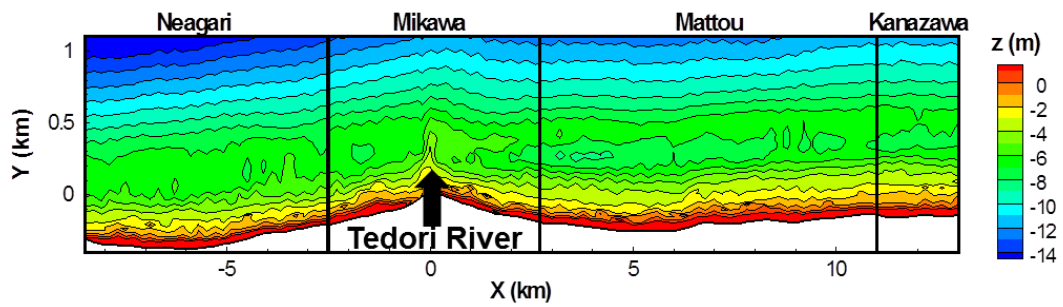
Figure 5.26. The topography of Ishikawa Coast
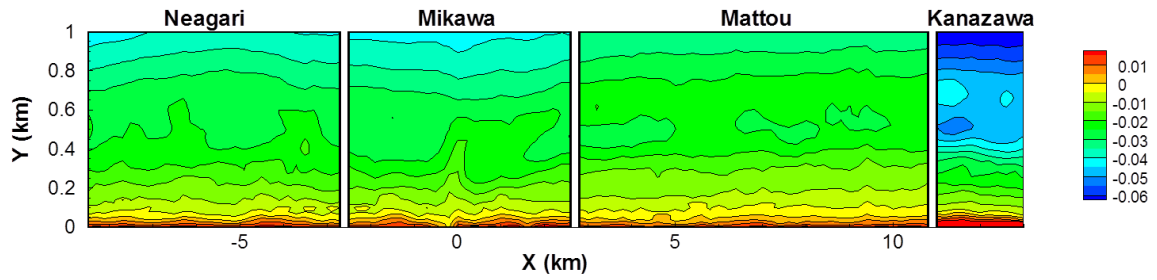
a)The spatial function of the 1st mode of the Ishikawa Coast
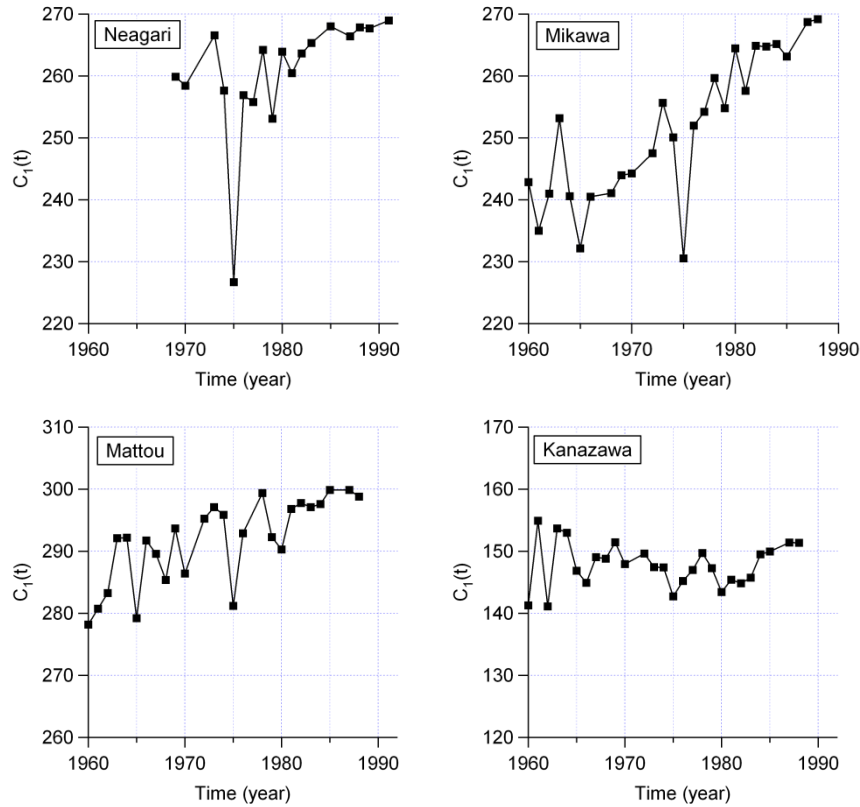
b)The temporal function of the 1st mode of the Ishikawa Coast

Figure 5.27. The 1st mode of the Ishikawa Coast (Yuhi et al., 2013).

Finally, EOF analysis was applied to the riverbed variation of the sub reaches 1 and 2 during 1950-1979 to compare with the corresponding variation in neiboring coast. Figure 5.24 and 5.25 describe the temporal and spatial eigen-funtions for the two first modes in each sub reach. In two sub reaches, the first spatial function $e_1(x)$ corresponds to the mean riverbed profile during 1950-1979. The temporal function $C_1(t)$ was closely related to the curve describing the cumulative temporal variation in sediment volume.

In the most downstream sector (0-2 km), the inset of accelerated erosion was around 1960. It continued until 1968. After that the segment volume became stable

for several years. Then the trend turned into accretion after the early 1970s. In the neighboring segment of 2-7 km, the erosion was most intensive during relatively short period of 1960 to 1966. The sediment volume became stable after 1966. The 2nd mode represents the morphological variation after 1966 in this segment. It indicated that the channel became steeper until 1972 and then the slope tend to change gentler.

To highlight the correlation between the river and downcoast erosion (Fig. 5.26), the EOF analysis was applied for the coastal area (Yuhi et al., 2013). Figure 5.27 describe the spatial and temporal functions for the first mode during 1960 to 1988 in Mikawa district of the Ishikawa Coast which is located near the river mouth. Similar to the riverbed results, the first spatial function $e_1(x)$ corresponds to the mean bed profile during the period. Since $e_1(x)$ is negative in underwater area and the 1st mode variation is expressed as the product of $e_1(x)$ and $C_1(t)$, the increase (decrease) of $C_1(t)$ represents the degradation (accretion) of bed elevation. In 1962, the erosion in Mikawa district was accelerated. The erosion in this area was intensive from the late 1960s to the late 1980s, and the magnitude of erosion was most significant among the four districts along the coastline. This is related to the direct influence of reduction in sediment discharge from the Tedori River. The time lag of the onset of accelerated erosion was several years when compared with that in the downstream river. The coastal erosion in this district was accelerated when the erosion of downstream sub reaches of the river slowed down and turned into accretion. It is considered that the sediment material, which could be an important beach component, was trapped in the river channel on the downstream area during the recovery process of sediment volume in the 1970s. This could reduce the sediment supply to the coast, resulting in the acceleration of the sand deficit in Mikawa district.

6.Conclusion

Comprehensive understanding of the long-term variation in the riverbed in relation to its controlling factors is essential to the rational management of disturbed rivers. The present study uses a 58-year topographic survey of the lower Tedori River, Japan and related data on human impacts to clarify the characteristics of long-term vertical adjustments of the riverbed. The main conclusions are summarized as follows.

1. Rapid and vertical adjustment was clearly observed from 1950 to 1991. The amount of sand and gravel extracted from the river was at least 8.9×10^6 m^3,

which significantly exceeded the sediment supply from the upstream area. Consequently the riverbed degraded in excess of 0.5–3.5 m in the entire study area, and the RSV decreased by 12.7×10^6 m^3. Besides, in the period of 1975 to 1990, the sediment mean diameter in the main course bacame smaller than that in the lateral lane. DA with a volume of 2.1×10^6 m^3 and imbalance between sediment transport capacity and sediment supply were other reasons for the degradation of the riverbed.

2. From 1991 when SGM was completely prohibited, the Tedorigawa Dam became the dominant factor affecting the lower riverbed. This led to a reduction in the mean total stream power per unit channel length by 25%, and a subsequent increase in the riverine vegetation cover. The sediment transport capacity of the flood decreased and sediment transported from the Ozo River deposited in the lower riverbed. Consequently, the RSV increased by 0.6×10^6 m^3 in the period 1991–2007.

3. The temporal adjustment of the riverbed elevation at each cross section indicates that the riverbed experienced five phases of adjustment: first three phases strongly depended on the rate and magnitude of sediment extraction from the river while the final phase was purely dominated by Tedorigawa Dam operation.

4. The first four modes of EOF analysis fully capture the main trends in the vertical adjustments and its dominant factors over the period 1950–1979. The first mode explained the mean profile of the riverbed and temporal variation of RSV. The second to fourth eigenfunctions reflected the characteristics of vertical adjustment for phase I-B, I-C and I-A, respectively. The corresponding temporal functions explained the respective effects of SGM, of imbalance in sediment transport, and of DA on the riverbed. In addition, a collation of river and coastal EOF result indicates that the time lag of the onset of accelerated erosion in Mikawa coast was several years when compared with that in the downstream river.

For the other rivers in which variations in riverbed are due to a complex interaction of natural and anthropogenic factors, EOF analysis is considered as a powerful tool to provide a relative measure between the rate and magnitude of channel response and the drivers for change.

Part III. Numerical study on bore propagation over a channel with complex topography

1. Introduction

Recently, tsunami intrusions on inland in general and into rivers in particular following massive earthquakes have more frequently taken place in several countries. As a result of this, increasing water level in the river may cause damages in the upstream area far from the coastline, i.e inundation and wave overtopping over the river embankments (Adityawan et al., 2012). Note that similar types of problems may be induced by the surge in canals due to sluice gate failure or in rivers after dam-break in the field of river and hydraulic engineering. In order to mitigate destruction of the tsunami intrusion, it is necessary to understand the behavior of bore under different boundary conditions. For this purpose, numerical simulation is considered as a powerful tool to reproduce various hydrodynamic process.

Bore propagation in rivers is mathematically described by the Nonlinear Shallow Water Equation. Many researches on improving the accuracy of the numerical schemes for solving the hyperbolic equation system have been conducted (as shown in literature). However, the treatment of source terms in that equation system and the modeling of the moving wet-dry interface at a shallow water wave front remain difficult (Liang et al., 2009; Wei et al., 2006). The problem becomes more difficult when simulating bore propagation over a complex topography in which artificial numerical wave may be generated in free water surface. This imposes a need to further study the well-balanced numerical schemes which are more accurate and robust to model discontinuous free-surface shallow flows like tsunami propagation over the complex boundary.

The object of this part is to develop a numerical model which is capable of solving the Nonlinear Shallow Water Equations based on the TVD-MacCormack scheme, which is 2nd order accurate in time and space. It aims to achieve well-balancing property through modifying local bed elevation and using the surface gradient instead of the depth gradient for TVD corrections. Concurrently, the model is capable of capturing the moving wet-dry interface well by incorporating a surface gradient method. The accuracy and robustness of the model will be tested against several analytical solutions and experimental data in order to confirm that the model is able to simulate the 1D, 2D discontinuous flow over a complex topography. The model is then applied to the study of wave run up over banks of a curved channel with a parabolic cross-section.

2. Literature review

Shock-capturing is an popular approach for dealing with discontinuities in solution of the shallow water equation. In shock-capturing models, explicit schemes rather than implicit schemes are typically used (Zoppou and Roberts, 2003). Although the usual Courant restriction is accounted for in computational procedures, the explicit schemes require less computational time. The existing methods of computational fluid dynamics consists of two major families of shock-capturing schemes (Liang et al., 2007). The first is the Godunov method, which solves Riemanm problems at the interfaces of grid cells. The other is the arithmetical combination method of 1st- and 2nd-order upwind schemes. TVD-MacCormack scheme is belong to the second category.

Various high-resolution Godunov-type schemes have been introduced to solve the shallow water equations with source terms such as bed slope and bed shear stress. Through validation with analytical or/and experimental data, such numerical schemes prove the accuracy, effectiveness and robustness. Namely, Alcrudo and Garcia-Navarro (1993) introduced a high resolution Godunov-type scheme to achieve second-order accuracy. Fraccarollo and Toro (1995) modified the Godunov-type scheme with the weight averaged flux (WAF) method. They also conducted a laboratory dam break experiment to validate their simulation results. An upwind method for shallow water equations with bed slope source term was proposed and applied (Bermudez and Vazquez, 1994; Vázquez-Cendón, 1999). However, the way to treat the source term in that scheme remains cumbersome. LeVeque (1998) advanced a treatment for the bed slope source term which preserved the balance between source terms and flux gradients. The scheme successfully deal with a quasi-steady problem, but it is difficult to apply for steady transcritical flow with shock waves. Recently, Hubbard and Garcia-Navarro (2001) introduced a method balancing source terms and flux gradients, in which a upwind method is used for source terms.

Compared with other high-resolution shock-capturing schemes, TVD-MacCormack type predictor–corrector-updating method provides a natural way to take into account the source terms without any additional treatment (Delis and Skeels, 1998; García‑Navarro et al., 1992; Ming and Chu, 2000a; Ming and Chu, 2000b). For example, Fennema and Chaudhry (1990) proposed a finite difference approach to implement the MacCormack scheme with an artificial viscosity to simulate the

65

supercritical channel flow. García-Navarro et al. (1992) incorporated TVD steps into a simple finite difference MacCormack explicit scheme for simulation of one-dimensional open channel flows. The scheme does not cause any additional difficulty dealing with the source terms of the equation and remains second-order accuracy in both time and space. Liang et al. (2007) used a TVD-MacCormack scheme to discretize the shallow water equation in terms of non-conservation form. By using this, the numerical model requires modest computational power, yet has the ability to resolve all flow regimes with a high level of accuracy and stability.

Bermudez and Vazquez (1994) introduced a definition of the ''exact C-property'', which require a numerical model to produce a constant surface elevation in a frictionless flow over varying bathymetry. Then, various numerical solution of SWEs based on Godunov-type methods including complex source terms have been developed. Among such tasks, several well-balanced methods have been proposed (Aureli et al., 2008; Begnudelli and Sanders, 2006; Canestrelli et al., 2010; Canestrelli et al., 2009; George, 2008; Liang and Marche, 2009; Song et al., 2011a; Song et al., 2011b; Xing et al., 2010). For example, George (2008) developed an augmented Riemann solver accounting for bottom slope. The solution with a key ingredient of wave propagation algorithm (LeVeque, 2002) can conserve a large class of steady states in one-dimensional applications. Considering the water level and discharge as dependent variables, Liang et al. (2009) proposed a scheme for solving the pre-balanced SWEs. However, the limitation of the scheme is that negative water depth appears near the wet/dry fronts, and the mass error due to artificial modification of flow variables exists. To overcome this problem, Liang and Marche (2009) suggested the nonnegative reconstruction of water depth, and derived additional source terms, which were introduced to cope with the occurrence of dry areas, for balancing spurious fluxes. As a result, there is no need for modifications of flow variables, and the mass conservation is exactly preserved. The one-dimensional shallow flow model (Liang and Marche, 2009) was later extended to two-dimensional and simplified to remove the additional source terms for practical applications by Liang (2010b). Begnudelli and Sanders (2006) introduced the flux correction terms to preserve the well-balanced property in fully wet cell, whereas the velocity in partially wet cell is set to zero. Therefore, the stationary solutions can be maintained in both fully and partially wet cell when the still steady state is encountered. All well-balanced schemes, mentioned above, was developed based on the Godunov-type methods while ones based on

TVD-MacCormack are very rare. Typically, Vincent et al. (2001a) proposed a numerical model based on TVD-MacCormack scheme and discretization ensuring balance between source term and flux gradient. Well-balanced property of the model was preserved for on the bottom with linear slopes and on sandy beach profiles varying smoothly. When the topography abruptly changes, artificial numerical wave appears. Tseng (2003) introduced a improved gradient method to eliminate or reduce the artificial numerical error caused by strong channel bed slope variations for TVD-MacCormack scheme. The improved surface gradient method is more suitable for simulating open-channel flow with highly irregular bed topography by using the surface gradient instead of the depth gradient for TVD corrections, considering the balancing of the source terms and the flux gradients. However, well-balanced characteristic of this model was broken when the domain consists of emergent islands. To simulate the flow on abruptly varying topography, it requires further improvement of existing numerical schemes.

3.Governing equations

This study considers horizontally two-dimensional, depth-integrated flows in the Cartesian coordinate system. The Nonlinear Shallow Water Equations (NSWE), which consists of a continuity equation and two momentum equations, define the fluid motion. The conservative form of NSWE can be written as follows:

$$\frac{\partial \mathbf{q}}{\partial t} + \frac{\partial \mathbf{F}}{\partial x} + \frac{\partial \mathbf{G}}{\partial y} = \mathbf{S} \tag{3-1}$$

where $\mathbf{q}$= vector of conserved variables; $\mathbf{F}$ and $\mathbf{G}$= flux vectors; and $\mathbf{S}$= source terms. These vectors are expressed in terms of the total flow depth $h(x,y,t)$ and the depth-averaged velocity $u(x,y,t)$ and $v(x,y,t)$ as

$$\mathbf{q} = \begin{bmatrix} h \\ hu \\ hv \end{bmatrix}, \ \mathbf{F} = \begin{bmatrix} hu \\ hu^2 + \frac{1}{2}gh^2 \\ huv \end{bmatrix}, \ \mathbf{G} = \begin{bmatrix} hv \\ huv \\ hv^2 + \frac{1}{2}gh^2 \end{bmatrix}, \ \mathbf{S} = \begin{bmatrix} 0 \\ -gh\frac{\partial Z_f}{\partial x} - \frac{\tau_x}{\rho} \\ -gh\frac{\partial Z_f}{\partial y} - \frac{\tau_y}{\rho} \end{bmatrix} \tag{3-2}$$

In the above, $Z_f(x,y)$ is the bed elevation and g is the gravitational acceleration; The bed stress terms τ_x and τ_y represent the effect of bed roughness on the flow and may be estimated using following formula:

$$\tau_x = \rho C_f u \sqrt{u^2 + v^2} \quad \text{and} \quad \tau_y = \rho C_f v \sqrt{u^2 + v^2}$$

The bed roughness coefficient C_f can be evaluated using $C_f = gn^2/h^{1/3}$, where n=Manning coefficient.
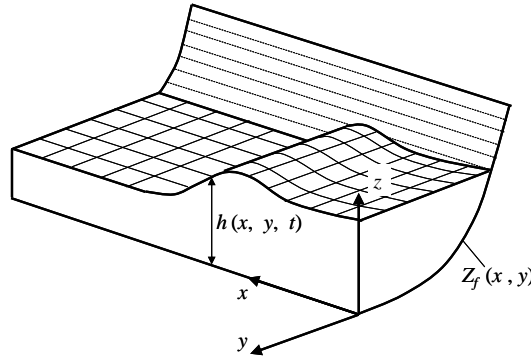
Figure 3.1. Definition Sketch

4.Numerical scheme

4.1.TVD-MacCormack scheme

The numerical model in the present study is based on a TVD MacCormack method, which is second order accurate in space and time. The classical MacCormack scheme is expressed in two steps (e.g.MacCormack, 1969; MacCormack and Paullay, 1972):

(a) predictor step

$$\mathbf{q}_{i,j}^{p} = \mathbf{q}_{i,j}^{n} - \lambda_x \left(\mathbf{F}_{i+1,j}^{n} - \mathbf{F}_{i,j}^{n} \right) - \lambda_y \left(\mathbf{G}_{i,j+1}^{n} - \mathbf{G}_{i,j}^{n} \right) + \varDelta \mathbf{S}_{i,j}^{n} \qquad \textbf{(4-1)}$$

(b) corrector step

$$\mathbf{q}_{i,j}^{c} = \frac{1}{2} \left[\mathbf{q}_{i,j}^{p} + \mathbf{q}_{i,j}^{n} - \lambda_x \left(\mathbf{F}_{i,j}^{p} - \mathbf{F}_{i-1,j}^{p} \right) - \lambda_y \left(\mathbf{G}_{i,j}^{p} - \mathbf{G}_{i,j-1}^{p} \right) + \varDelta \mathbf{S}_{i,j}^{p} \right] \qquad \textbf{(4-2)}$$

where $\lambda_x = \Delta t/\Delta x$ and $\lambda_y = \Delta t/\Delta y$.

It is known that the MacCormack scheme yields good solutions in regular zones where surface gradient is relatively small, but shows oscillatory behavior near steep gradients and shocks. Following the work of Yee (1987) and Vincent et al. (2001a), accordingly, we have added the TVD correction step in order to suppress the numerical oscillations.

(c) TVD step

$$\mathbf{q}_{i,j}^{n+1} = \mathbf{q}_{i,j}^{c} + \lambda_x \left[(\mathbf{R}_A)_{i+1/2,j}^{n} (\mathbf{\Phi}_x)_{i+1/2,j}^{n} - (\mathbf{R}_A)_{i-1/2,j}^{n} (\mathbf{\Phi}_x)_{i-1/2,j}^{n} \right] + \lambda_y \left[(\mathbf{R}_B)_{i,j+1/2}^{n} (\mathbf{\Phi}_y)_{i,j+1/2}^{n} - (\mathbf{R}_B)_{i,j-1/2}^{n} (\mathbf{\Phi}_y)_{i,j-1/2}^{n} \right]$$

(4-3)

where R_A and R_B is the right-eigenvector matrix associated with the flux Jacobian matrix $A = \partial F/\partial q$ and $B = \partial G/\partial q$, respectively (e.g.Toro, 2003).

The l-th component of Φ_x is expressed as

$$(\phi_x)_{i+1/2,j}^{l} = \frac{1}{2} \left[\xi \left((a_x)_{i+1/2,j}^{l} \right) - \lambda_x \left((a_x)_{i+1/2,j}^{l} \right)^2 \right] \times \left[(\alpha_x)_{i+1/2,j}^{l} - (Q_x)_{i+1/2,j}^{l} \right]$$

(4-4)

In order to avoid the scheme converging to non-physical solutions an entropy correction function has been used:

$$\xi(z) = \begin{cases} |z| & |z| \geq \varepsilon \\ (z^2 + \varepsilon^2)/2\varepsilon & |z| < \varepsilon \end{cases}$$

(4-5)

In (4) a_x^{l} represents the l-th component of the vector of local characteristic speeds. The difference in characteristic variable is defined as (Leveque and Yee, 1990)

$$(\boldsymbol{\alpha}_x)_{i+1/2} = (\mathbf{R}_A)_{i+1/2,j}^{-1} (\mathbf{q}_{i+1,j} - \mathbf{q}_{i,j})$$

(4-6)

A simple limiter for the l-th component of vector α_x (Harten, 1983; Leveque and Yee, 1990) is defined as

$$(Q_x)_{i+1/2,j}^{l} = minmod(\alpha_{i-1/2,j}^{l}, \alpha_{i+1/2,j}^{l}, \alpha_{i+3/2,j}^{l})$$

(4-7)

in which Q_x^{l} is the flux after correction by the limiter. The minmod function is defined as

$$minmod(a,b,c)=\begin{cases} s\,min(\,|a|,|b|,|c|\,) & s=sgn(\,a\,)=sgn(\,b\,)=sgn(\,c\,) \\ 0 & otherwise \end{cases} \tag{4-8}$$

At the interface of the grid, $\mathbf{q}_{i+1/2,j}$ is computed on the basis of Roe's averaging (Roe, 1981) as follows:

$$h_{i+1/2,j}=\frac{h_{i+1,j}+h_{i,j}}{2} \tag{4-9}$$

$$u_{i+1/2,j}=\frac{\sqrt{h_{i+1,j}}\,u_{i+1,j}+\sqrt{h_{i,j}}\,u_{i,j}}{\sqrt{h_{i+1,j}}+\sqrt{h_{i,j}}} \tag{4-10}$$

Following the similar formulation, an identical set of equations corresponding to $\mathbf{\Phi}_y$, $\mathbf{a}_y$, $\mathbf{Q}_y$, and $\mathbf{q}_{i,j+1/2}$ can likewise be developed in a straightforward way.

4.2. Well-balanced property and treatment of dry front

If the bathymetry is not horizontal, the NLSW involves source terms. It is known that these source terms should be treated carefully especially when the bottom topography has steep slopes, since the bottom variations terms may generate artificial numerical waves. In the case of the smoothly varying bathymetry, in order to avoid the occurrence of spurious oscillations, several methods have been proposed (Vincent et al., 2001a). Among them the surface gradient method, which gives rise to a well-balanced formulation of the flux and source terms, is adopted in this study. Detailed explanation on the surface gradient method can be found by Zou et al. (2001) and Wei et al. (2006). For dealing with high irregular bathymetry, the model was additionally incorporated an improved gradient method (Tseng, 2003) which uses the surface gradient instead of the depth gradient for TVD corrections, considering the balancing of the source terms and the flux gradients.

Various techniques have been proposed on the treatment of wave propagation on drybed. Representative approaches include the wetting and drying methods (e.g.Balzano, 1998), slot models (Kennedy et al., 2000; Madsen et al., 1997), and linear extrapolation method (Lynett et al., 2002). In the present study, a simple wetting and drying method is adopted from a practical point of view, in which a thin water layer (typical depth is 10^{-4} m) is imposed in dry zones.

5. Model validation

To verify and validate the ability of the model, we have conducted several bench-mark tests. The numerical computation was verified with either analytical solution or experimental data. Through such comparison, the accuracy and robust of the model were addressed.

5.1.Tidal wave over steps

To meet the well-balanced criteria, a numerical model must be capable of keeping a constant surface elevation in a frictionless flow over varying bathymetry. Accordingly, tidal wave over two steps is investigated to validate the well-balanced ability of the model in reproducing the flow over the abruptly varying topography. This test is first introduced by EU CADAM project. Then the test is investigated by Liang and Marche (2009) and Zhou et al. (2002). The bed profile is defined by

$$z_b = \begin{cases} 8 & if \quad /x-750/\leq 187.5 \\ 0 & otherwise \end{cases} \tag{5-1}$$

And the channel has length of 1500m.
The initial conditions is set as follows.

$$h(x,0)=H(x)$$

$$u(x,0)=0$$

and the upstream and downstream boundary conditions are assigned by

$$h(0,t) = H(0) + 4 - 4\sin\left[\pi\left(\frac{4t}{86400} + \frac{1}{2}\right)\right] \tag{5-2}$$

$$u(L,0)=0$$

Where H(x)=H(0)-Z(b) with H(0)=16m

According to Bermudez and Vazquez (1994), with the aforementioned conditions, the tidal wave is a relatively short; therefore, an asymptotic analytical solution is derived as:

$$h(x,t) = H(x) + 4 - 4\sin\left[\pi\left(\frac{4t}{86400} + \frac{1}{2}\right)\right] \tag{5-3}$$

$$u(x,t) = \frac{(x-L)\pi}{5400h(x,t)} cos\left[\pi\left(\frac{4t}{86400} + \frac{1}{2}\right)\right] \quad \text{(5-4)}$$

The computational domain is divided into 200 uniform cells with Δx=7.5m. In this case, the vertical step is simulated by the very steep slope that is ratio between the step height and the grid size. The numerical computation is conducted with Δt=0.2s. A collation of numerical and analytical results is conducted at t=10800 s (the half-risen tidal flow) and t=32400 (the half-ebb tidal flow). Figures 5.1 and 5.2 reveal that the numerical results for both water surface and velocity agree very well with the analytical ones. The water surface is constant along the channel. Although no cumbersome treatment for the head loss at the vertical steps is added to the source terms, yet the model has proven its well-balanced capability of dealing with the steep topography.
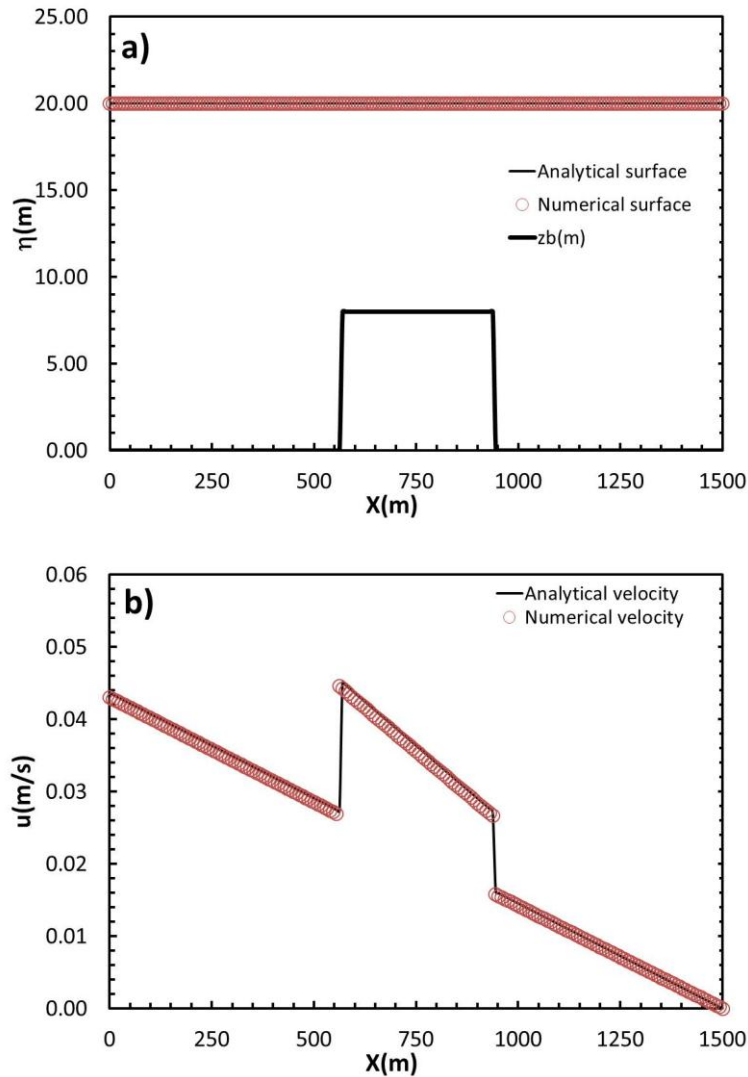
Figure 5.1. Tidal wave over steps: free surface (a) and velocity profiles (b) at t=10800s
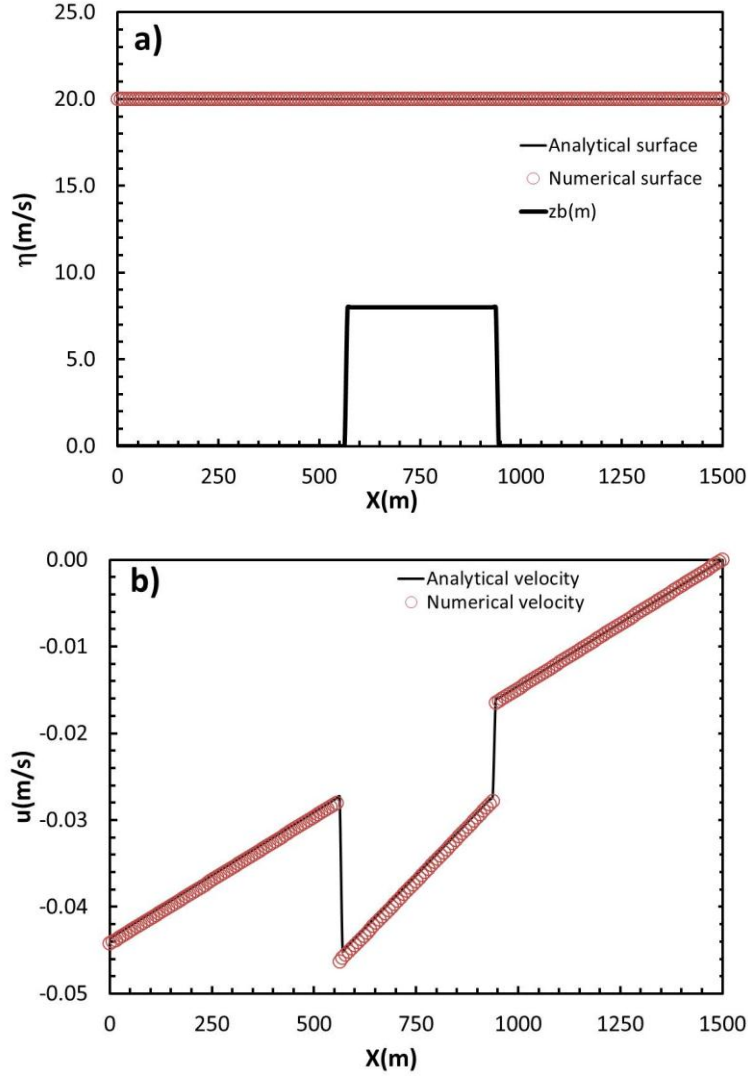
Figure 5.2. Tidal wave over steps: free surface and velocity profiles at t=32400s

5.2. Preservation of still water surface

To examine whether the still water surface runs up at dry-wetting interface or not, we simulate the still water surface surrounding an emerged island during the time period of 200s. Accordingly, the island is located at the center of a 1m long friction-less channel, with the bed topography defined by:

$$z_b = \begin{cases} 0.2 & if \quad /x - 750/ \leq 187.5 \\ 0 & otherwise \end{cases}$$ (5-5)

The still surface elevation given by $\eta = \max(0.1, z_b)$ is set as the initial condition. The upstream and downstream boundaries are closed. The domain is descreted into 100 uniform cells. The time step is assigned as $\Delta t = 0.002$ s. During the running time of

200s, the water surface remains static as observed in Fig. 5.3. This results is similar to that of the numerical model developed by Liang and Marche (2009).
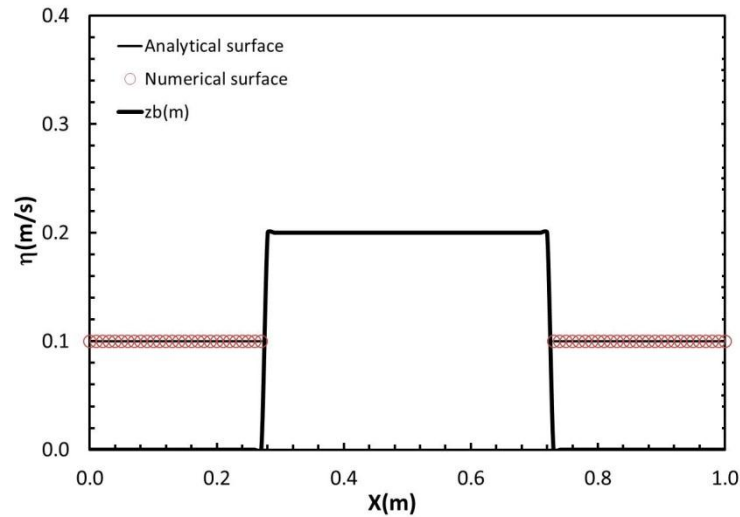
Figure 5.3. Still water test: undisturbed still water surface after t=200s

5.3. Dam-Break on wet bottom

Firstly, the dam-break problem on wet bottom is considered. To establish this problem, a thin partition is located at the section $x = 0$. For $x<0$ the water has the depth h_0 and for $x>0$ the depth h_1. The water is assumed to be at rest on both side of dam initially. The partition is then suddenly released at time $t = 0$.

A comparison between the analytical solutions (Stoker, 1957) and the numerical results based on the TVD MacCormack scheme are shown in Fig. 5.4. The initial water depths are set as $h_0 = 12.0$ m and $h_1 = 4.0$ m. A grid interval of $\Delta x = 0.5$ m is used with $\Delta t = 0.01$ s. It is recognized that very good agreement is obtained between analytical and numerical results. The flow evolves with the generation of a right-moving shock (bore). The shock front is captured sharply without numerical oscillations. The propagation speed of shock agrees very well with the characteristic theory. The agreement in velocity field is also quite satisfactory.
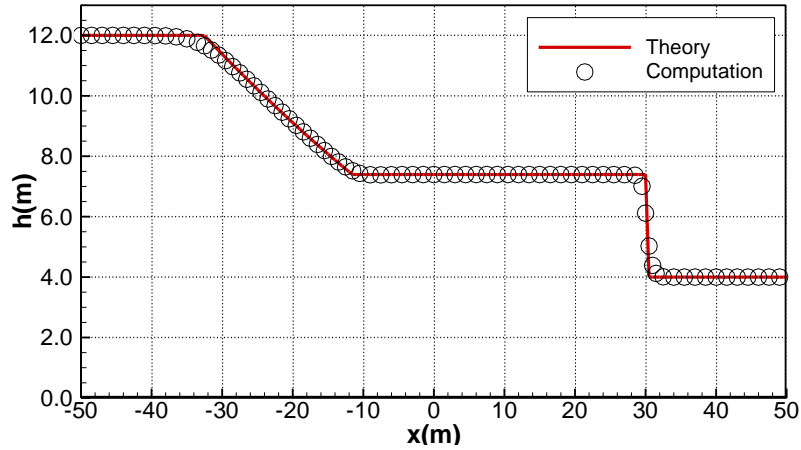
a) Water surface profile at *t*=3s
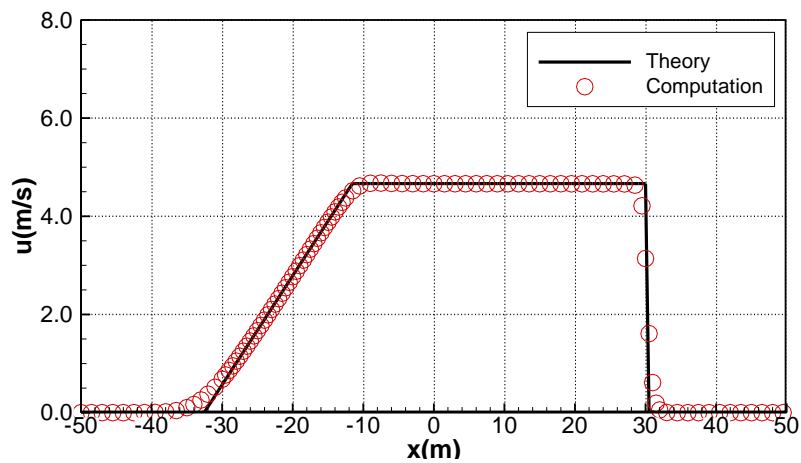
b) Velocity profile at *t*=3s

Figure 5.4. Comparison between the analytical solutions and the numerical results for a dam-break problem on wet bottom

5.4. Dam-Break on dry bottom

The numerical model is then applied to a dam-break problem on dry bottom. The initial water depths are set as $h_0 = 12.0$ m and $h_1 = 10^{-4}$ m. We use a grid interval of $\Delta x = 0.5$ m with $\Delta t = 0.01$ s. A comparison between the theoretical solutions of Stoker (1957) and the numerical results are shown in Fig. 5.5. For the water surface profile, the agreement between the numerical and analytical results is very good. The transition between the wet and the dry zone is calculated stably. At the front edge, the transition of surface profile is monotonic and smooth: No artificial hump appears. On the velocity profile, the numerical results from the TVD-MacCormack scheme capture the general features of the analytical solution, but some discrepancies appear near the wave front. The numerical profile becomes more diffusive and the wave front

in the numerical solution is slightly behind the corresponding one in the analytical solutions. A reason for is that when a peak appears on the velocity profile, the accuracy of TVD scheme becomes 1st order surrounding it. Additionally, according to Vincent et al. (2001b), the thin water layer in the dry zone impacts on the dynamics near the wet-dry interface inducing approximation errors, which cause a delay in the numerical solution. Nevertheless, the results are globally accurate and totally non-oscillatory. The present results are comparable to existing studies.

5.5. Long wave oscillation in a canal with a parabolic cross-section

The numerical model is further validated through comparison with the theory for the long wave oscillation in a canal with a parabolic cross-section. Thacker (1981) presented an analytical solution to the NSWE, where the free surface water elevation (Z) and the basin shape (Z_f) are given as.

$$Z = 2\eta \frac{D_0}{L} \cos \omega t \left(\frac{x}{L} - \frac{\eta}{2L} \cos \omega t \right) + D_0 \, , \omega = \sqrt{\frac{2gD_0}{L^2}}$$

(5-6)

$$Z_f = D_0 \frac{x^2}{L^2}$$

(5-7)

where D_o = representative water depth at the basin center, x = distance from the center point, L = representative shoreline location, η = amplitude of the oscillation, and ω= oscillation frequency. The numerical values used for this test are: D_o = 2.0 m, $L = 10\sqrt{10}$ m, and η = 10 m. A grid interval of $\Delta x = \Delta y = 5$ m is used with $\Delta t = 0.01$s
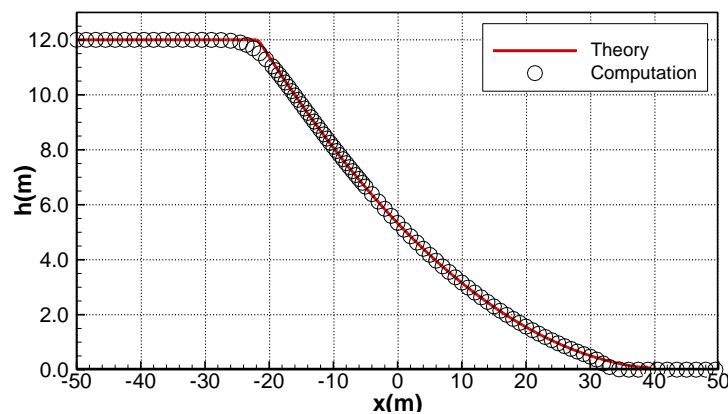
a) Water surface profile at t=2s
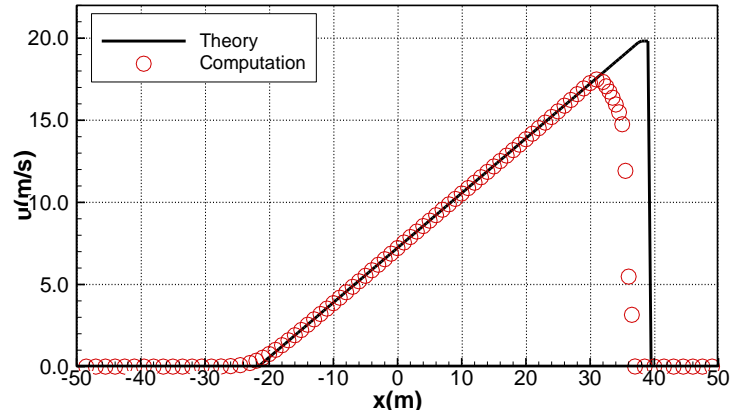
b) Velocity profile at *t*=2s

Figure 5.5. Comparison between the analytical solutions and the numerical results for a dam-break problem on dry bottom
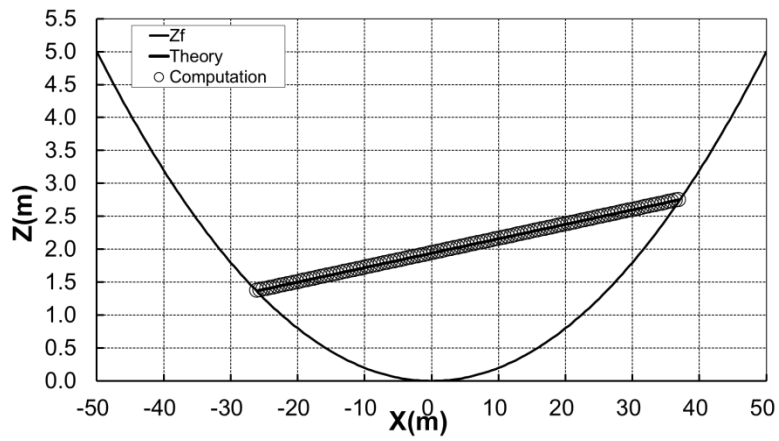
a) Water surface profile at t=5s
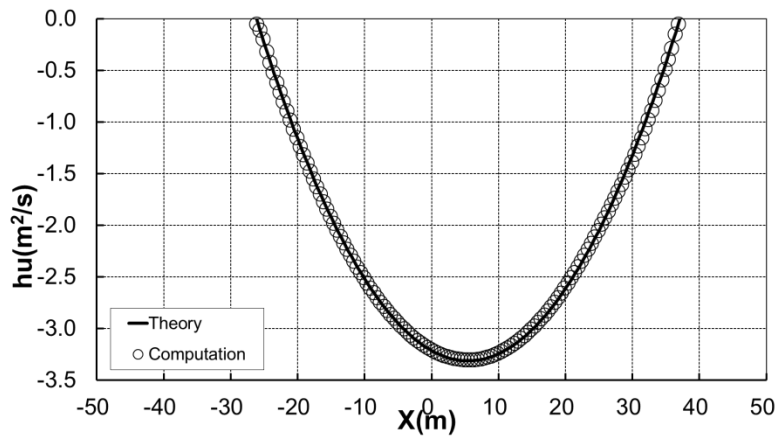
b) Flux profile at t=5s
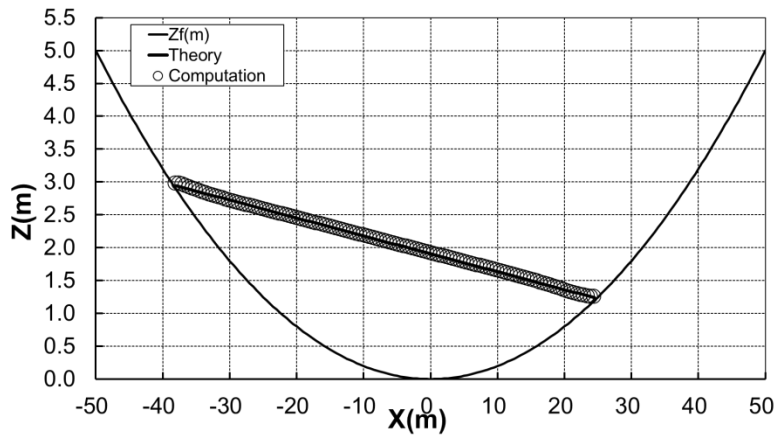
c) Water surface profile at t=20s
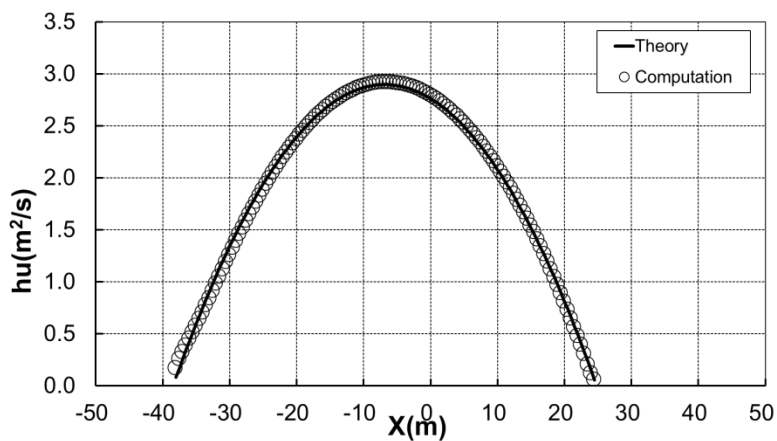
d) Flux profile at t=20s

Figure 5.6. Comparison between the analytical solutions and the numerical results for water oscillation

The comparison between the numerical and analytical results is shown in Fig. 5.6. The results including water surface (Z) and unit-width discharge in the x-direction (hu) are considered at $t=$ 5s and $t=20$s. The comparison reveals very good agreements. No obvious distortion is found in the wet-dry interface. In addition, the agreement with the analytical solution during the back-wash phase has been confirmed to be satisfactory. These results thus validate the high capability of the numerical model in tracking the moving boundary on a sloping bathymetry.

5.6. Dam -break wave over a triangular bottom sill
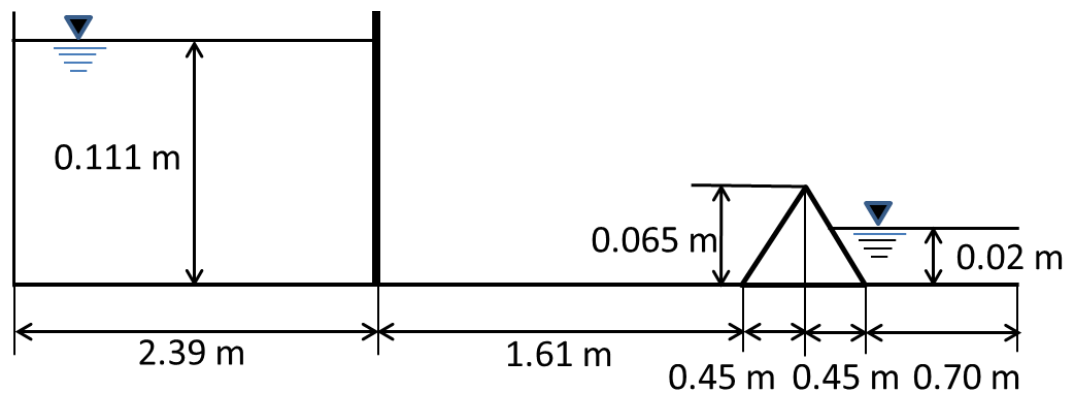
Figure 5.7. Sketch of dam break over a triangular bottom

The bore propagation over the dry adverse and normal slopes is investigated numerically. In this case, the experiment conducted by IMPACT project is reproduced by the present model. The sketch of the laboratory experiment is shown in Fig 5.7. The upstream and downstream ends are assumed as solid walls. A gate is located at 2.69 m far from the upstream boundary. A reservoir with an initial water depth of 0.111m is established from the upstream boundary to the gate. A triangular hump is put at 4m far from the upstream boundary. The height of hump is 0.065m. The projected length of both adverse and normal slopes of the hump is 0.45 m. Another reservoir with initial water depth of 0.02m is set from the downstream of the hump to the downstream boundary. In the dry area, the friction is zero and in the wet area, the Manning coefficient is assigned as n=0.011 $sm^{-1/3}$. Computation is implemented for 45 s on a grid with uniform resolution of 5cm.

At t=0s, the gate is suddenly opened, releasing the initial still water at the reservoir into the downstream area. After t=1.3s, the front wave reaches the bottom of the hump and flow runs up along the adverse slope (Fig. 5.8a). During the run up, the bore wave is partially reflected by the hump, generating a bore propagating in an opposition direction toward the upstream end. At t=1.8s, the wave starts to overtop the hump and subsequently flows on the downward slope as a supercritical flow. The bore wave reaches the still water surface at t= 2.3s. The still water makes the front wave be suddenly slowed down, forming a bore which propagates toward the downstream end (Fig. 5.8b). The bore wave reaches the downstream end and is reflected back by the downstream end at t=3.4s (Fig. 5.8c). After that, the water wave propagates backward but not overtop the hump at this time. The second bore induced by the 2nd reflection

79

against the downstream wall is strong enough to overtop the hump at $t=8.3$s (Fig. 5.8d). Then, it joined with the bore induced by the refection from the upstream side of the hump and propagates toward the upstream end. The bore wave is reflected by the upstream wall at $t=9.4$ s. Several reflections of the flow against the wall and the hump are observed until the end of simulation. Figure 5.8 indicates that the numerical water surface agrees very well with the experimental water surface conducted by Soares-Frazão (2007) .
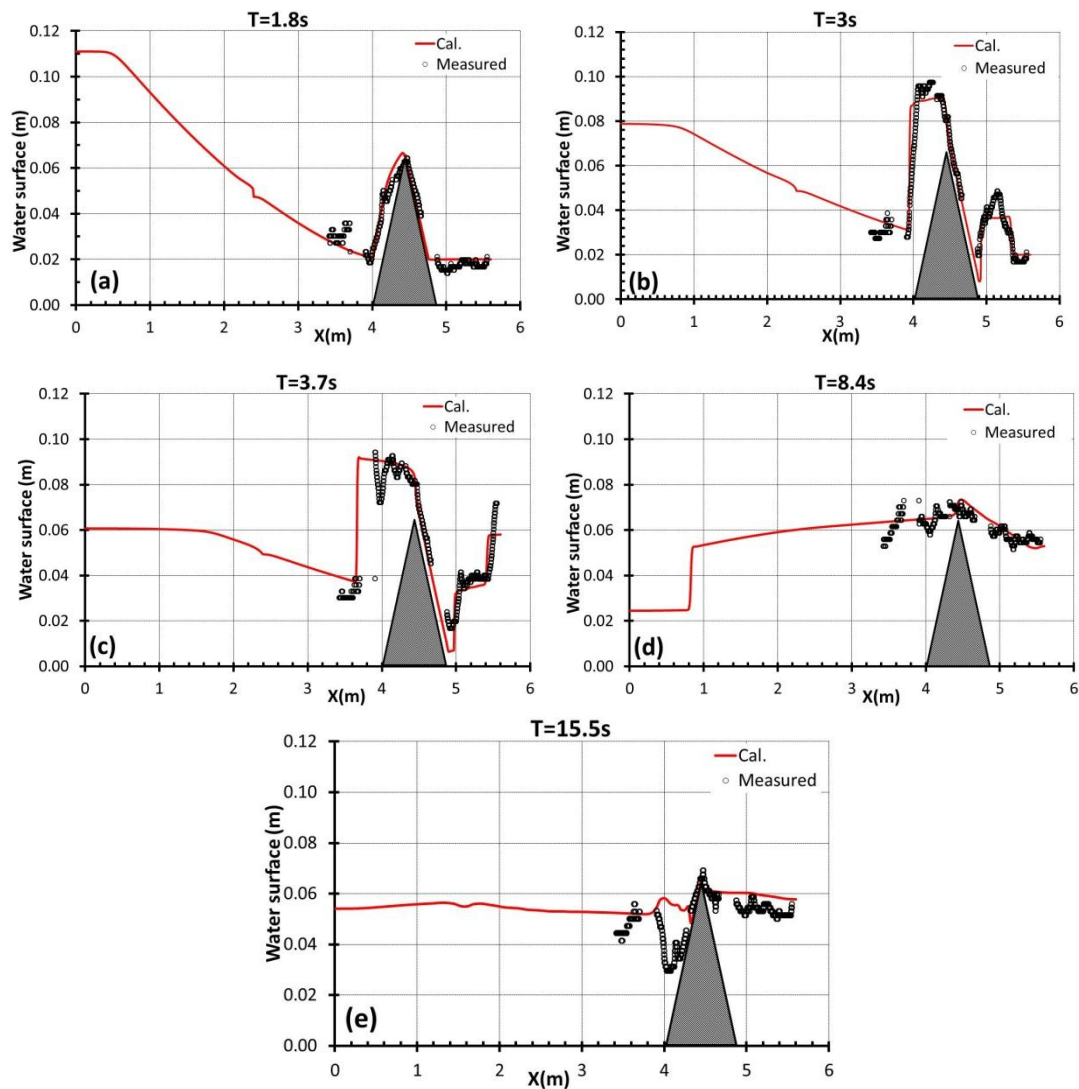
Figure 5.8. Longitudinal profile of water surface at different time
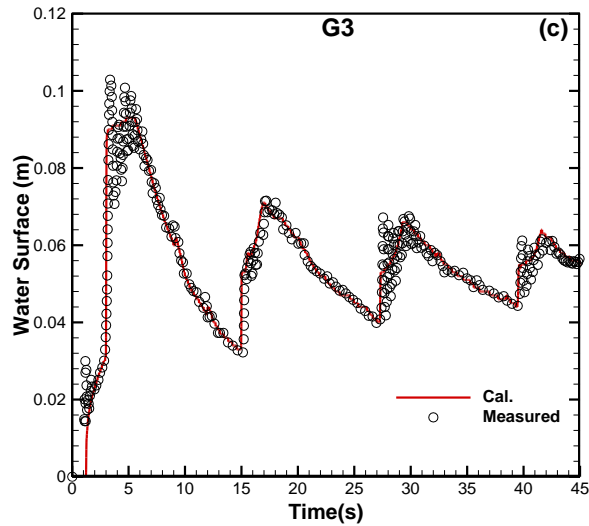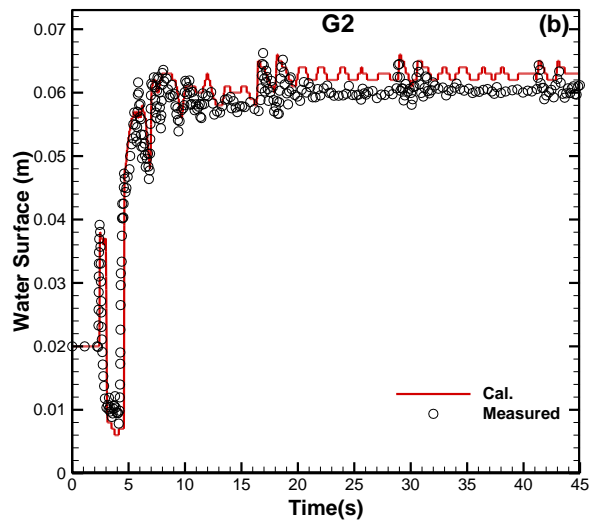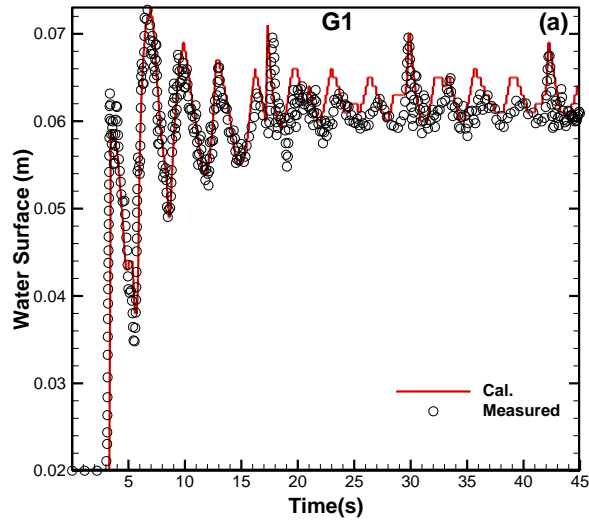
Figure 5.9. Comparison of experimental and numerical water surface at three gauges

Time series of water surface are recorded at three gauges in order to describe the complicated variation of the flow and to compare with the laboratory experiment. Gauge G3 is located upstream from the hump, at x=3.935 m (x=0 at the upstream boundary). Gauges G2, G1 are located downstream from the hump, at x=4.925 m and x=5.575 m, respectively. It is recognized that there was an excellent agreement between numerical and measured water surface at three gauges (Fig. 5.9). Gauge G2 is located immediately downstream from the hump. As mentioned above, at t=2.3s, a bore is generated as a transition between the supercritical flow on the downstream side of the hump and the still water surface, causing the water level at G2 to increase rapidly (Fig. 5.9b). Subsequently, while the bore travelled toward the end boundary, the water with high energy running down played an role as a jet that made the water level lower (Fig. 5.9b). Upon reaching the end boundary, the water level at G1 increased sharply (Fig 5.9a), generating a surge which moved back to the hump. The bore runs up the downstream side of the hump and be totally reflected by the hump. Therefore, the water level at G2 increases sharply again and the second surge is created to travel toward the downstream end. After the second reflection of the downstream boundary, the energy of the surge is adequate to partly overtop the hump. As a result of this, amplitude of the water level at G1 decreases generally until the end of simulation. Similarly, gauge G3 describes the propagation and reflection of several bores (Fig 5.9c). It is clear that the water level at G3 is more variable than those at G1 and G2. This can be explained that in the upstream area, the initial flow with high momentum flows over the dry and long bottom while in the downstream area, the flow with lower momentum flows over the wet and short bottom.

Overall, the dam-break wave over the mixed wet-dry bottom consisting of the triangular hump experiences many reflections against the boundaries and the hump. This makes the flow very complex. Yet, the present model is able to accurately capture such complex characteristics of the flow. It proves that the model could reproduce the one dimensional dam-breaking wave propagating over the highly irregular topography.

5.7. Dam-break wave propagation over a complex topography

In previous validation, it is realized that shallow water equation solved by TVD-MacComack scheme reproduces accurately the dam break wave travelling over the triangular hump. In this validation, we further examine how accurate the model can simulate the dam break wave propagating over a triangular hump and subsequently overtopping a vertical wall. Accordingly, a trapezoid hump was put at $x=0$ m (x was distance far from the hump)(Fig. 5.10). The height of the hump is 0.04 m. Immediately, above the hump, a thin gate divides the entire domain into two parts: the upstream part and the downstream part. The upstream part is considered as a reservoir. The initial water depth in the reservoir is h_1, which is a range of 0.15-0.3 m. When $x \geq 3.06$ m, the bed level is set as 0.105m and the initial water depth is 10^{-4} m. When $0<x<3.06$ m, the initial water depth is 0.05 m. The upstream boundary is close while the downstream boundary is transmissive. The boundary and initial condition of the simulation is adapted from the laboratory experiment conducted by Umeda et al. (2013). The grid size is set as $\Delta x=0.01$m. The simulation is run for 9 s with time step $\Delta t=0.002$s. The Manning coefficient is assigned as $n=0.0105$ sm$^{-1/3}$ in the wet area. In the dry area, the friction is zero.

To examine the hydrodynamic response of the flow at different sites along the channel, four wave gauges are located along the channel. The gauges W_1 and W_2 are placed between the hump and the vertical step, at $x=1.99$ m and $x=3.05$ m, respectively. These gauges measures the interaction of the bore against the hump and the vertical step. The positions of W_3 and W_4 are $x=3.82$ m and $x=4.81$ m, respectively. These gauges defines how the flow varies after overtopping the vertical step. In this study, we simulate for 4 cases of h_1 including $h_1=15$cm, 20cm, 25 cm and 30 cm. Here, we only show the simulated result of the case $h_1=20$cm.
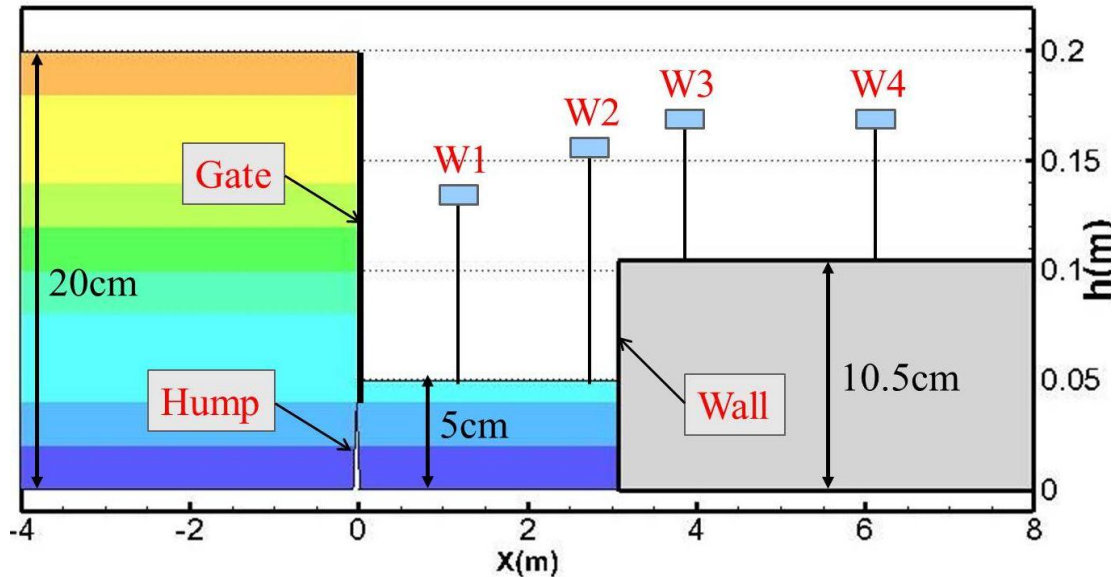
Figure 5.10. Sketch of dam break over a complex topography

Figure 5.11 shows the comparison between the numerical and experimental results at four gauges. It indicates that there is a very good agreement at gauges W_1 and W_2. At t=2.2 s, the bore reaches the vertical step. Immediately, the bore overtops the vertical step. Simultaneously, it is partially reflected by the vertical step, causing the water surface at W_2 sharply increase (Fig. 5.11b). Subsequently, the reflective bore travells back toward the hump and crosses the gauge W_1 at t=3.9s. As a result of this, the water surface at W_1 increases rapidly at t=3.9s (Fig. 5.11a). It is recognized that there remains small discrepancy between the numerical and experimental water surface at gauges W_1 and W_2. This could be due to the occurrence of wave breaking at the bore front, which is not incorporated in the present model. At the gauges W_2 and W_3, the computational arriving time of the bore which is important in dam-break flow agrees very well with the experimental one. However, the numerical water surface elevation is overestimated compared with the experimental water surface. In this case, the reason is attributed to that the hydrostatic assumption of shallow water equation is violated when the water flows over the vertical step. Comparison between the numerical and experimental results in terms of water surface and ariving time at W_3 and W_4 is conducted for the case h_1=25cm. It indicates that the numerical model predicts the arriving time very well, but overestimates the water surface. By using the different numerical schemes, other researchers (e.g.(Liang and Marche, 2009)) also encounters the similar phenomenon.
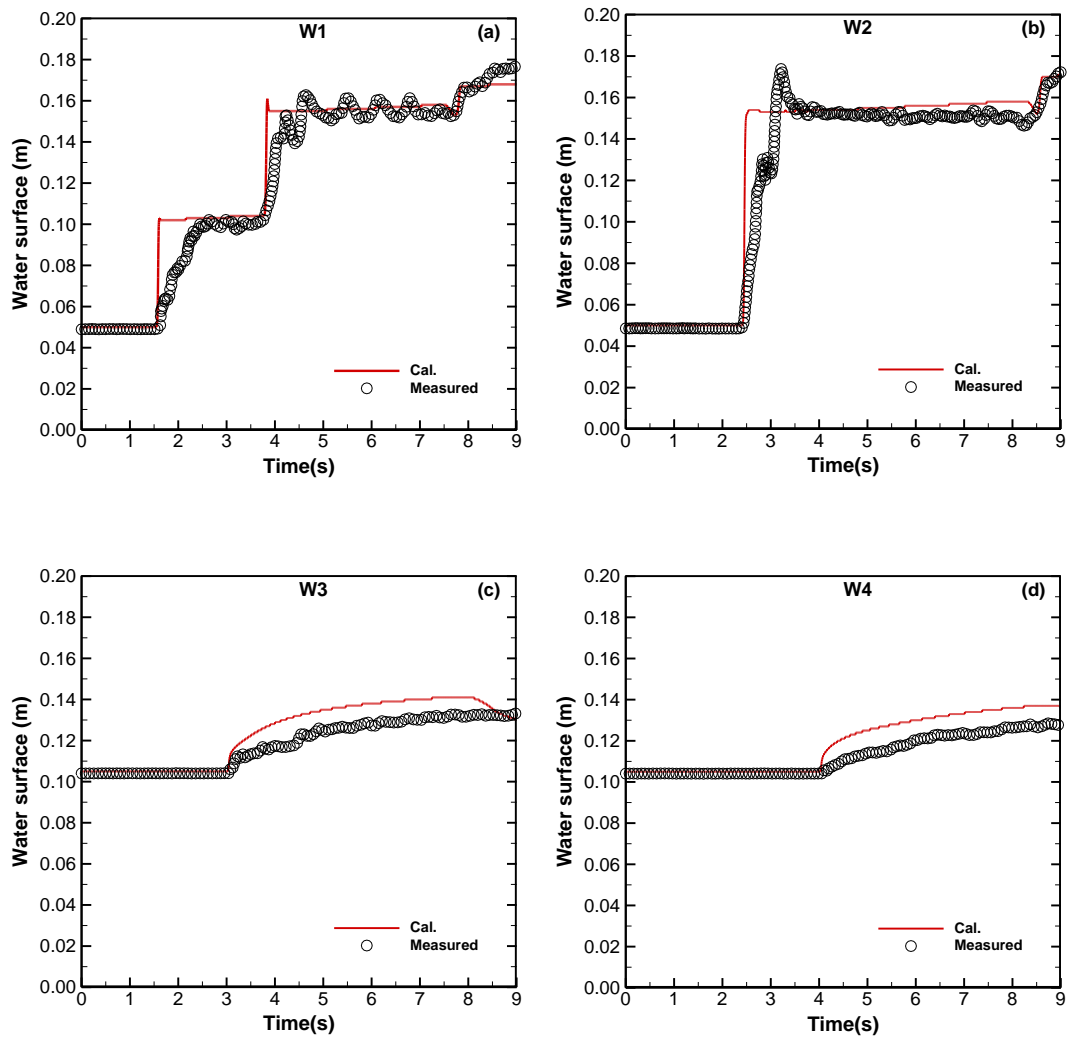
Figure 5.11. Comparision of experimental and numerical water surface at four gauges.
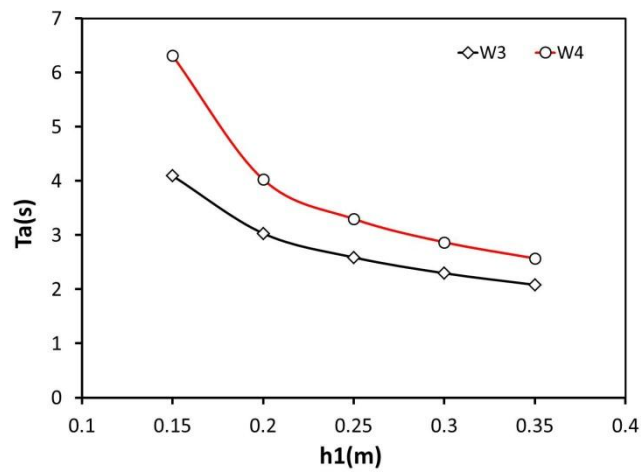
Figure 5.12. Relation between arriving time and the initial water height of the reservoir
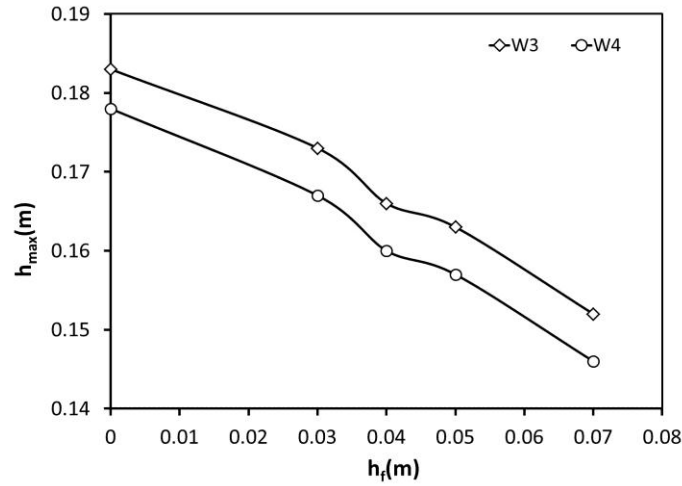
Figure 5.13. Relation between the height of the fence and the maximum inundation height of the downstream area.

Figure 5.12 indicates the relation between arriving times of bores at W_3 and W_4 and the initial water depth of the reservoir (h_1). Clearly, the higher the h_1 is the shorter the arriving time of the bore is at W_3 and W_4. In addition, in order to exame influence of a fence on maximum inundation heighs at W_3 and W_4, we put a fence with varying heighs at the vertical steps. Figure 5.13 describes that when the heigh of the fence increases, the maximum inundation heighs at W_3 and W_4 decrease.

5.8. Three dimensional schematic dam break

Although the shallow water equation is proper to describe the depth-integrated flow, yet it is interesting to examine how reasonable a two horizontally dimensional model can reproduce a three dimensional flow. For a practical purpose, such task brings reduction in computational expense in comparison with 3D model. Accordingly, in this section, we use the present model to simulate a 3D breaking-dam flow on the basis of the experiment conducted by the Maritime Research Institute Netherlands (Fig. 5.14). A large tank of $3.22 \times 1 \times 1$ m is used. The leftmost boundary is set as x=0 m. A door is placed at x=1.228 m. Behind the door, a still water depth is set as 0.55 m. The downstream of the door is dry. A box of $0.403 \times 0.161 \times 0.161$ m is put at x=2.476 m. Four lateral boundaries are close. The domain is descritized into a uniform grid with size $\Delta x = \Delta y = 0.005$ m. We assign time step Δt=0.001 s. Duration of simulation is 7.4 s. The Manning friction coefficient for the tank bed was estimated as 0.01.
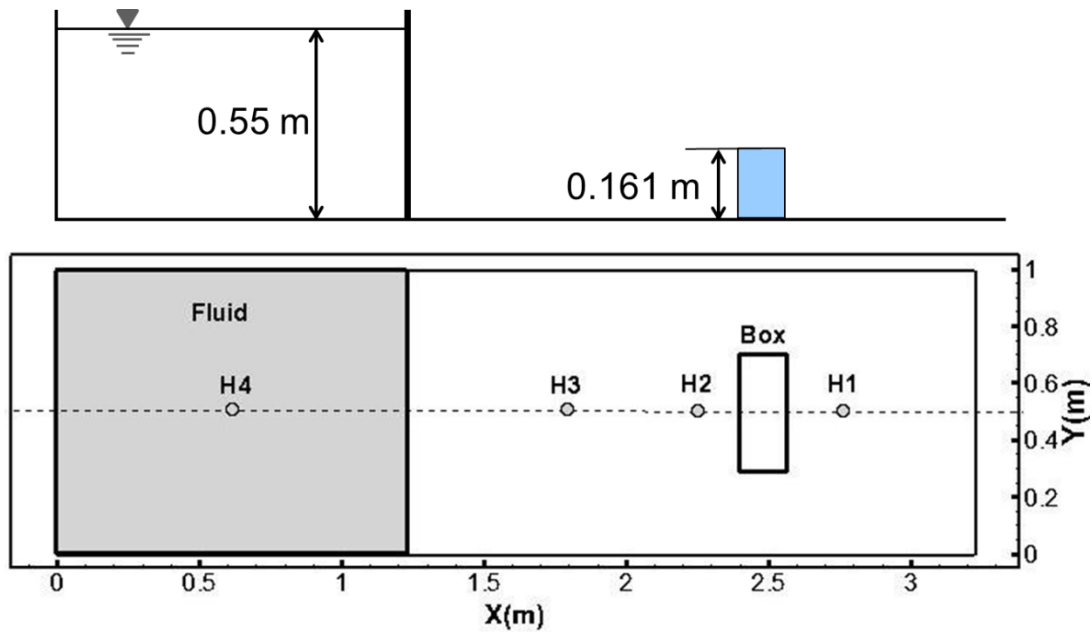
Figure 5.14. Sketch of 3D dam-breaking flow

Four gauges are located within the tank: H_4 in the reservoir; H_3 between the reservoir and the box; H_2 immediately in front of the box, H_1 immediately behind the box (Fig. 10.14). Comparison between the numerical and experimental results indicates that the numerical model describe well the general characteristics of the flow. The numerical model captures well the reflective waves of the boundaries and the box. However, in some periods, the magnitude of the computed water surface is considerably different from that of the measured water surface. Nearly similar result is also obtained when we applied the DART model (Liang, 2010a) to simulate the existing problem (Fig. 5.15). It is therefore considered that less precise prediction of the present model to a 3D flow could be due to an inherent disadvantage of the existing mathematical model. Namely, as mentioned above, non-hydrostatic pressure distribution surrounding the box may be a reason of such less accurate prediction. In addition, the Manning–Strickler formula used to express the bottom friction may be inadequate for dam-break waves since it is originally derived for uniform-flow conditions (Frazão and Guinot, 2007). Nevertheless, with being ease to treat source terms together with less expensive cost of computation, the developed model has high potential to reproduce the 3D real flow for practical purposes.
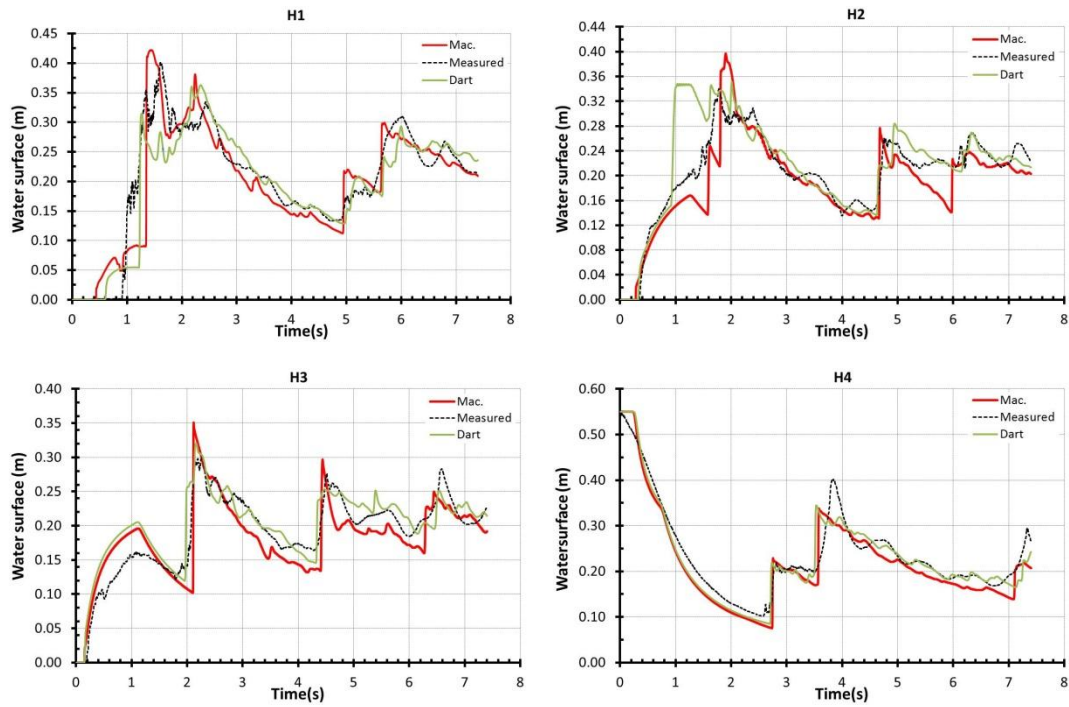
Figure 5.15. Comparison of experimental and numerical water surface at four gauges

6.Wave run up over a bank

To mitigate the damage of disasters such as flood events and tsunami, it is essential to numerically investigate the process where the flood wave or tsunami runs up over the river banks into adjacent areas. In this section, accordingly, we first indicate how a bore propagates along a channel. Subsequently, we study how the bore overtops the river banks and consequently induces the inundation of the adjacent areas. For these purpose, the propagation of the bore in a curved channel with a parabolic cross-section is simulated. The channel is composed of a circular bend (with radius R) plus upstream and downstream legs. The bore is made by a similar procedure as in the dam-break problem in the previous section . A gate is located at $x = 900$ m and divides the whole domain two spatial regions: in the upstream part still water of initial depth $h_0 = 4.0$ m is present, while in the downstream part the initial still water depth is set as $h_1 = 0.0$ m. The gate is suddenly released at time $t = 0$. The top elevation of channel banks is set as 2.5 m . The elevation of adjacent area is set as 0.0 m. In the computation, a grid interval of $\Delta x = \Delta y = 5$ m is used with $\Delta t = 0.1$ s.

Figure 6.1 illustrates the evolution of water surface in time and space. Once the water is released, bore wave propagates downstream. In the upstream leg of the channel, the shape of bore is symmetric through the center line of the channel. When entering the curved bend, the bore tilts higher outward against the outer bank. This phenomenon results from effect of inertial force. The water surface elevation at the outer region is higher than that at the inner region, which induces the higher propagating speed of wave at the outer region than at the inner one. Additionally, Fig.5a and b indicate clearly the effect of radius of the curved bend (R) on overtopping degree of the wave. Namely, the smaller the radius is, the stronger the wave runs up. A series of snapshots of free surface elevations obtained from the numerical results are shown in Fig 6.2. The numerical model reproduces the complicated flow field with steep front in a stable manner.

a)R=600 m   b) R=300 m
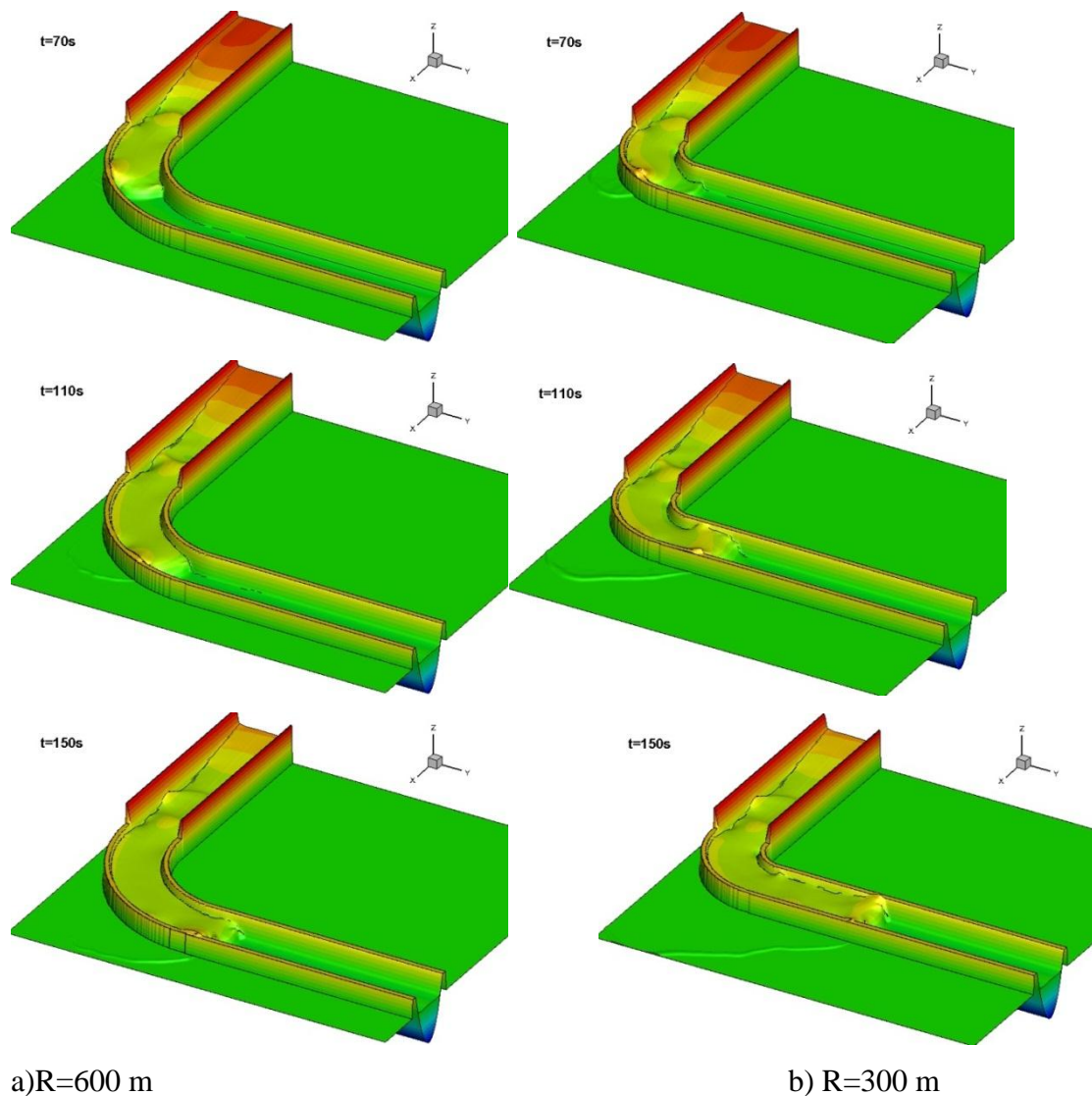
Figure 6.1.Temporal and spatial evolution of water surface
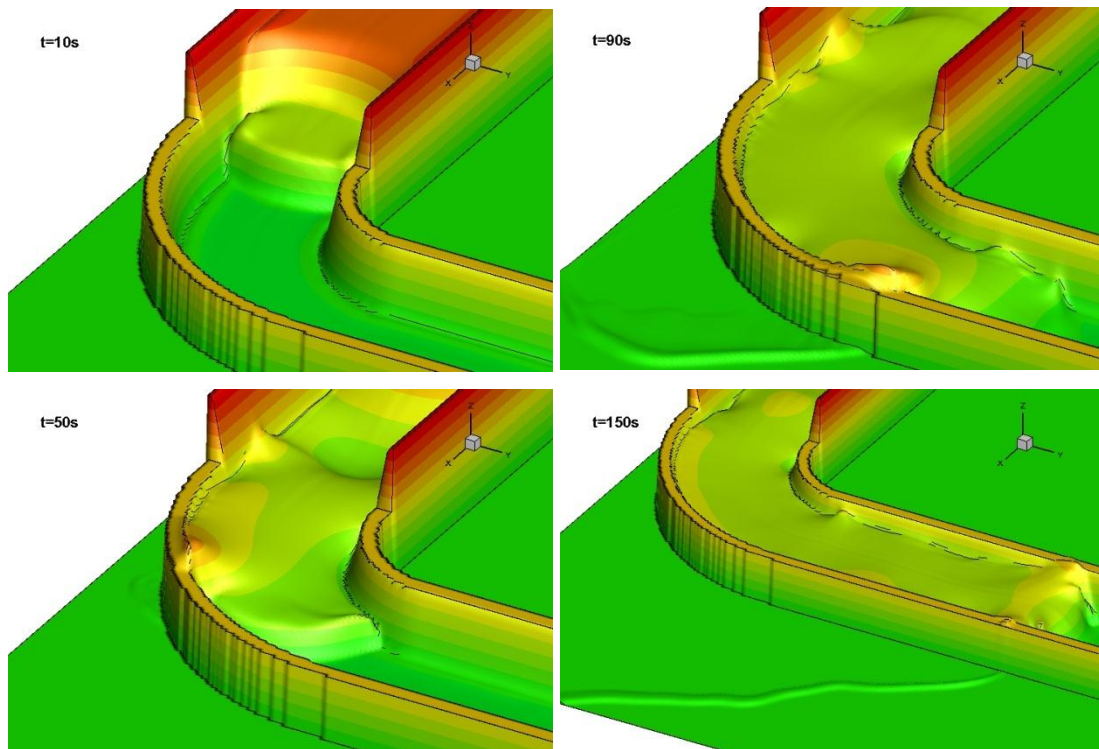
Figure 6.2.Close-up view of wave running up over the channel banks for the case R=300m

(Vertical scale is exaggerated.)

7.Conclusions

In the present study, a numerical model is developed to solve the Nonlinear Shal-low Water Equations based on the TVD-MacCormack scheme, which has the 2nd order accuracy in time and space. Effective treatments have been implemented to achieve well-balancing through modifying local bed and using the water surface gradient instead of the depth gradient for TVD corrections. Concurrently, the model is capable of capturing well the moving wet-dry interface by incorporating with the surface gradient method.

The applicability of the numerical model is verified through comparison with ex-isting theoretical studies. The shock-capturing ability of the model is tested against two frictionless transcritical flow problems: the dam-break on wet bottom and the dam-break on dry bottom. These tests prove that the numerical model captures very well the moving shock in both the wet and dry bottom. Then, the well-balanced property of the model is confirmed when the water surface remains constant along the channel in the case where tidal wave runs over two steps. In addition, the high capa-bility of the numerical model in tracking the moving boundary on a sloping

bathymetry is examined. The results reveal that the water surface keeps planar during the simulated duration. No distortion appears adjacent to the wet-dry interface. In all above tests, very good agreement between the numerical and analytical results is obtained.

In a second step, the performance of the numerical scheme is validated with several laboratory experiments. Firstly, the present model is able to accurately capture the complex characteristics of the flow, which is induced by the dam-break wave over the mixed wet-dry bottom consisting of the triangular hump. It proves that the model could reproduce the one-dimensional dam-breaking wave propagating over the highly irregular topography. More difficultly, the model is applied to a dam break wave propagating over a triangular hump and subsequently overtopping a vertical wall. The model reasonably describes the response of the flow until the flow reaches the vertical wall, but after that, there is a discrepancy between the computed and measured water surfaces due to the violation of the key assumption of the shallow water equation at the vertical wall. However, the model predicts the arriving time very well after the flow overtops the vertical wall. Subsequently, dynamics of the 3D flow is simulated by using the existing model. The numerical model captures well the reflective waves of the boundaries and the box. However, in some periods, the magnitude of the computed water surface is considerably different from that of the measured water surface. Yet, for practical purposes, the model has advantage of being easy to treat the source term together with less expensive cost of computation in comparision with alternative 2 D or 3 D models. Finally, the model is utilized to study the behavior of wave overtopping river banks of a curved channel with a parabolic cross-section. Characteristic behavior of wave transformation during propagation and overtopping processes is realized clearly.

Part IV. Conclusion

1.Summary

Comprehensive understanding of the long-term variation in the riverbed in relation to its controlling factors is essential to the rational management of disturbed rivers in the first part. The present study uses a 58-year topographic survey of the lower Tedori River, Japan and related data on human impacts to clarify the characteristics of long-term vertical adjustments of the riverbed. The main works in part I are summarized as follows.

First, high water level (HWL) in river channel was computed by using a hydraulic model (RIC-Nays). Next, the mean riverbed level of each cross-section was mathematically averaged over the cross-sectional extent located below HWL. Subsequently, a comparative analysis was conducted to quantify the river bed variation trends in time and space. Namely, the decadal variation in the riverbed was analyzed following the presence or absence of human activities. More specifically, the yearly response of the riverbed elevation to the varying rate of the human impacts was addressed by using nonlinear regression analysis.

The channel variation was examined by a collation of the cross-sections surveyed in 1950, 1979, and 2007. Thanks to such work, change in the erosion/deposition along the cross-sectional direction with respect to change in human activities also was indicated. Additionally, temporal and spatial variation in widths of the river transporting bankfull discharge was analyzed. By using aerial photographs of the lower Tedori river at various years, change in river pattern was observed. Simultaneously, the alteration of boundary condition such as sediment mean diameter, vegetation cover was found as a consequence of sand and gravel extraction and Tedori dam construction.

To explain the change in the morphological characteristics of the lower Tedori river, balance equation of sediment was established. Based on this equation, the variation in the riverbed sediment volume was analyzed in relation to change in incoming and outgoing sand and gravel due to natural or/and anthropogenic factors. The riverbed sediment volume was computed on the basis of the topographic survey. The incoming sand and gravel volume was estimated upon the sediment deposition in the Tedorigawa dam. The volume of sediment extraction was defined according to

surveyed data. Through using sediment balance equation, the sand and gravel transport rate along the lower Tedori river was extracted for different decades.

Empirical Orthogonal Function (EOF) analysis was conducted in order to highlight the long-term characteristics of channel variation and the effect of anthropogenic activities over the periods 1950–1979 and 1991-2007. In addition, a collation of river and coastal erosion by EOF analysis was conducted.

In the second part, in order to reproduce the bore propagation over complex topography, a numerical model is developed to solve the Nonlinear Shallow Water Equations on the basis of TVD-MacCormack scheme. The model incorporates a surface gradient method , a simple wetting and drying method and an improved surface gradient method. The applicability of the numerical model is tested through comparison with existing theoretical and experimental studies. The verification of the model against with analytical solution include tide wave over steps, preservation of still water surface, dam-break, run-up and back-wash on a sloping bathymetry. The validation of the model with experimental data consist of dam -break wave over a triangular bottom sill, dam-break wave propagation over a complex topography, 3D schematic dam break. Finally, tsunami propagation and run up over a river bank was modeled.

2.Conclusion

For the morphological response of the lower Tedori river to material extraction and dam construction, several conclusions were extracted as follows.

Rapid and vertical adjustment was clearly observed from 1950 to 1991. The amount of sand and gravel extracted from the river was at least 8.9×10^6 m^3, which significantly exceeded the sediment supply from the upstream area. Consequently the riverbed degraded in excess of 0.5–3.5 m in the entire study area, and the RSV decreased by 12.7×10^6 m^3. Besides, in the period of 1975 to 1990, the sediment mean diameter in the main course was smaller than that in the lateral lane. DA with a volume of 2.1×10^6 m^3 and imbalance in sediment transport were other reasons for the degradation of the riverbed.

From 1991 when SGM was completely prohibited, the Tedorigawa Dam became the dominant factor affecting the lower riverbed. This led to a reduction in the mean

total stream power per unit channel length of 25%, and a subsequent increase in the riverine vegetation cover. The sediment transport capacity of the flood decreased and sediment transported from the Ozo River deposited in the lower riverbed. Consequently, the RSV increased by $0.6 \times 10^6 \, \mathrm{m}^3$ in the period 1991–2007.

The temporal adjustment of the riverbed elevation at each cross section indicates that the riverbed experienced five phases of adjustment: first three phases strongly depended on the rate and magnitude of sediment extraction from the river while the final phase was purely dominated by Tedorigawa Dam operation. An empirical model was established to describe such phases.

An overall decrease in channel width of the lower Tedori river was observed through the period of 1950-2007. The variation in the channel width was accompanied with the variation in the riverbed elevation: namely, channel narrowing and the river bed degradation; channel widening and the river bed aggradation. Prior to 1991 sand and gravel mining induced a considerable reduction in sediment budget along the lower Tedori river; after 1991 sediment budget slightly recovered partially along the lower Tedori river.

The first four modes of EOF analysis fully capture the main trends in the vertical adjustments and its dominant factors over the period 1950–1979. The first mode explained the mean profile of the riverbed and temporal variation of RSV. The second to fourth eigenfunctions reflected the characteristics of vertical adjustment for phase I-B,I-C and I-A, respectively. The corresponding temporal functions explained the respective effects of SGM, of imbalance in sediment transport, and of DA on the riverbed. In addition, a collation of river and coastal EOF results indicate that the time lag of the onset of accelerated erosion in the Mikawa coast was several years when compared with that in the downstream river.

The early presence of the dykes with embankment disrupting the connection between the river channel and its floodplain makes the adjustment of the lower Tedori River different from that of other disturbed rivers in U.S.A. and Europe. The embankment has confined the river channel, resulting in no widening due to bank failure in the lower Tedori River during the period 1950-2007. However, due to high energy of the Tedori River, a significant amount of sediment, generated from the erosion in the upstream riverbed and tributaries was still transported to the downstream riverbed, inducing an aggradation phase following an intensive degradation phase.

In the second part of the present study, a numerical model is developed to solve the Nonlinear Shallow Water Equations based on the TVD-MacCormack scheme, which is 2nd order accurate in time and space. Effective treatments have been implemented to achieve well-balancing through modifying local bed and using the surface gradient instead of the depth gradient for TVD corrections. Concurrently, the model is capable of capturing the moving wet-dry interface well by incorporating a surface gradient method.

The applicability of the numerical model is verified through comparison with existing theoretical studies. The shock-capturing ability of the model is tested against two frictionless transcritical flow problems: the dam-break on wet bottom and the dam-break on dry bottom. These tests prove that the numerical model captures the moving shock very well in both the wet and dry bottom. Then, the well-balanced property of the model is confirmed when the water surface remains constant along the channel in the case where tidal wave runs over two steps. In addition, the high capability of the numerical model in tracking the moving boundary on a sloping bathymetry is examed. The results reveal that the water surface keeps planar during the simulated duration. No distortion appears adjacent to the wet-dry interface. In all tests above, very good agreement between the numerical and analytical results is obtained.

In a second step, the perfomance of the numerical scheme is validated with several laboratory experiments. Firstly, the present model is able to accurately capture complex characteristics of the flow, which is induced by the dam-break wave over the mixed wet-dry bottom consisting of the triangular hump. It proves that the model could reproduce the one-dimensional dam-breaking wave propagating over the highly irregular topography. As a case with more difficulty, the model is applied to a dam break wave propagating over a triangular hump and subsequently overtopping a vertical wall. The model reasonably describes the response of the flow until the flow reaches the vertical wall, but after that, there is a discrepancy between the computed and measured water surfaces due to the violation of the key assumption of the shallow water equation at the vertical wall. However, the model predicts the arriving time very well after the flow overtops the vertical wall. Subsequently, dynamics of the 3D flow is simulated by using the developed model. The numerical model captures well the reflective waves of the boundaries and the box. However, in some periods, the magnitude of the computed water surface is considerably different from that of the

measured water surface. Yet, for practical purposes, the model has advantage of being easy to treat the source term together with less expensive cost of computation in comparision with alternative 2D or 3D models. Finally, the model is utilized to study of wave overtopping river banks of a curved channel with a parabolic cross-section. Characteristic behavior of wave during propagation and overtopping processes is realized clearly.

3. Recommendation

1. In this thesis, role of vegetation on change in river morphology was explained based on the general mechanism which occurred at similar rivers. Therefore, it is interesting to further investigate how riverine vegetation influences on the river morphology by using hydrodynamic model.

2. An estimation of sediment transport from the downstream Tedori river to the coast of Mikawa, Neagari and Mattou districts should be conducted to clearly quantify the effect of human impacts on morphological variation of the integrated watershed consisting of the Tedori river and the Ishikawa coast.

3. Results from this study clearly quantify how anthropogenic activities can adjust the river morphology. For other rivers in which variations in riverbed are induced due to a complex interaction of natural and anthropogenic factors, EOF analysis is considered as a powerful tool to provide a relative measure between the rate and magnitude of channel response and the drivers for change.

4. In future work, it is vital to develop a numerical scheme with nonuniform grid which can be applied to simulate the real dam break flow. A model of turbulence should be incorporated into account the developed model.

References

Adityawan, M.B., Roh, M., Tanaka, H., Farid, M., 2012. The effect of River Mouth Morphological Features on Tsunami Intrusion. Proceedings of The 8th International Conference on Disaster management, 75-83.

Alcrudo, F., Garcia-Navarro, P., 1993. A high-resolution Godunov-type scheme in finite volumes for the 2D shallow-water equations. International Journal for Numerical Methods in Fluids, 16(6), 489-505.

Alekseevskiy, N.I., Berkovich, K.M., Chalov, R.S., 2008. Erosion, sediment transportation and accumulation in rivers. International Journal of Sediment Research, 23(2), 93-105.

Arroyo, S., 1925. Channel improvement of Rio Grande and El Paso. Eng. News-Rec., 95, 374-376.

Aubrey, D.G., 1978. Statistical and dynamic prediction of changes in natural sand and beaches. Ph.D Thesis, Univ. of California, San Diego, 193pp.

Aureli, F., Maranzoni, A., Mignosa, P., Ziveri, C., 2008. A weighted surface-depth gradient method for the numerical integration of the 2D shallow water equations with topography. Advances in Water Resources, 31(7), 962-974.

Balzano, A., 1998. Evaluation of methods for numerical simulation of wetting and drying in shallow water flow models. Coastal Eng, 34, 83-107.

Beaumont, P., 1978. Man's impact on river systems: a world wide view. Area 10, 38-41.

Begnudelli, L., Sanders, B., 2006. Unstructured Grid Finite-Volume Algorithm for Shallow-Water Flow and Scalar Transport with Wetting and Drying. Journal of Hydraulic Engineering, 132(4), 371-384.

Bermudez, A., Vazquez, M.E., 1994. Upwind methods for hyperbolic conservation laws with source terms. Computers & Fluids, 23(8), 1049-1071.

Bridge, J.S., 2003. Rivers and floodplains: forms, processes, and sedimentary record. a Blackwell Publishing company.

Bull, W.B., 1979. Threshold of critical power in streams. Geological Society of America Bulletin, 90(5), 453-464.

Canestrelli, A., Dumbser, M., Siviglia, A., Toro, E.F., 2010. Well-balanced high-order centered schemes on unstructured meshes for shallow water equations with fixed and mobile bed. Advances in Water Resources, 33(3), 291-303.

Canestrelli, A., Siviglia, A., Dumbser, M., Toro, E.F., 2009. Well-balanced high-order centred schemes for non-conservative hyperbolic systems. Applications to shallow water equations with fixed and mobile bed. Advances in Water Resources, 32(6), 834-844.

Church, M., 1995. Geomorphic response to river flow regulation: Case studies and time-scales. Regulated Rivers: Research & Management, 11(1), 3-22.

Collins, B.D., Dunne, T., 1989. Gravel Transport, Gravel Harvesting, and Channel-Bed Degradation in Rivers Draining the Southern Olympic Mountains, Washington, U.S.A. Environmental Geology, 13(3), 213-224.

Dai, Z., Liu, J.T., Fu, G., Xie, H., 2013. A thirteen-year record of bathymetric changes in the North Passage, Changjiang (Yangtze) estuary. Geomorphology, 187(0), 101-107.

Dang, M.H., Umeda, S., Matsuda, R., Yuhi, M., 2012. Influence of Anthropogenic Activities on the lower Tedori river, Japan. Japan Sea Research, Kanazawa University, 43, 19-34.

Delis, A.I., Skeels, C.P., 1998. TVD schemes for open channel flow. International Journal for Numerical Methods in Fluids, 26(7), 791-809.

Dick, J.E., R.A.Dalrymple, 1984. Coatal changes at Bethany Beach, Delaware. Proc. 29th Coastal Engineering Conf. (ASCE), 1650-1667.

Dietrich, W.E., Kirchner, J.W., Ikeda, H., Iseya, F., 1989. Sediment supply and the development of the coarse surface layer in gravel-bedded rivers. Nature, 340, 215-217.

Erskine, W.D., 1990. Environmental impact of sand and gravel extraction on river systems. In:P.Davie, E.Stock amd D.Low Choy (eds.), The Brisbane River: A Source Book for the Future, Australian Littoral Society Inc. and Queensland Museum, Brisbane, 295-302.

Fennema, R., Chaudhry, M., 1990. Explicit Methods for 2‐D Transient Free Surface Flows. Journal of Hydraulic Engineering, 116(8), 1013-1034.

Fergus, T., 1997. Geomorphological response of a river regulated for hydropower: River Fortun, Norway. Regul. Rivers, 13, 449-462.

Fraccarollo, L., Toro, E.F., 1995. Experimental and numerical assessment of the shallow water model for two-dimensional dam break type problems. J. of Hydraulic Research, IAHR, 33(6), 843-864.

Frazão, S.S., Guinot, V., 2007. An eigenvector-based linear reconstruction scheme for the shallow-water equations on two-dimensional unstructured meshes. International Journal for Numerical Methods in Fluids, 53(1), 23-55.

Galay, V.J., 1983. Causes of river bed degradation. Water Resources Research, 19(5), 1057-1090.

García‐Navarro, P., Alcrudo, F., Savirón, J., 1992. 1‐D Open‐Channel Flow Simulation Using TVD‐McCormack Scheme. Journal of Hydraulic Engineering, 118(10), 1359-1372.

George, D., 2008. Augmented Riemann solvers for the shallow water equations over variable topography with steady states and inundation. J Comput Phys, 227(6), 3089–3113.

Germanovski, D., Ritter, D.F., 1988. Tributary response to local base level lowering below a dam. Regul. Rivers, 2, 11-24.

Gilvear, Winterbottom, 1992. Tributary response to local base level lowering below a dam. Regul. Rivers, 2(11-24).

Graf, W.L., 1977. The rate law in fluvial geomorphology. American Journal of Science, 277(February), 178-191.

Grant, G.E., 2012. The Geomorphic Response of Gravel-Bed Rivers to Dams: Perspectives and Prospects, Gravel-Bed Rivers. John Wiley & Sons, Ltd, pp. 165-181.

Harten, A., 1983. High resolution schemes for hyperbolic conservation laws. J. Comp. Phys., 49, 357-393.

Hathaway, G.A., 1948. Observations on channel changes degradation and scour below dams. Report of the 2nd Meeting of the Int. Assoc. Hydraul. Res., Stockholm, 267-307.

Hey, R.D., 1979. Dynamic process-response model of river channel development. Earth Surface Processes, 4(1), 59-72.

Hsu, T.-W., Jan, C.-D., Chang, K.-C., Wang, S.-K., 2006. Analysis and prediction of riverbed changes using empirical orthogonal functions. Journal of Hydraulic Research, 44(4), 488-496.

Huang, G., 2011. Time lag between reduction of sediment supply and coastal erosion. International Journal of Sediment Research, 26(1), 27-35.

Hubbard, M., Garcia-Navarro, P., 2001. Flux difference splitting and the balancing of source terms and flux gradients. Journal of Computational Physics, 165, 89-125.

Inoue, M., 2009. Promotion of Field-verified Studies on Sediment Transport Promotion of Field-verified Studies on Sediment Transport Quaterly Review, No.33, 89-108.

Isik, S., Dogan, E., Kalin, L., Sasal, M., Agiralioglu, N., 2008a. Effects of anthropogenic activities on the Lower Sakarya River. Catena, 75(2), 172-181.

Isik, S., Dogan, E., Kalin, L., Sasal, M., Agiralioglu, N., 2008b. Effects of anthropogenic activities on the Lower Sakarya River. Catena, 75.

Jackson, J.E., 1991. A user's guide to principal components. Wiley, New
York.

Jang, C., Shimizu, Y., 2005. Numerical Simulation of Relatively Wide, Shallow Channels with Erodible Banks. Journal of Hydraulic Engineering, 131(7), 565-575.

Kennedy, A.B., Chen, Q., Kirby, J.T., Robert, A.D., 2000. Boussinesq modeling of wave transformations, breaking, and runup. J Waterway, Port, Coastal, and Ocean Eng,, 126(1), 39-47.

Kondolf, G.M., 1994. Geomorphic and environmental effects of instream gravel mining Landscape and Urban Planning, 28, 225-243.

Kondolf, G.M., 1997. Hungry water: Effects of dams and gravel mining on river channels. Environmental Management, 21(4), 533-551.

Kondolf, G.M., Swanson, M.L., 1993. Channel adjustments to reservoir construction and gravel extraction along Stony Creek, California Environmental Geology, 21, 256-269.

Lane, E.W., 1947. Grade changes in Cherry Creek, Denver. Transactions, American Geophysical Union, 28(3), 443-444.

Lane, E.W., 1955. The importance of fluvial morphology in hydraulic engineering. Proceedings of the American Society of Civil Engineers, 81, 17.

Larson, M., Hanson, H., Kraus, N.C., Newe, J.r., 1999. Short - and long- term responses of beach fills determined by EOF analysis. Journal of Waterway, port, coastal, and ocean engineering, 125(6), 285-293.

Lawson, J.M., 1925. Effect of Rio Grande storage on river erosion and deposition. Eng. News-Rec., 327-334.

LeVeque, R., 2002. Finite volume methods for hyperbolic problems. Cambridge: Cambridge University Press.

LeVeque, R.J., 1998. Balancing source terms and flux gradients in high-resolution Godunov methods: the quasi-steady
wave-propagation algorithm. Journal of Computational Physics, 146, 346-365.

Leveque, R.J., Yee, H.C., 1990. A study of numerical methods for hyperbolic conservation laws with stiff source terms. Journal of Computational Physics, 86(1), 187-210.

Liang, D., Lin, B., Falconer, R.A., 2007. Simulation of rapidly varying flow using an efficient TVD–MacCormack scheme. International Journal for Numerical Methods in Fluids, 53(5), 811-826.

Liang, G., J.Seymour, 1991. Complex Principal Component analysis of wave-like sand motions. Proc. Coastal Sediment'91 Conf. ASCE(2175-2186).

Liang, Q., 2010a. Flood Simulation Using a Well-Balanced Shallow Flow Mode. Journal of Hydraulic Engineering, 136(9), 669-675.

Liang, Q., 2010b. Flood Simulation Using a Well-Balanced Shallow Flow Model. Journal of Hydraulic Engineering, 136(9), 669-675.

Liang, Q., Borthwick, L., A.G., 2009. Adaptive quadtree simulation of shallow flows with wet-dry fronts over complex topography. Computers & Fluids, 38(2), 221-234.

Liang, Q., Marche, F., 2009. Numerical resolution of well-balanced shallow water equations with complex source terms. Advances in Water Resources, 32(6), 873-884.

Losada, M.A., R.Medina, C.Vidal, A.Roldan, 1991. Historical evolution and morphological analysis of "el Puntal" Spit, Santander(Spain). J. Coastal Res., 7(3), 711-722.

Lynett, P.J., Wu, T.R., Liu, P.L.F., 2002. Modeling wave runup with depth-integrated equations. Coastal Eng, 46, 89-107.

Lyons, J.K., Puchrelli, M.J., Clark, R.C., 1992. Sediment trasport and channel characteristics of a sand-bed portion of the Green River below Flaming Gorge dam, Utah, USA. Regul. Rivers, 7, 219-232.

MacCormack, R.W., 1969. The effect of viscosity in hypervelocity impact cratering. AIAA Paper 69-354, Cincinnati, Ohio, USA, 7pp.

MacCormack, R.W., Paullay, A.J., 1972. Computational efficiency achieved by time splitting of finite difference operators. AIAA Paper 72-154, San Diego, California, U.S.A., 1972, 8pp.

Madsen, P.A., Sorensen, O.R., Schaffer, H.A., 1997. Surf zone dynamics simulated by a Boussinesq-type model: Part I. Model description and cross-shore motion of regular waves. Coastal Eng, 32, 255-287.

Makkaveyev, N.I., 1974. The impact of large water engineering projects on geomorphic processes in stream valleys. Geomorphogia, 2, 28-34.

Malhotra, S.L., 1951. Effects of barrages and weirs on the regime of rivers. Proc. Int. Assoc. Hydraul. Res., 4th Meeting(335-347).

Martín-Vide, J.P., Ferrer-Boix, C., Ollero, A., 2010. Incision due to gravel mining: Modeling a case study from the Gállego River, Spain. Geomorphology, 117, 261-271.

Medina, R., Losada, M.A., Dalrymple, R.A., Roldan, A., 1991. Cross-shore sediment transport determined by E.O.F. Method Coastal Sedimentd'91 Proceedings. ASCE, 2160-2174.

Miller, J.K., Dean, R.G., 2007. Shoreline variability via empirical orthogonal function analysis: Part I temporal and spatial characteristics. Coastal Engineering, 54(2), 111-131.

Ming, H.T., Chu, C.R., 2000a. The simulation of dam-break flows by an improved predictor–corrector TVD scheme. Advances in Water Resources, 23(6), 637-643.

Ming, H.T., Chu, C.R., 2000b. Two-dimensional shallow water flows simulation using TVD-MacCormack Scheme. Journal of Hydraulic Research, 38(2), 123-131.

Nunomoto, H., Takase, N., Kawaguchi, T., 1980. A study on mechanism of the riverbed variation in the Tedori River. Proc. of the 35th Annual Meeting of JSCE, 35(2), 350-351(in Japanese).

Oguchi, T., Saito, K., Kadomura, H., Grossman, M., 2001. Fluvial geomorphology and paleohydrology in Japan. Geomorphology, 39(1–2), 3-19.

Petts, G.E., 1984. Impounded Rivers. Chichester, John Wiley & Sons, Ltd.

Phillips, J.D., 2010. The job of the river. Earth Surface Processes and Landforms, 35(3), 305-313.

Piégay, H., Hicks, D.M., 2005. Sediment management in river systems: a need to assess changing processes in the long term and at a large scale. River Research and Applications, 21(7), 689-691.

Preisendorfer, R.W., 1988. Principal component analysis in meteorology and oceanography. Developments in atmospheric science, 17, Elsevier Science, Amsterdam.

Pruszak, Z., 1993. The analysis of beach profile change using Dean's method and empirical orthogonal functions. Coastal Engineering 19, 245-261.

R.Medina, Losada, M.A., C.Vidal, I.J.Losada, 1992. Temporal and spatial cross-shore distributions of sediment at " El Puntal" spit, Santander, Spain. Proc. 33th Coastal Engineering Conf. (ASCE), 2251-2264.

R.Medina, Losada, M.A., I.J.Losada, C.Vidal, 1994. Temporal and spatial relationship between sediment grain size and beach profile. Marine Geology, 118, 195-208.

Rinaldi, M., 2003. Recent channel adjustments in alluvial rivers of Tuscany, central Italy. Earth Surface Processes and Landforms, 28, 587-608.

Rinaldi, M., B.Wyzga, N.Surian, 2005. Sediment mining in alluvial channels: physical effects and management perspectives. River Research and Application, 21, 805-828.

Rinaldi, M., Simon, A., 1998. Bed-level adjustments in the Arno River, central Italy. Geomorphology, 22(1), 57-71.

Robbins, C.H., Simon, A., 1983. Man-induced channel adjustment in Tennessee streams. Water-resources investigations report ;82-4098. U.S. Dept. of the Interior, Geological Survey ; Open-File Services Section, U.S. Geological Survey [distributor], Nashville, Tenn. : Lakewood, CO.

Roe, P.L., 1981. Approximate Riemann solvers, parameter vectors and difference schemes. J Comp Phys, 43, 357-372.

Rovira, A., Batalla, R.J., M.Sala, 2005. Respone of a river sediment budget after historical gravel mining (the lower Tordera, NE Spain). River Research and Application, 21, 829-847.

Sandecki, M., 1989. Aggregate mining in river systems. Calif. Geol., 42(4), 88-94.

Sato, S., Kajimura, T., Abe, M., Isobe, M., 2004. Sand movement and long-term beach evolution in a fluvial system composed of the samegawa river and the Nakoso coast

Coastal Engineering Journal, 46(2), 219-241.

Schumm, S.A., Lichty, R.W., 1965. Time, space, and causality in geomorphology. American Journal of Science, 263(2), 110-119.

Sear, D.A., 1995. Morphological and sedimentological changes in a gravel-bed river following 12 years of flow regulation for hydropower. Regul. Rivers, 10, 247-264.

Sherrard, J.J., Erskine, W.D., 1991. Complex response of a sand-bed stream to upstream impoundment. Regul. Rivers, 6, 53-70.

Simon, A., 1989. A model of channel response in disturbed alluvial channels. Earth Surface Processes and Landforms, 14(1), 11-26.

Simon, A., 1992. Energy, time, and channel evolution in catastrophically disturbed fluvial systems. Geomorphology, 5(3–5), 345-372.

Simon, A., Rinaldi, M., 2006. Disturbance, stream incision, and channel evolution: The roles of excess transport capacity and boundary materials in controlling channel response. Geomorphology, 79(3), 361-383.

Soares-Frazão, S., 2007. Experiments of dam-break wave over a triangular bottom sill. Journal of Hydraulic Research, 45(sup1), 19-26.

Song, L., Zhou, J., Guo, J., Zou, Q., Liu, Y., 2011a. A robust well-balanced finite volume model for shallow water flows with wetting and drying over irregular terrain. Advances in Water Resources, 34(7), 915-932.

Song, L., Zhou, J., Li, Q., Yang, X., Zhang, Y., 2011b. An unstructured finite volume model for dam-break floods with wet/dry fronts over complex topography. International Journal for Numerical Methods in Fluids, 67(8), 960-980.

Stanley, J.W., 1951. Retrogression of the Lower Colorado River after 1935. Trans. Am. Soc. Civ. Eng., 116(943-957).

Stoker, J.J., 1957. Water Waves. Interscience, New York, 567pp.

Surian, N., Rinaldi, M., 2003. Morphological response to river engineering and management in alluvial channels in Italy. Geomorphology, 50(4), 307-326.

Syvitski, J.P.M., Peckham, S.D., Hilberman, R., Mulder, T., 2003. Predicting the terrestrial flux of sediment to the global ocean: a planetary perspective. Sedimentary Geology, 162(1–2), 5-24.

T.Hack, J., 1960. Interpretation of Erosional Topography in Humid Temperate Regions. American Journal of Science, 258-A, 80-97.

Thacker, W.C., 1981. Some exact solutions to nonlinear shallow-water wave equations. J Fluid Mech, 107, 499-508.

Topping, D.J., Rubin, D.M., Jr., L.E.V., 2000. Colorado River sediment transport 1. Natural sediment supply limitation and the influence of Glen Canyon Dam. Water Resources Research, 36(2), 515-542.

Toro, E.F., 2003. Shock-Capturing Methods for Free-Surface Shallow Flows. John Wiley & Sons LTD, 30-35.

Tseng, M.-H., 2003. The improved surface gradient method for flows simulation in variable bed topography channel using TVD-MacCormack scheme. International Journal for Numerical Methods in Fluids, 43(1), 71-91.

Tsujimoto, T., 1999. Fluvial processes in streams with vegetation. Journal of Hydraulic Research, 37(6), 789-803.

Tsujimoto, T., Teramoto, A., 2004. Transitional change in vegetation and bar-morphology comparison between gravel-bed river and sandy river. Advances in Hydro-science and Engineering, 6, 1-9.

Umeda, S., Saitoh, T., Furumichi, H., Nakaguchi, A., Ishida, H., 2013. Reduction of tsunami inundation flow and tsunami force by a porous vertical barrier mouted on a seawall. Journal of Japan Society of Civil Engineers, Ser. B3 (Ocean Engineering) 69 No.2, (in press) (in Japanese)

Vázquez-Cendón, M.a.E., 1999. Improved Treatment of Source Terms in Upwind Schemes for the Shallow Water Equations in Channels with Irregular Geometry. Journal of Computational Physics, 148(2), 497-526.

Vincent, S., Caltagirone, J.P., Bonneton, P., 2001a. Numerical modeling of bore propagation and run-up on sloping beaches using a MacCormack TVD scheme. J. Hydraulic Res., 39, 41-49.

Vincent, S., Caltagirone, J.P., Bonneton, P., 2001b. Numerical modelling of bore propagation and run-up on sloping beaches using a MacCormack TVD scheme. Journal of Hydraulic Research, 39(1), 41-49.

Wei, Y., Mao, X.Z., Cheung, K.F., 2006. Well-balanced finite-volume model for long-wave runup. J Waterway, Port, Coastal, and Ocean Eng., 132(2), 114-124.

Wijnberg, K.M., Wolf, F.C.J., 1994. Three-dimensional bahaviour of a multile bar system. Proc. Coastal Dynamics'94, ASCE, 59-73.

Williams, G.P., Wolman, M.G., 1984. Dowstream effects of dams on alluvial rivers. U.S. Geological Survey Professional Paper 1286, 83pp.

Winant, C.D., Inman, D.L., Nordstorm, C.E., 1975. Description of seasonal beach changes using empirical eigenfunctions. Journal of Geophysical Research, 80(15), 1979-1986.

Wolman, M.G., 1967. Two problems involving river channels and their background observations. Northwest. Univ. Stud. Geogr, 14, 67-107.

Xing, Y., Zhang, X., Shu, C.-W., 2010. Positivity-preserving high order well-balanced discontinuous Galerkin methods for the shallow water equations. Advances in Water Resources, 33(12), 1476-1493.

Yamamoto, Y., Kawai, K., Takano, T., 2008a. Sedimentation control of coastal zone with large-scale sandy beach. Proc. Civil Eng. in Ocean, JSCE, 24.

Yamamoto, Y., Kawai, K., Takano, T., 2008b. Sedimentation control of coastal zone with large-scale sandy beach. Proc. Civil Eng. in Ocean, JSCE, 24, 1339-1344 (in Japanese).

Yee, H.C., 1987. Upwind and symmetric shock-capturing schemes. NASA technical memorandum, 89464.

Yoshimura, C., Omura, T., Furumai, H., Tockner, K., 2005. Present state of rivers and streams in Japan. River Research and Applications, 21(2-3), 93-112.

Yuhi, M., 2008a. Impact of anthropogenic modifications of a river basin on neighboring coasts: A Case Study. Waterway, Port, Coastal and Ocean Engineering, ASCE, 134(6).

Yuhi, M., 2008b. Impact of Anthropogenic Modifications of a River Basin on Neighboring Coasts: Case Study. Journal of Waterway, port, coastal, and ocean engineering, 134(6), 336-344.

Yuhi, M., Dang, M.H., Umeda, S., 2013. Comparison of accelerated erosion in riverbed and downstream coast by EOF analysis. Journal of Coastal Research(65), 618-623.

Yuhi, M., S.Umeda, K.Hayakawa, 2009. Regional analysis on the decadal variation of sediment volume in an integrated watershed composed of the Tedori River and the Ishikawa Coast, Japan. Journal of Coastal Research, SI 56, 1701-1705

Yuhi, M., Yamada, F., Ishida, H., 2007. Preconditioned EOF study of multi-scale morphodynamics on eroding coast. Proceedings of Coastal Engineering Conference, ASCE(30), 3529-3541.

Zarillo, G.A., J.T.Liu, 1988. Resolving bathymetric components of upper shoreface on a wave-dominated coast. Marine Geology, 82, 169-186.

Zhou, J.G., Causon, D.M., Ingram, D.M., Mingham, C.G., 2002. Numerical solutions of the shallow water equations with discontinuous bed topography. International Journal for Numerical Methods in Fluids, 38(8), 769-788.

Zoppou, C., Roberts, S., 2003. Explicit Schemes for Dam-Break Simulations. Journal of Hydraulic Engineering, 129(1), 11-34.

Zou, J.G., Causon, D.M., Mingham, C.G., Ingram, D.M., 2001. The surface gradient method for the treatment of source terms in the shallow-water equations. J Comp Phys, 168(1), 1-25.